

Synthesis, Physical Properties and Application of NaSbO₃



Sumaira Kanwal

A thesis submitted in partial fulfillment of requirements for the degree of
Master of Science in Chemistry

Supervised by

Dr. Zahida Malik

Department of Chemistry

School of Natural Sciences

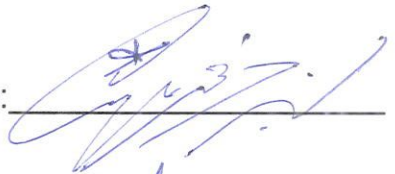
National University of Sciences and Technology

Islamabad, Pakistan

2018

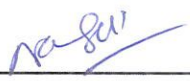
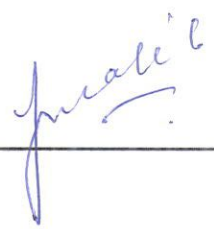
National University of Sciences & Technology**MS THESIS WORK**

We hereby recommend that the dissertation prepared under our supervision by: SUMAIRA KANWAL, Regn No. NUST201463664MSNS78214F Titled: Synthesis, Physical Properties and Applications of Pyrochlore-Type NaSbO₃ be accepted in partial fulfillment of the requirements for the award of **MS** degree.

Examination Committee Members1. Name: DR. AZHAR MAHMOODSignature: 2. Name: DR. NASEEM IQBALSignature: 

3. Name: _____

Signature: _____

External Examiner: DR. NASIR MEHBOOBSignature: Supervisor's Name: DR. ZAHIDA MALIKSignature: 


Head of Department

08-02-18

Date
COUNTERSIGNEDDate: 08/02/18


Dean/Principal

THESIS ACCEPTANCE CERTIFICATE

Certified that final copy of MS/M.Phil thesis written by Ms. Sumaira Kanwal, (Registration No. NUST201463664MSNS78214F), of School of Natural Sciences has been vetted by undersigned, found complete in all respects as per NUST statutes/regulations, is free of plagiarism, errors, and mistakes and is accepted as partial fulfillment for award of MS/M.Phil degree. It is further certified that necessary amendments as pointed out by GEC members and external examiner of the scholar have also been incorporated in the said thesis.

Signature: _____

Name of Supervisor: Dr. Zahida Malik

Date: 8.2.2018

Signature (HoD): _____

Date: 28-02-18

Signature (Dean/Principal): _____

Date: 08/02/18

Dedicated to

My parents, Teachers ,loving siblings and friends.

Contents

Chapter no. 1: Introduction

| | | |
|-------|---|-----------|
| 1.1 | Antimony and its compounds | 12 |
| 1.1.1 | Antimony oxide | 12 |
| 1.1.2 | Doping in Sb_2O_3 | 12 |
| 1.1.3 | Properties of metals doped Sb_2O_3 | 13 |
| 1.1.4 | Application of Antimony oxide | 13 |
| 1.1.5 | Lubricating oil Additives | 14 |
| 1.2 | Characterization | 14 |
| 1.2.1 | X-Ray Powder Diffraction technique(XRPD) | 14 |
| 1.2.2 | Scanning electron Microscopy | 16 |
| 1.2.3 | LCR Meter | 19 |
| 1.2.4 | Diffuse reflectance spectroscopy (DRS) | 22 |
| 1.3 | Mechanical properties | 24 |
| 1.3.1 | Hardness | 24 |
| 1.3.2 | Density | 25 |
| 1.3.3 | Specific gravity | 25 |
| 1.3.4 | Viscosity | 26 |
| 1.3.5 | Flash point | 27 |
| 1.4 | Effect of additives on Properties of lubricating oil | 27 |
| 1.4.1 | Viscosity index | 27 |
| 1.4.2 | Volatility and flash point | 28 |
| 1.4.3 | Pour point | 28 |
| 1.4.4 | Alkalinity | 28 |
| 1.4.5 | Oxidation | 28 |
| 1.5 | Aims and objectives of research | 29 |
| | Chapter no. 2: Literature review | 31 |
| 2.1 | Synthesis of inorganic material | 31 |
| 2.2 | Alkali metals doping in Sb_2O_3 | 32 |
| 2.2.1 | Lithium (Li) doping | 32 |
| 2.2.2 | Sodium doping | 32 |
| 2.2.3 | Potassium doping | 34 |
| 2.2.4 | Rubidium doping | 34 |
| 2.3 | Alkaline earth metals doping in Sb_2O_3 | 35 |
| 2.3.1 | Magnesium doping | 35 |
| 2.3.2 | Calcium doping | 35 |
| 2.3.3 | Barium doping | 36 |
| 2.3.4 | Strontium doping | 37 |
| 2.4 | Transition metals doped antimony oxide | 38 |
| 2.4.1 | Scandium doped antimony oxide | 38 |
| 2.4.2 | Titanium doped antimony oxide | 38 |
| 2.4.3 | Vanadium doped antimony oxide | 40 |
| 2.4.4 | Doping of chromium in antimony oxide | 44 |
| 2.4.5 | Doping of manganese in antimony oxide | 44 |

| | | |
|---|--|----|
| 2.4.6 | Doping of iron in antimony oxide | 45 |
| 2.4.7 | Doping of cobalt in antimony oxide | 48 |
| 2.4.8 | Doping of nickel in antimony oxide | 49 |
| 2.4.9 | Doping of copper in antimony oxide | 50 |
| 2.4.10 | Doping of zinc in antimony oxide | 53 |
| 2.5 | Lubricating oil | 54 |
| 2.5.1 | Addition of chemicals in lubricating oil | 55 |
| 2.5.2 | Zinc dialkyl di thio phosphate ZDDP | 55 |
| 2.5.3 | CuO, TiO ₂ and nano diamond as an additives | 56 |
| 2.5.4 | Cuo additive | 56 |
| 2.6 | Properties of antimonates | 56 |
| 2.7 | Properties of lubricating oil | 57 |
| 2.8 | Properties of doped antimonates | 57 |
| 2.8.1 | Optical properties | 57 |
| 2.8.2 | Photoluminescence properties | 60 |
| 2.8.3 | Surface photovoltage properties | 61 |
| 2.8.4 | Electrical properties | 62 |
| 2.8.5 | Electrochemical properties | 64 |
| 2.8.6 | Ion exchange properties | 65 |
| 2.8.7 | Magnetic properties | 65 |
| 2.8.8 | Catalyst | 68 |
| 2.8.9 | Acid base property | 70 |
| 2.8.10 | Sorption behavior | 70 |
| 2.8.11 | Opacifying agent | 70 |
| 2.8.12 | Flame retardants | 70 |
| 2.8.13 | Gas sensing ability | 71 |
| Chapter no. 3: Materials and method | | 73 |
| 3.1 | Synthesis of precursors | 73 |
| 3.2 | Synthesis of NaSbO ₃ | 73 |
| 3.3 | Characterization | 74 |
| Chapter no. 4: Results and discussions | | 76 |
| 4.1 | Structural and morphological analysis | 76 |
| 4.2 | Scanning electron microscopy | 78 |
| 4.3 | Optical properties | 80 |
| 4.3.1 | Diffuse reflectance spectroscopy | 81 |
| 4.4 | Dielectric properties | 83 |
| 4.5 | Mechanical properties | 89 |
| 4.5.1 | Hardness | 89 |
| 4.6 | Flash point elevation | 90 |
| 4.7 | Effect on density of lubricating oil | 91 |
| 4.8 | Specific gravity | 92 |
| 4.9 | Viscosity | 92 |
| Summary and future prospects | | 94 |
| References | | 96 |

List of Abbreviations

| | | | |
|--------------------------------|------------------------------|---------------|----------------------------------|
| Sb ₂ O ₃ | Antimony oxide | d | Day |
| NaSbO ₃ | Sodium antimonate | C | Capacitance |
| SEM | Scanning electron microscope | D | Dissipation factor |
| LaB ₆ | Lanthanum hexa boride | DRS | Diffuse reflectance spectroscopy |
| kV | kilo volt | UV | Ultra violet |
| eV | Electron volt | % | Percentage |
| SE | Secondary electron | nm | Nanometer |
| LCD | Liquid crystal display | TLC | Thin layer chromatography |
| XRPD | X-Ray powder diffraction | Hv | Vicker hardness |
| XRD | X-Ray diffraction | Å | Angstrom |
| Cu | Copper | ϵ | Dielectric Constant |
| Mg | Magnesium | ϵ'' | Dielectric loss |
| W | Tungsten | $\tan\delta$ | Tangent Loss |
| Fe | Iron | σ_{ac} | AC conductivity |
| Cr | Chromium | $\ln(F)$ | Natural log of Frequency |
| Mo | Molybdenum | PVA | Poly vinyl alcohol |
| kHz | kilo hertz | μ | Dynamic viscosity |
| h | Hour | ρ | Density |

List of Figures

- Figure 1.1: Working of XRPD.
- Figure 1.2: Illustration of Bragg's law.
- Figure 1.3: Instrumentation of a SEM.
- Figure 1.4: Interaction of electron beam with specimen.
- Figure 1.5: LCR meter.
- Figure 1.6: Diffuse and specular reflection from glossy surface.
- Figure 1.7: General mechanism of diffuse reflection by solid surface.
- Figure 1.8: Light scattering through powdered sample.
- Figure 1.9: Micro Vickers hardness tester.
- Figure 1.10: Specific gravity bottle.
- Figure 1.11: Viscometer.
- Figure 1.12: Close cup flash point tester.
- Figure 1.13: Oxidation cycle.
- Figure 2.1: Ilmenite type crystal structure FeTiO_3 .
- Figure 2.2: represent Anatase and rutile phase of titanium oxide.
- Figure 2.3: Structure of FeSb_2O_4 . shaded octahedral are shaded Fe ion are located within octahedral, O ion are in black sphere and Sb ion are in white.
- Figure 2.4: CoSb_2O_6 SEM image.
- Figure 2.5: Delafossite structure.
- Figure 2.6: Delafossite honeycomb crystal structure of Cu_5SbO_6 . (a) View perpendicular to the honeycomb layer with the Cu^{2+} honeycomb arrangement emphasized (black dashed lines and dots). Sb(V)O_6 octahedral are shown in blue (dark) while Cu(II)O_6 octahedra are shown in yellow (light). A schematic illustration of the relationship of the unit cell axes between the hexagonal (light-gray dashed-dot arrows) and monoclinic (red solid arrows) cells is also included. (b) View parallel to the honeycomb layers. The two types of O -Cu(I) -O sticks that separate the planes a.
- Figure 2.7: Crystal structure of ZnSb_2O_6 . Edge-shared octahedrons represent the rutile chain.
- Figure 2.8: Optical absorption spectrum converted from optical diffuse reflectance spectrum for polycrystalline sample of strontium antimonates.
- Figure 2.9: Optical band gap estimated from the plots of $(\alpha h\nu)^{1/2}$ versus energy (h ν) for polycrystalline sample of $\text{Ba}_2\text{Sb}_7\text{O}_{13}(\text{OH})$
- Figure 2.10: UV-visible degradation spectra of $\text{CaSb}_2\text{O}_5(\text{OH})_2$ prepared at pH=1 and cubic CaSb_2O_5 .
- Figure 2.11: Temporal changes of RhB concentration as monitored by the UV-vis absorption spectra at 554nm over illuminated ZnSb_2O_6 , illuminated P25 and UV irradiations only
- Figure 2.12: Excitation power intensity-dependent PL of the nanostructures measured at room temperature, where I_0 is about 20 kW/cm^2 . Position (b) and integrated intensity.
- Figure 2.13: SPS spectra of ZSO(900) undoped and N-ZSO(900)doped ZnSb_2O_6 without external bias.

Figure 2.14: Variation of conductivity vs temperature.

Figure 2.15: The ac complex impedance spectrum of ilmenite NaSbO_3 .

Figure 2.16: Arrhenius plot for NaSbO_3 ionic conductivity for ilmenite phase.

Figure 2.17: Potential (vs Li/Li^+) vs capacity for CoSb_2O_4 under galvanostatic charge/discharge at 30 mA/g between 0.05 and 1.3 V for the second, third, and tenth cycles. The inset shows the initial discharge and charge curves.

Figure 2.18: Magnetic properties of FeSbO_4 .

Figure 2.19: Temperature dependence of the magnetization (M) and the susceptibility (M/H) of CoSb_2O_6 compounds measured at various magnetic Fields (H)

Figure 2.20: Temperature dependence of the magnetic susceptibility of the CuSb_2O_6 sample. The solid line represents a result of the curve fitting S¹² 1-D antiferromagnetic Heisenberg model.

Figure 2.21: Sulfur yield as a function of reaction temperature.

Figure 2.22: Percentage response characteristics as a function of temperature toward different concentrations of H_2 gas exhibited by the sensors fabricated using 300°C calcined FeSbO_4 powder..

Figure 2.23: SEM analysis of thin film

Figure 4.1: X-Ray powder diffraction pattern of NaSbO_3 annealed at different temperatures

Figure 4.2: Rietveld refinement result of NaSbO_3

Figure 4.3: Crystal structure of NaSbO_3

Figure 4.4: SEM images of samples annealed at (a) 700°C (b) 800°C (c) 900°C (d) 1000°C.

Figure 4.5: EDS spectra of samples prepared at different temperatures; (a) 700°C, (b) 800°C, (c) 900°C, (d) 1000°C.

Figure 4.6: UV-DRS spectra of NaSbO_3 samples % Reflectance vs $\ln F$.

Figure 4.7: Taucplot of $[\text{h}\nu \times F(R)]^2$ vs energy for sample annealed at: (a) 700°C, (b) 800°C, (c) 900°C (d) 1000°C

Figure 4.8: Variation of dielectric constant with frequency.

Figure 4.9: (a) plot of dielectric loss vs $\ln F$ (b) plot of tangent theta loss vs $\ln f$.

Figure 4.10: Variation of AC conductivity with frequency

List of tables

Table 1.1: Dielectric constants of common materials.

Table 2.1: Product of solid state reaction of Mn_2CO_3 with Sb_2O_3 at different temperature.

Table 2.2: Sb_2O_3 and CuO phase relation at different temperature.

Table 4.1: Unit cell data of NaSbO_3

Table 4.2: Optical band gaps of samples at different temperatures

Table 4.3: Vickers hardness of samples.

Table 4.4: Effect of NaSbO_3 on flash point of lubricating oil

Table 4.5: Effect of NaSbO_3 addition on densities of lubricating oil.

Table 4.6: Effect of NaSbO_3 addition on specific gravities of lubricating oils.

Table 4.7: Effect of NaSbO_3 addition on kinematic viscosity of lubricating oils

Table 4.8: Effect of NaSbO_3 addition on Dynamic viscosity of lubricating oils.

Acknowledgments

All praises to Allah who deemed man worthy to be the foremost of His creation and all blessings for Prophet(PBUH) whose life is a doubtless model for the mankind.

*Thanks to almighty Allah for giving me this opportunity, the patience and strength to do this huge task in the field of science. I am thankful to my research supervisor **Asst. Prof.Dr. Zahida Malik** at SNS NUST for her motivation, patience, enthusiasm, support, kind consideration and guidance regarding my research work.*

*I am also thankful to Principal of SNS **Prof. Dr. Habib Nasir**. I am paying my special thanks to my GEC members, **Asst .Prof. Azhar Mahmood** and **Assoc. Prof. Dr.Naseem Iqbal**. I am conveying my sincere and deepest gratitude to **Mr. Faisal Waqar** for his assistance in improving my internet skill needed for my research purpose. Laboratory staff including **Ishrat Nadeem** and **Raza** helped me during my research project and they deserve special thanks.*

*My friends including **Maryam, Natasha, Mamoona, Hajra, Yusra, Humaira, Sara and Asad Ali** are worthy for their moral support. My parents deserve special mention for their support and prayers. Words fail to express my father,s devotion, he is the person in first place who made the foundation for my higher education, showed me the joy of intellectual pursuit, Whose dedication, affection, love and persistant confidence in me has taken the load of my shoulders.*

In the last I am greatly thankful to School of Natural Sciences (SNS) NUST, School of Chemical and Material Engineering (SCME) NUST, US Pakistan Centre for Advance Study in Energy (USPCAS-E) NUST, Institute of Space Technolo(IST)andNationalCentre of Physics (NCP) Islamabad for providing me technical assistance in my research work.

Sumaira Kanwal

Abstract

Present research work is based on development of an innovative method for synthesis of sodium antimonate using commercial grade (NaCl). There are few reports on the synthesis of this compound from expensive precursors. Present study aimed to produce NaSbO₃ by Wet chemical synthesis of Sb₂O₅ followed by its solid state reaction with NaCl at 700°C, four different annealing temperatures (700, 800, 900, 1000°C) have been employed to investigate the structure and properties. Characterization by XRD revealed the purity, phase analysis and crystallite size of synthesized material and also indicated the change of single phase to multi phase at higher annealing temperature. Crystal structure obtained after Rietveld refinement is pyrochlore type, in that structure Na is present between the layers of Sb and O. SEM analysis exposed the same chemical composition and gave information about the morphology of NaSbO₃. Material synthesized at 1000°C showed better morphological aspect as compared to other samples annealed at lower temperatures. Dielectric properties and AC conductivity have been measured at room temperature. It has been found that by increasing the annealing temperature, conductivity decreases because material is shifting from semiconductor to insulator. The value of optical band gap increased on increasing the annealing temperature which indicated that material becomes insulator at higher temperatures. NaSbO₃ is subjected to hardness measurement by using micro Vickers hardness tester and material synthesized at 700°C exhibited maximum hardness. NaSbO₃ is introduced as an additive into engine lubricating oil to check its effectiveness quality parameters of lubricating oils were measured after addition and compared with virgin oil. Flash point measurements have also been reported here, involving the effect of NaSbO₃ concentration on the flash point of lubricating oil. Density, specific gravity and viscosity of lubricating oils after addition of little amount of NaSbO₃ is measured and results obtained indicates elevation in density and specific gravity and viscosity of the lube oil decreases. Further research will prove NaSbO₃ as a good additive for lubricating oil to enhance its flash point and has little effect on its density.

ChapterNo.1

Introduction

1.1. Antimony and its compounds

Antimony is a metalloid with silvery lustrous appearance and resistant against acids. Antimony compounds have been used since prehistoric time in cosmetics. Recently, metallic antimony is used as an alloying material for tin and lead, improving their hardness for applicability in preparation of solders, plain bearings, bullets and microelectronics [1]. Antifriction alloys are also made by antimony, used in bullets, lead shots, cable sheathing, solders and other hardening alloys that are employed for organ pipe manufacturing [2]. Its compounds include, oxide, hydroxide, halides, hydrides, antimonides and organo-antimony, etc [3] some are used as a stabilizers and catalysts for PET production, e.g as fining agent to remove tiny bubbles in glass for TV screens and as a pigment in paints [4]. In addition to above mentioned applications it is widely used as a dopant for n type silicon wafers in semiconductor industry and in the production of diodes, IR detectors, and Hall Effect devices [5-6]. Anti-protozoan and schistosomal drugs are made by antimony and it is also useful for veterinary medicine [7-8]. Besides wide variety of antimony compounds, in this study the main focus is on antimony oxide doped with alkali and alkaline earth metals.

1.1.1 Antimony oxides

Antimony oxides exists two different state i.e. +3 (Sb_2O_3) and +5 (Sb_2O_5) both are amphoteric in nature and are synthesized by open air oxidation of Sb [9]. In nature Sb_2O_3 exist as an important compound of antimony in the form of minerals e.g. valentinite and senarmonite.

1.1.2 Doping in Sb_2O_3

Metals like Li, Na, K, Rb, Cs, Mg, Ca, Sr, Al, Sc, Ti, V, Cr, Mn, Fe,Co, Ni, Cu, and Zn etc are doped into Sb_2O_3 and new properties of resultant compounds are studied [10-86]. There are numerous reports on optical, electrical, photocatalytic, semiconducting, magnetic and

electrochemical properties of Sb_2O_3 doped with alkali, Alkaline earth and transition metals [87].

1.1.3 Applications of Antimony oxide

Compounds of metal antimony oxide have received increasing attention in recent years because of their diverse structure chemistry and potential applications in different fields, like photocatalysis, nonlinear optics, piezoelectricity and luminescence materials [87]. Metals including alkali, alkaline earth and transition doped Sb_2O_3 has following applications given below:

- **Flame retardant:** Antimony trioxide and its halides are used as a flame retarding materials. These materials are used in children's clothing, toys, air craft, automobile seat covers and fiberglass composites etc. The Sb_2O_3 is also employed as additive in polyester resins of aircraft engine cover. It makes resin to burn till the time it is in contact with flame but soon extinguishes upon disconnection of flame. [88-91]. Antimonates of Na are used in textiles, ropes and coatings [92] because of their flame retarding ability. Composite of Sb_2O_3 with $\text{Mg}(\text{OH})_2$ and talc also show flame retardant ability and possess high mechanical strength.
- **Electronics & Solar Cell:** Lithium antimonates have ionic conductivity used in batteries and other electronic devices such as an electrodes material. V, Co and Zn antimonates also possess electrical property used in electrical appliances [93],[94],[86]. Co, Fe, and Zn antimonate show electrochemical ability use in electrochemical application including cells and batteries [74],[71]. Antimonate of Sr have double perovskite like structure used in fuel cell, solar cell [32], and as a semiconducting material in various fields [95]. Co antimonites are the candidate oxidants in the time delays for mining detonators [96] other metals antimonates also have unique and worthwhile properties which serve as a milestone for the researchers to do extensive research on synthesis of antimony oxide doped with different metals. The Al, Ti, Cr and Nickel doped antimony oxide yields ion exchange material used as ion exchangers in industries [68], [97],[62] [78].

- **Magnetic & Sensing material:** V, Co and Nickel antimonates show magnetic susceptibility [50], [74]. Whereas Antimonates of Fe serve as LPG sensing material [70] and Co antimonates also act as chemical sensor [98].
- **Paints & Glass Industry:** Antimonates of Ca are used in glass industry as opacifying agents [99],[100]. Ni antimonates are used as heat resistant pigment in paints [101].
- **Photocatalysis:** Antimonates of Ca, Fe, Co, V and Zn are used as a photocatalyst against environmental pollution [102], [98], [72], [85].

1.1.4 Lubricating Oil Additives: Friction between two moving parts are reduced by presence of certain chemicals such chemicals are known as lubricants. Large number of lubricants are used for lubrication purposes in vehicles engines and machineries out of which lubricating oils are most extensive in use. In order to save the energy given to a mechanical system it is necessary to improve the properties of lubricants [103]. Scientist are keen to improve the quality of lubricating oils by adding certain chemicals additives. Usually antioxidant, dispersant, detergent, antiwear agents, viscosity modifier and antifoam agents are added into lubricating oil as additives. Additives expand the properties of lubricating oil by affecting the quality parameters, e.g flash point, viscosity, surface tension, density and specific gravity, etc [104].

1.2 Characterization Techniques

The techniques used for characterization and to ascertain the physical properties are given below:

- 1.2.1 X-Ray Powder diffraction
- 1.2.2 Scanning Electron Microscope (SEM)
- 1.2.3 L.C.R meter
- 1.2.4 Diffuse Reflectance spectroscopy

1.2.1 X-Ray Powder Diffraction (XRPD)

XRPD is used for studying crystal structure, phases, preferred orientation, crystallinity, strain and crystal defects, etc. It is nondestructive technique with the principle based on constructive

interference of scattered beam, scattered by lattice planes in a sample. Each crystalline material has its own specific X-Ray powder pattern which acts as a fingerprint for its identification. It is used to find structure; position of atoms, atomic packing in the structure, interatomic distances and angles.

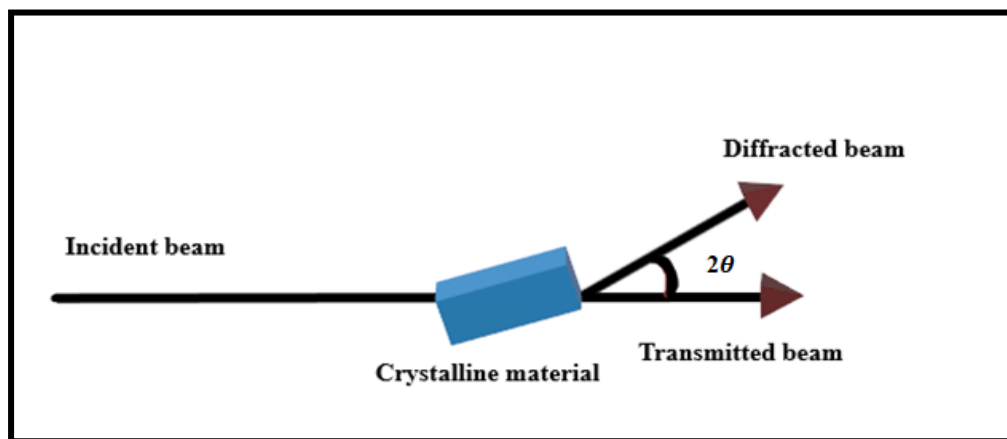


Figure 1.1: Working of XRD.

XPRD technique is based on Bragg's law developed by two English scientists Sir W.H.Bragg and Sir W.L.Bragg.

$$n \lambda = 2d \sin \theta$$

Distance between atomic layers of crystal is given by d , λ represents wavelength of incident X-Ray beam and n is an integer. Crystal is made up of unit cell which are periodically arranged in a lattice. When rays 1 and 2 fall on material it causes diffraction and after passing through the planes of material it come back and recorded in the form of spectrum.

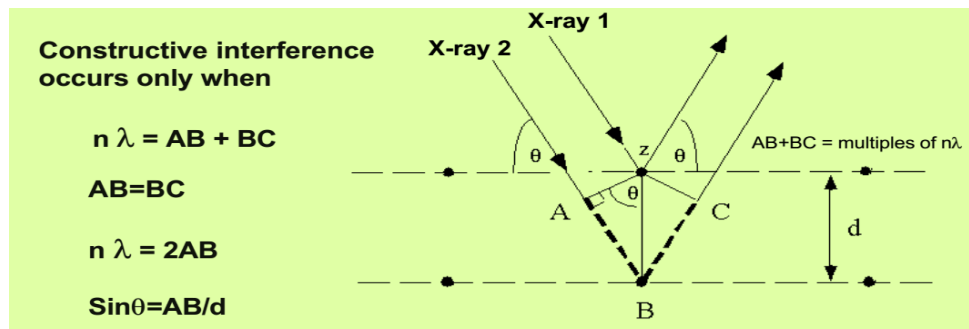


Figure 1.2: Illustration of Bragg's law.

1.2.2 Scanning Electron Microscopy (SEM)

SEM uses electron beam instead of light for analyzing the object under investigation and generates sample micrographs. When electron beam falls on the surface of a sample they interact with its atoms and produce different signals which contain information about sample topography, composition, crystalline structure and orientation of material. In the early 1950, SEM was developed and used in the medical and physical sciences. Scientists are now able to control the magnification limits greater than 1nm which makes SEM one of the more powerful and useful instrument for analysis [105]. It produces images of maximum magnification and resolution. It is very powerful tool in the field of metals and material for solving problems regarding to product and its processing. Every field of life is aided by SEM including electronics, petrochemicals, plastics, pharmaceuticals, aerospace, medical devices, engineering, chemicals, automotives, materials and metallurgy, glass, metals, ceramics, semiconductors, plastics, polymer, powders and dust, composite materials, fibres all can be studied by SEM. It also allows studying defects in products and process failure, airborne contamination identification and analysis of surfaces, particle size and powder morphology, chemical etching and cleaning problems, corrosion identification and oxidation study, stain and contaminants investigation. Joining technology and welding quality evaluation, failure study, coating, paints, adhesives, sealant, gasket filler, fingerprinting, delamination study are all applications of SEM [106].

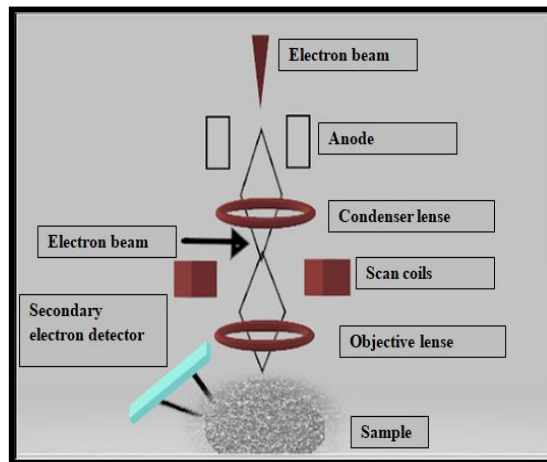


Figure 1.3: Instrumentation of a SEM

SEM consist of following parts:

- (a) Vacuum system
- (b) Sample Stage
- (c) Electron Source ("Gun")
- (d) Detectors for all signals of interest
- (e) Display / Data output devices

- **Vacuum system:** Vacuum pump is used to evacuate the specimen chamber under high vacuum at 10^{-3} to 10^{-4} pa. SEM usually has one detector but in some cases additional detectors can be present [107].

- **Specimen stage:** In an electron microscope specimen is observed at high magnification. So a specimen stage is required in a smooth fashion, horizontally (x,y direction), vertically (z direction), tilting (t) and rotation (r).

- **Image display and recording:** Signals from SE detectors are amplified and transmitted to display unit Cathode ray oscilloscope is used as a display unit but now day's LCD's are used. Scanning speed of electrons beam can be changed in several steps. Fast scanning speed is used for observation purposes and slow scanning speed is used for saving of images. Image is recorded in digital formatting.

- **Sample preparation:** Sample preparation is required before SEM analysis. Sample should be tightly mounted on sample stud and the size of the sample should be in range of

sample holder. Sample should be electrically conductive in nature at least sample surface should be conductive. in case of nonconductive sample it will be coated with thin layer of electrically conducting material, Conducting material used for sample coating are gold, gold/palladium alloy, Pt, Os, Ir, W, graphite C, and Cr.

- **Principle of SEM**

Various types of signals produced by SEM are due to different type of electron including SE or BSE, characteristic X-Ray and light absorbed current, visible light (Cathodeluminescence) and transmitted electrons. All SEMs are equipped with SE detectors. Mostly in standard detection mode SE are emitted closely from the surface of specimen. SEM produce very high resolution image of surface of the sample and details about the sample less than 1nm in size can be disclosed. Elastic scattering of the electron beam with sample produce back scattered electron. These emit from the depth of the sample. Resolution of secondary electron images is greater than back scattered electron images.

Intensity of backscattered electrons signals is related to atomic number of the sample so they are mostly used for analysis purpose from SEM with characteristic X-Ray spectra. Images of back scattered electrons deliver information about different elements present in the sample. When high energy electron beam removes an electron from the inner shell of the sample and cause the electrons of higher energy shell to fill the vacant underlying shell and release energy in the form of characteristic X-Rays. Abundance of element in the sample and identification of sample composition is done by characteristic X-Rays. SEM gives three dimensional imaging of sample which is helpful for complete analysis of surface of a specimen.

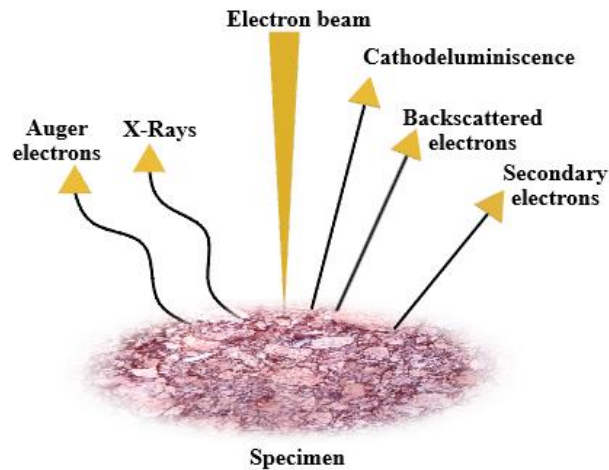


Figure 1.4: Interaction of electron beam with specimen.

1.2.3. LCR Meter

An electronic equipment which is used to measure the inductance (L), capacitance (C) and resistance (R) of a material is known as LCR meter. It is an automated computer controlled device for measurement of sample conductivity at a frequency range of 10kHz to 2MHz. It is used for measurement of impedance by measuring current, voltage and phase angle between voltage and current. LCR meter is used to measure conductance, inductance, capacitance, dissipation factor.

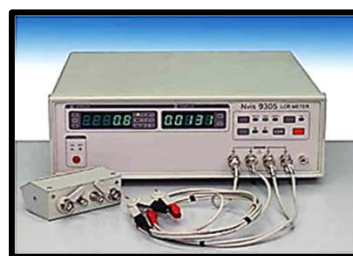


Figure 1.5: LCR meter.

Measurement of impedance is a substantial income of electronic components and material evaluation. Every material has specific set of electrical features which depend on its dielectric or insulating properties. When these properties are accurately measured, they provide essential information for its use and applications. In LCR meter impedance is internally measured and converted to capacitance and inductance for displa. Measurement of dielectric

material give us information which is useful for many electronic application. Dielectric properties are related to impedance of a substrate, frequency of dielectric resonator and loss of cable insulator [108]. Dielectric information of a material is also useful for packing design, microwave in which food is processed, ceramic, rubber and plastic etc.

- **Measurement Principle**

Measurement through LCR meter is based on automatic balancing bridge method. An electric current is drained through a resistor when amplifier having high gain level automatically adjusts its gain. Current flow through device under test is equal to R whereas, The value of potential for device under test is also equal to virtual ground level potential. At this stage feedback resistance, input voltage output voltages are used to calculate impedance of test material. when AC voltage is passed through testing material then LCR meter is used for measuring voltage and current across the testing material. Measurement by LCR meter involves connection of a material to the instrument which require special fixture depending on material type. Powder materials and other compound can be compressed into a disk or slab having a measured thickness than fixed into dielectric cell. Dielectric cell is a test fixture with two adjustable plates in which test sample is fixed for measurement of its electrical behaviour. After connecting the sample to LCR meter capacitance and loss factor can be readout directly and give fast result.

- **Measurements of Solid Materials:** American society for testing and materials (ASTM) and international electrotechnical commission (IEC) have established the methods which are published for measuring dielectric constant and dielectric loss. One method which is easy and require minimum calculation but has little accuracy, is contacting electrode method. Actual measurement involves making the pellet of the powder material and then insert of the test sample in the cell and after insertion electrodes are closed by micrometer until they tightly touch the sample. The spacing of micrometer is recorded for test sample. Value of capacitance C and value of dissipation factor D are measured by LCR meter. Sample is removed from the cell and micrometer is adjusted back to its original position calculation is repeated in air. Impedance measurement on material can be easily performed by using LCR

meter. Insulation properties vary with frequency so instrument has wide range of frequency which is programmable. Accuracy of result can be improved by averaging several measurements and obtained results can be simplified by computer programs. This all result increased efficiency , superior product results and better control over process.

- **Dielectric Constant:** Relative permittivity is also called dielectric constant its measurement is a basic tool for finding insulating behaviour of rubber, plastic and powders. Ability of a material to store electrical energy is find by dielectric constant measurements. Dielectric constant is a ratio of capacitance of a material with the capacitance of air,

$$k' = \frac{C_x}{C_0}$$

C_x represents the capacitance of a material and C_0 represent the capacitance of vacuum. Dielectric constant value of dry air is 1.00053, therefore, a material which is used for insulating material should have low value of dielectric constant or its value needs to be closer to air and for electronic purposes for electrical charge storage a material is used which have high value of dielectric constant. Charge storage will be maximum if more dielectric material is present between the plates of capacitors. Dielectric constant is greater than 1 for any solid or liquid.

Table 1.1: Dielectric constants of common materials.

| Materials | Dielectric constant |
|--------------|---------------------|
| Vacuum | 1.0 |
| Air | 1.0005 |
| Pure Teflon | 2.04 |
| Fused Quartz | 3.78 |
| Water | 78 |

- **Dissipation Factor:** At specific frequency, the ratio of resistance of an insulating material to its capacitive reactance is called dissipation factor. Its value is always greater than 0 and very smaller than dielectric constant. It measures the loss of material and gives an idea

about contamination and deterioration so it is an indication of quality control parameter. Presence of moisture also influence the value of dissipation factor. Purity of epoxy and some raw material also checked by dissipation factor measurement [108-109].

1.2.4. Diffuse Reflectance Spectroscopy (DRS)

In diffuse reflectance spectroscopy, there is no need to make pellets all the material which are not soluble or make suspension in different solvents their band gap is calculated accurately by DRS.

Incident rays are reflected at many angles after falling on the sample. Surfaces like plaster, fibers and polycrystalline materials, reflect light diffusively. Formation of the object image is due to diffused reflection of light [110].

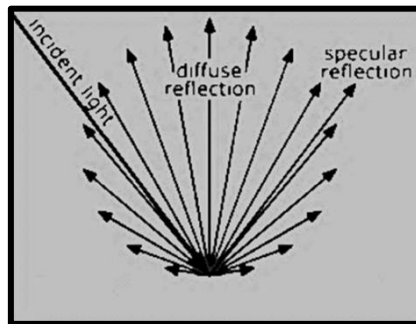


Figure 1.6: Diffuse and specular reflection from glossy surface.

Surfaces of materials are not only responsible for reflection but below the surface of material scattering occurs [109]. Certain materials do not allow diffuse reflection including metals, liquids, gases, glass and transparent plastics, single crystal like gems and salt crystal. In case of glossy paints in homes painting gives specular and diffuse reflection [111].

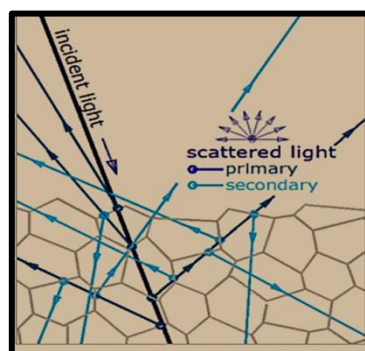


Figure 1.7: General mechanism of diffused reflections by solid surface.

- **Principle of diffuse Reflectance spectroscopy**

DRS principle is similar to that of UV/Visible spectroscopy, in both techniques, visible light is used for electronic excitations. UV/Visible spectroscopy is used to find relative change of transmittance of light when it passes through the solution whereas, DRS is used to find the relative change in the reflected light when it is reflected from the sample surface. If test material has electronic energy levels which are separated by small energy difference which is equal to visible region energy then such material absorb light and undergo electronic transition from valence band to conduction band. Amount of energy in the particular light after absorption is reduced than reference source and % transmittance and reflectance will be reduced.

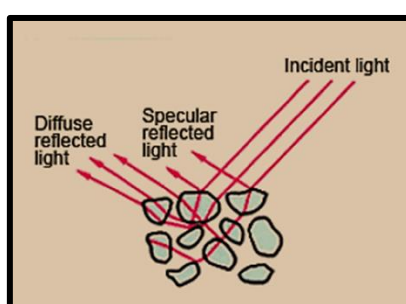


Figure 1.8: Light scattering through powdered sample.

Powder samples which possess particles having random orientation and size, reflect light in different directions. This combined effect of reflection, diffraction, absorption and refraction of

light waves by particles of test sample oriented in different direction and shape is called diffused reflection.

- **Measurement by DRS**

Light can not pass through opaque objects it is reflected back from the surface. In front of incident light window sample is placed. light is falling on the sample and reflected from the sample. Reflected light is move toward detector. This movement of reflected light toward detector is brought about by spheres which are coated with barium sulphate inside. Values obtained for DRS is reflectance of light with reflectance of standard sample which is taken to be 100%. When light directed angle on sample is 0 then specular reflected light exit from the sphere and not detected. In this case only diffuse reflected light is measured.

1.3. Mechanical properties

1.3.1. Hardness

It is property of a material due to which it tends to resist against applied force. Broadly knoop and vicker methods are used for hardness measurement of composites and teeth denture [112-115]. Material hardness is a complex property and is greatly influenced by crystallographic orientation inside the material, applied force and size of the indentation [116-119]. Microscope usually monitors the object surface and indentation of the diamond. Material, used for measurement of hardness, is placed on the stud of the machine and then its image is focused and finally required load for for certain time period is applied and record the digital value. Vickers hardness tester is used for measurement of hardness of a material; it consists of a pyramid shape diamond which is suppressed onto the surface of material during operation. Then length of diagonal is measured from the machine and applied load is also taken from the Vickers hardness tester, formula for hardness calculation is given below [119],

$$Hv = 2F \sin(\theta/2) / d^2$$

This formula indicates that hardness is ratio between applied load and area influencing that load. In this formula, d represents diagonal in mm, sin theta represents angle between opposite faces and Hv is hardness in Vickers number and F is applied load.



Figure 1.9: Micro Vickers hardness tester.

1.3.2. Density

The mass of the substance in unit volume is called its density. It is important parameter for oil analysis. Oil thickness is deduced by density.



Figure 1.10: Specific gravity bottle.

Density is determined by the following formula [120],

$$\text{Density} = m / V$$

1.3.3. Specific gravity

It is heaviness of a material compared to that of water. It is measured by following formula [121]:

$$\text{Specific gravity} = d_1/d_2$$

1.3.4. Viscosity

Most important parameter for lubricating oil analysis is its viscosity. It is thickness and internal friction of the liquid and important parameter for prediction of oil properties. Lubricating oil consist of series of fluid layers that are superimposed above one another and oil viscosity is the measure of resistance produce between the individual layers. High viscosity indicates high resistance to flow and low viscosity offer low resistance to flow. It is inversely related to temperature. pressure and load increases the viscosity of oil. Lubricating oil viscosity is measured in two ways either kinematic or dynamic viscosity [122].

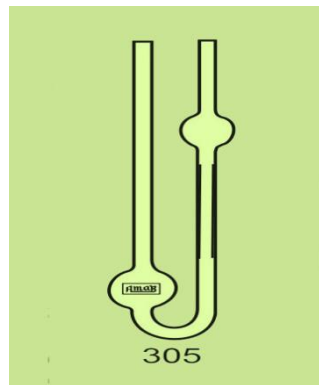


Figure 1.11: Viscometer.

1: Kinematic viscosity

It is resistance to flow and shear due to gravity. It is measured by timing the flow rate and it is ratio of absolute or dynamic viscosity to the density of oil

$$V = \mu/\rho$$

Where V= Kinematic viscosity

μ = Dynamic viscosity

ρ =Density of liquid

2: Dynamic viscosity

It is tangential force per unit area required for the movement of one horizontal plane over the other at unit velocity when a unit distance is maintained between the layers.

1.3.5. Flash point

Flammability of combustible and volatile substances is measured by flash point. This parameter is also important from safety point of view for handling of flammable liquids. It is the minimum temperature at which a substance catches fire in air in the presence of flame. Two standard methods are employed for flash point measurement 1-open cup method and - close cup method. Open cup method gives error so close cup method is widely used for measurement of flash point. It consists of sample holder which is closed and material to be analysed is injected into it by injection. [123-124]. Lubricating oils used in engines and machinery of industries require high flash point in order to avoid fire hazards. Additives in lubricating oil raises the flash point of oil. Motor oils and engine oils have high flash point which prevent the engine from capturing fire.



Figure 1.12: Close cup flash point tester.

1.4. Effect of additives on lubricating oil properties

The high viscosity index, high flash point, corrosion resistance, oxidation resistance and thermal stability are vital quality parameters to evaluate the performance of lubricating oil. A good quality oil, lubricates the engine parts under all operating conditions and remains unchanged and prevents the damage of metal parts. To establish these necessities the operating temperature of system, physical and chemical properties of lubricating oils, all are within the definite limits [125].

1.4.1. Viscosity Index: Viscosity index describes the effect of flow with temperature changes. Lubricating oils having high viscosity index are good for service due to proper lubrication inside the engine at higher temperatures. Whereas, low viscosity index describes poor quality of lubricating oil because it leads to poor wear resistance which consequently

reduce the engine life. Additives of high molecular weight polymers improves the viscosity index of lubricating oils [126-127].

1.4.2. Volatility & Flash Point: Lubricating oils should be of low volatility otherwise can be hazardous. Flash point of lubricating oils in turn is controlled by the volatility. Flash point is the temperature at which vapours produce from the oil mixes with air and form combustible mixture and cause fire. In order to reduce fire hazards which result deterioration of whole system lubricating oils having high flash points are preferred. Lubricants having low flash points easily capture fire it should blended with additives which raise its flash point before application. Scientists are trying to introduce such chemicals which greatly enhance the flash point of the lubricants [128].

1.4.3. Pour point: It is a temperature below which lubricating oil ceases to flow and becomes a gel like wax or in other words it is the lowest temperature at which oil maintains its quality. The pour point of lubricating oil should be low in order to obtain good lubricity. For this purpose pour point depressant additives are added to retard its pour point to ambient conditions at least, e.g. below 10°C. The pour point depressants are certain polymers designed to lower the pour point of lubricating oil. e.g. polymethylmethacrylates PMMA, chlorinated wax, polyacrylates, acrylate styrene copolymers, maleic anhydride etc [129].

1.4.4. Alkalinity: Large number of additives are present in lubricating oil to enhance its performance which in addition enhance the base number of oil. Base number is the quality parameter which measures the amount of basic substances in the oil, relative amount of such substances are measured by using *base number calculation method* by treating the oil with acid. [130]. Failure to keep oil alkaline results in damage to bearing and engine parts due to acidic attacks and increased wear.

1.4.5. Oxidation: The lubricity of engine oil is directly related to its antioxidant property. Antioxdants are added into lubricating oil to retard its oxidation and prevent formation of corrosive substances. The antioxidants are the additive chemicals which are added in lubricating oil to prolong its life by raising oxidative resistance. These chemicals also allow the lubricating oil to function properly at higher temperature otherwise. Antioxidants action is described in two ways they inhibit peroxides and radicals scavenging. Oxidation process is

carried out by formation of reactive free radicals and peroxides, antioxidants retard their propagation these oxidation product result thickening of lubricating oil during service [131-132].

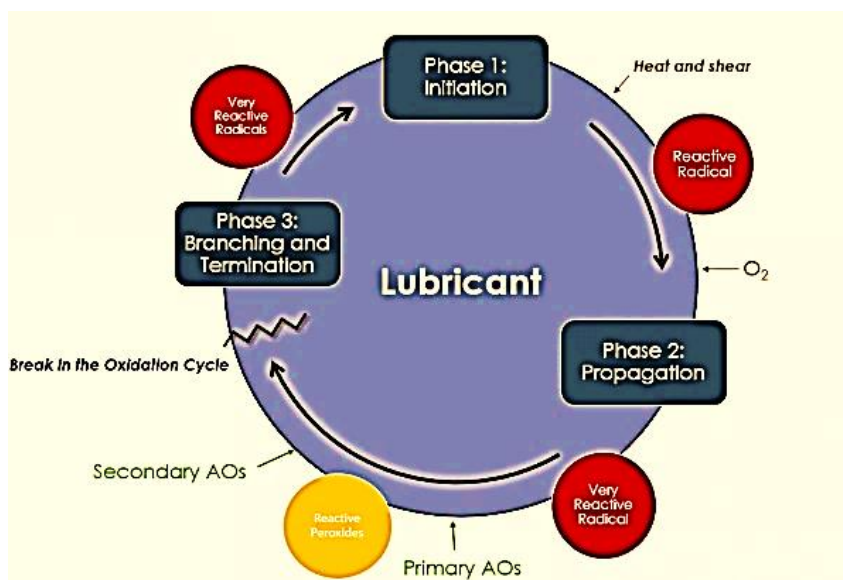


Figure: 1.13: oxidation cycle

Two types of antioxidants are used in lubricating oil primary and secondary antioxidants. primary antioxidants consist of aromatic amines and phenolic substances and secondary antioxidants comprises of phosphites and sulphur containing compounds including thioethers and thioesters. primary antioxidant act as free radical scavengers and secondary retard peroxide propagation.

1.5. Aims and objectives of research

This research work concentrates on synthesis, properties and applications of antimony oxide doped with alkali metal because such doping prompts extra ordinary changes in properties. New method of synthesis was introduced by using cheap precursors. Being a flame retardant material NaSbO_3 , an attempt was made to introduce its little amount into lubricating oil as an additive. And changes produce after addition of sodium antimonates into lubricating oil was observed by mean of measuring quality parameters of lubricating oil and compared with

virgin oil. Quality parameters includes density, specific gravity, viscosity (kinematic, dynamic) , flash point and surface tension. Followings are the aims and objectives of this research project

- To develop the synthesis procedure.
- Try to introduce easily available precursors for synthesis.
- To make the use of NaSbO_3 additives in different products lubricating oils for improved performance.

Chapter 2

Literature Review

2.1. Synthesis of Inorganic Materials

The synthesis of inorganic materials is one of the most important aspect of material sciences. The proper choice of chemical precursor and synthesis technique to obtain a material with desired chemical and physical properties is a challenge for both material scientist and in organic chemist [133]. Large number of elements are reported which are doped into antimony oxide, and the product after doping is called either antimonate or antimonite, depending upon oxidation state of antimony in the compound, e.g., alkali and alkaline earth metals, transition metals and various other elements are doped into antimony oxide following different synthetic routes; hydrothermal, solid state (sintering) methods are emphasized. These methods are widely used for synthesis of metal doped antimony oxide.

(a) Hydrothermal method

The hydrothermal method is a low cost synthesis method and depends on the solubility of materials in hot water under high pressure. The process is carried out in an autoclave in which chemicals along with water are supplied, usually maintaining the temperature below 300°C [134] under pressure.

The advantages of hydrothermal method over other synthesis method because the materials with high vapor pressure near their melting points can be synthesized and the good quality crystals can also be grown by controlling the precursors composition [135].

(b) Solid state reaction

Reactants in stiochemertic ratios are mixed properly in order to increase area of contact between them. After pelletizing the sample, heating at high temperature is carried out followed by keeping it at certain temperature in order to attain the equilibrium [136].

2.2. Alkali Metals Doping in Sb₂O₃

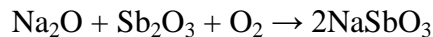
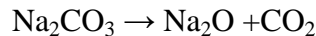
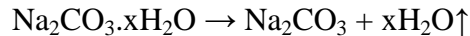
In order to study multipurpose changes in properties of antimony oxide alkali metals are doped into it. doping result into new compound with unique and useful properties. Metals like Li, Na, K, Rb, Cs are doped into antimony oxide and new properties of resultant compounds are studied.

2.2.1. Lithium (Li) Doping

The sodium and lithium antimonate have been synthesized by precipitation method. In 1st step Li[Sb(OH)₆] and Na[Sb(OH)₆] were prepared in the presence of potassium antimonate in the solutions. Dehydration and annealing at 850-1000°C yield sodium and lithium antimonates [10]. There is another report on Synthesis of LiSbO₂ compound in vacuum by continuous heating of Sb₂O₃ and Li₂O mixture in a silver tube covered by quartz tube for 72h [11]. All grindings and weighing were done in glove box under Ar atmosphere. Product structure has been analysed by XRPD and NPD techniques. The structure of LiSbO₂ crystal was monoclinic with the lattice parameters, a = 4.8550, b = 17.857, c = 5.5771Å, β = 90.061°.

2.2.2. Sodium (Na) Doping

Synthesis and crystal structure study of sodium antimonate has been reported by Ramirez *et al.*, the Na₂CO₃ and Sb₂O₃ mixture in 1:1 ratio have been sintered in a platinum crucible at 860°C (±4°C) for 273h in air. The mixture was analyzed in a TGA-DSC thermal analyzer fluxing with air 60 mL/min with heating rate of 10°C/min. The reactions taking place during heating,



Structural and morphological analysis indicated the trigonal geometry of sodium antimonate. SEM analysis indicated a homogenous product only possible after sintering below 750°C [12]. Long *et al.*, synthesize sodium antimonates by chloridizing leaching process following hydrolysis [13]. Chlorine was introduced as a leaching agent and chlorides were formed which upon hydrolysis were converted into oxide form. H₂O₂ was used as an oxidizing agent and final

product was sodium antimonates. Chen *et al.*, worked on effect of particle size on properties of a compound. Synthesis route and controlling precursors amount size of a nanocrystal can be altered [14]. Ultrasonic spray method was used for sodium antimonate synthesis which gives controlled size nanocrystal. Aerosol assisted synthesis followed by adding 15 mL of water in a vial containing sodium antimonyl tartarate (116 mg) and cesium nitrate (780 mg). This suspension was sparged with compressed air at 307 ccm for 30 minutes followed by nebulization. Growing of sodium antimonate crystal was observed and controlled by varying the temperature of furnace. Powder particles were collected in gas bottle filled with water. Centrifugation was done and supernatant was removed. After drying white sodium antimonate was obtained. David J.Stewart *et al.*, worked on structure of sodium antimonates crystal by different methods in order to fix it in pyrochlore type, which was only possible if Na:Sb ratio is less than 1:1.5 [15]. In order to prepare pyrochlore type of crystal structure for sodium antimonates required ratio should be emphasized. When synthesis of metal antimonates involve intermediate compound antimononic acid and that suspension (antimononic acid in water) was treated with excess of sodium salt. The resultant crystal structure will be pyrochlore. All other methods yield ilmenite (FeTiO_3) type crystal structure. $a=5.0884(1)\text{\AA}$ $c=14.0855(4)\text{\AA}$ $V=315.84(1)\text{\AA}^3$ [16].

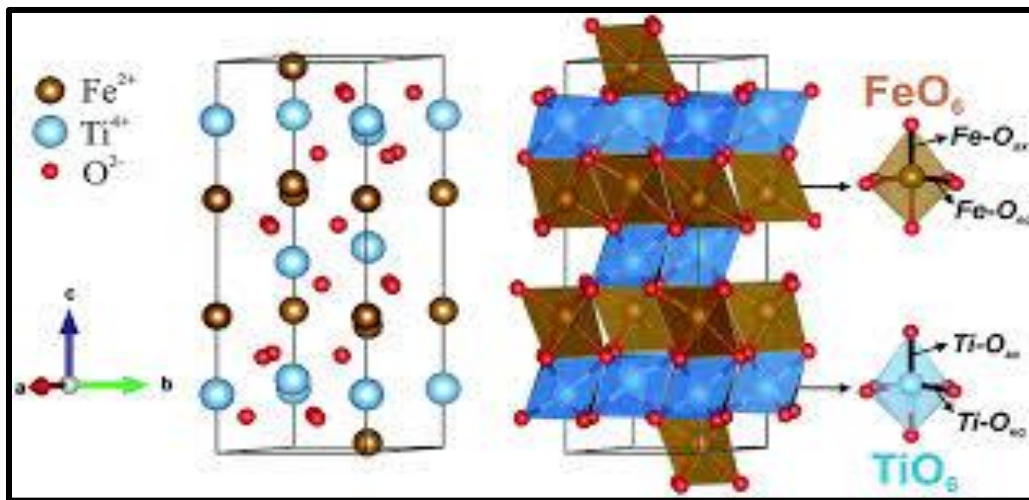


Figure 2.1: Ilmenite type crystal structure FeTiO_3 [17].

The crystal structure of ilmenite is highly ordered with alternating iron layers between the oxygen layers. The oxygen layers are hexagonally packed and each metal ion is bonded to three

oxygen layer above and three oxygen layer below. Synthesis of sodium antimonate has been reported by wet as well as by the dry method. In *wet method* several filterations were performed on the mixture of SbCl_5 and crushed ice until clear filterate was obtained. Precipitates were washed with cold water for many time. In order to get rid of Cl^- ions, washing with AgNO_3 solution has been performed. After drying at room temperature, distilled water was added into antimonite acid precipitates. The metal salt (carbonate, oxalate, nitrate or acetate) was added then along with the continuous shaking and boiling for many hours it produced crystalline sodium antimonates. While in dry method, the mixture of Sb_2O_3 or antimonite acid and metal salt (carbonate, oxalate, nitrate or acetate) was ground. This mixture was exposed to firing in an alumina crucible for many times. The mass deficit was estimated after each firing by weighing the sample. Sodium antimonate with ilmenite type crystalline structure was obtained. Waring *et al.*, constructed phase diagram for $\text{Sb}_2\text{O}_4 \leftrightarrow \text{NaSbO}_3$ system [18]. For this purpose sodium antimonate was prepared by oxidizing high purity antimony metal powder on platinum setter at elevated temperature in air. After 450°C there was formation of oxide coating on metal which stop further reaction of antimony with platinum. Mixture of Sb_2O_4 with sodium carbonate was prepared followed by its crushing. Mixture was placed on setter fabricated from platinum foil and calcined in air at 700°C for 60 h and again at 500°C for 60 h. Babkenovich studied exchange reactions of sodium antimonates by placing the ground mixture of NaNO_3 , Na_2CO_3 and Sb_2O_3 at 500°C for an hour followed by regrinding and calcination at 850°C for 2h [19]. The chemical and XRD analysis confirmed it as NaSbO_3 later it was treated with molten nitrates in order to check its ion exchange reaction.

2.2.3. Potassium (K) Doping

Brower *et al.*, synthesized ilmenite (FeTiO_3 structure type) type potassium antimonate by using 1:1 mixture of K_2CO_3 and Sb_2O_4 in platinum crucible by heating at 100°C for 1 month [20]. The same reactants yield body centered cubic potassium antimonate upon hot pressing at 800°C and 20 Kbar pressure for 5 min.

2.2.4. Rubidium (Rb) Doping

Kasenova Sh.B *et al.*, studied heat capacity of rubidium antimonites at 673 K which was prepared by reacting rubidium carbonates with antimony oxide [21]. Characterization was done

by XRD. Govindaraasan kalpana and weller reported the synthesis of rubidium antimonite single crystal by flux method [22]. Mixture of Rb_2CO_3 , Sb_2O_3 and H_3BO_3 after grinding was subjected to the heat treatment in different steps; 1st heated slowly and kept at 773 K for 12h, for next 12h at 923 K then adjusted at 1273 K for 24h and finally furnace was adjusted to room temperature. After 48 hour cooling, the melt was washed with hot water to remove excess of boric acid followed by filtration and drying in an oven at 353 K. The colorless nanocrystals of rubidium antimonate were obtained having monoclinic structure with the parameters; $a=19.504(11)$, $b=7.5681(4)$, $c=7.2115(4)$ Å and $\beta=95.203^\circ$ (3) revealed through X-ray single crystal and SEM analysis.

2.3. Alkaline Earth Metal Doping in Sb_2O_3

2.3.1. Magnesium (Mg) Doping

Brian Mason and Charles reported 1st time on crystal structure and properties of the mineral bystromite (MgSb_2O_6) and also compared it with the synthetic magnesium antimonate [23]. It was synthesized by heating MgO and Sb_2O_3 in air at 1000°C for 18 h. The lattice parameters were found the same for both the synthetic and natural MgSb_2O_6 compounds; $a=4.68$, $c=9.21$ and $c/a=1.968$ Å in space group $P4/mnm$, with $Z=2$.

2.3.2. Calcium (Ca) Doping

Barry Gdboer reported the results of an extensive work on structural analysis of Ca, Sr and Ba antimonates. Calcium meta antimonates were prepared from concentrated solution of $\text{Ca}(\text{NO}_3)_2$ in minimum amount of hot distilled water in a fused silica boat. Stirring was done by adding 50% Sb_2O_3 then this mud was dried at 378K for few h. Temperature was 773K for 1st hour until water and NO_2 will evolve meanwhile oxidation from Sb^{+3} to Sb^{+5} took place. The sample was kept at 1473K until white smoke of Sb_2O_4 finishes, boat (the sample holder) gets crack during cooling and calcium antimonate was obtained, XRD characterization revealed the following data, $a=5.2405(4)$, $c=5.0221(4)$ Å, $V=119.45(2)$ Å³ [24]. The electrical conductivity of calcium antimonates has been reported by Zyryanov *et al.*, synthesized by mechanochemical method. The fine ground mixture of CaO , Sb_2O_3 , and Bi_2O_3 was fired in open air to oxidize, followed by leaching in 1N HCl. The product obtained was CaSb_2O_6 and CaSb_4O_7 , only calcium passed into

the solution with some antimony oxide. Chemical analysis, XRD and thermal analysis in argon atmosphere (DTA+TG) revealed the structure of the compound, $(\text{Ca}_{0.82} \text{Sb}^{+3}_{0.18}) \text{Sb}^{+5}_{1.68} \text{O}_{5.29}$ with the lattice parameters, $a=5.238 \text{ \AA}$, $c=5.013 \text{ \AA}$. The synthesis of nanostructured calcium antimonite has also been reported by hydrothermal method in recent years [25]. Huang *et al.*, synthesized nanocrystalline calcium antimonite by hydrothermal method, using $\text{Ca}(\text{CH}_3\text{COO})_2 \cdot \text{H}_2\text{O}$ (0.441g, 2.5 mmol) and Sb_2O_5 (0.809 g, 2.5 mmol) were used as starting materials, mixed in 12 mL deionized water. After maintaining the pH of the solution by HNO_3 and NaOH , the mixture was loaded into 23 mL Teflon lined autoclave which was filled with 14 mL deionized water and sealed, maintained at 180°C for 48h. After 48h mixture was cooled down filtered and washed many times with deionized water and absolute alcohol followed by drying in air. Different samples of $\text{Ca}_2\text{Sb}_2\text{O}_7$ and $\text{Ca}_2\text{Sb}_2\text{O}_5$ have been prepared from pH value 1 to 14. pH changes effect the ratio of Ca and Sb in compound [26]. The pressure also influence the crystal structure of metal antimonates, Chelazzi *et al.*, reported the effect of high pressure on crystal structure of calcium antimonate. Calcium antimonate single crystals have been obtained by heating the CaCO_3 , MnO and Sb_2O_3 ground mixture at 1100°C for 30 days in air in Pt crucible. The calcium antimonate ($\text{Ca}_2\text{Sb}_2\text{O}_7$) crystals of $300 \mu\text{m}$ have been obtained as a result of little addition of $\text{Na}_2\text{B}_4\text{O}_7$. The high pressure X-ray diffraction gave $a=7.2818(4)$ $b=10.1839(5)$ $c=7.4467(4) \text{ \AA}$ $V=542.23(9) \text{ \AA}^3$ [27]. Cornelis *et al.*, compared the romeite ($\text{Ca}_2\text{Sb}_2\text{O}_7$) [naturally occurring calcium antimonates are called romeites] and the synthetic calcium antimonate [28]. The synthetic calcium antimonate has been prepared by mixing $\text{KSb}(\text{OH})_6$ 0.01M and $\text{Ca}(\text{NO}_3)_2 \cdot 9\text{H}_2\text{O}$ 0.005 M solutions in order to get a suspension, which was stirred for 24 h followed by aging at 60°C . Such suspension mixture gave Ca:Sb molar ratio as 1:2. $\text{Ca}[\text{Sb}(\text{OH})_6]_2$ was precipitated from this suspension at the $\text{pH}=6.5$, different samples were prepared by changing the pH of the suspension and amount of $\text{KSb}(\text{OH})_6$. The rietveld refinement of XRD data revealed the similarity between natural and synthesized romeites with formula $\text{Ca}_{1+x}\text{Sb}_2\text{O}_6\text{OH}_{2-2x}$.

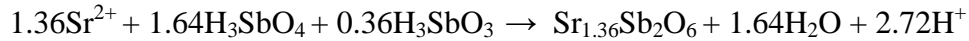
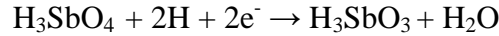
2.3.3. Barium (Ba) Doping

Geng *et al.*, synthesized barium antimonate single crystals by hydrothermal method by using KCl , 2 mmol Sb_2O_3 and 1 mmol $\text{Ba}(\text{OH})_2 \cdot 8\text{H}_2\text{O}$ in water. The Teflon lined autoclave was heated to 190°C for 4d followed by sample cooling. Product was filtered and washed with DI water in

ultrasonic bath. Two type of barium antimonates crystals different SbO_2 ratios were obtained; the pale brown $\text{Ba}_2\text{Sb}_7\text{O}_{13}(\text{OH})$ and the colorless $\text{BaSb}_3\text{O}_5(\text{OH})$ crystals. Addition of 10% more $\text{Ba}(\text{OH})_2 \cdot 8\text{H}_2\text{O}$ and introduction of KCl salts as a mineralizer has increased the pale brown product $\text{Ba}_2\text{Sb}_7\text{O}_{13}(\text{OH})$. The yield gets maximum at the precursor ratios $\text{Sb}_2\text{O}_3/\text{Ba}(\text{OH})_2 \cdot 8\text{H}_2\text{O}/\text{KCl}$ was 1.4:1:0.8 at 190°C [29].

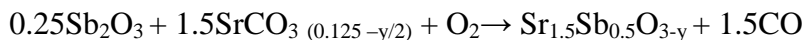
2.3.4. Strontium (Sr) Doping

Hun Xue *et al.*, reported synthesis of strontium antimonate nanocrystals by hydrothermal method from a solution of 0.88 gm $\text{Sr}(\text{CH}_3\text{COO})_2 \cdot 0.5\text{H}_2\text{O}$ and 0.9 gm Sb_2O_5 in 70 mL deionized water at different pH values. After pH adjustment with help of HNO_3 and NaOH samples were placed in a Teflon lined autoclave at 180°C for 48 h, following reaction occurred during heating .



The precipitates obtained after this operation were washed for many time with dist water and alcohol and dried in air at 80°C . The PXRD and SEM analysis indicated nanooctahedral structure of $\text{Sr}_{1.36}\text{Sb}_2\text{O}_6$, and octahedrons with diameters 40 –120 nm [30]. Recently, a new structure type for strontium doped antimony oxide by hydrothermal method was reported for $\text{Sr}_5\text{Sb}_{22}\text{O}_{38}$ [31]. The synthesis was carried out by the precursors; 0.1458g (0.5 mmol) of Sb_2O_3 , 0.0797g (0.3 mmol) $\text{Sr}(\text{OH})_2 \cdot 8\text{H}_2\text{O}$ and 0.0058g (0.1 mmol) KF in a Teflon lined autoclave at 190°C for 4d use water as solvent. After 4 d of heating, block shaped crystals of $\text{Sr}_5\text{Sb}_{22}\text{O}_{38}$ were obtained by cooling the mixture to room temperature then filtered and washed with DI water many time. The X-ray single crystal studies revealed the monoclinic crystal structure with lattice parameters; $a=11.739(9)$, $b= 12.014(10)$, $c=16.412(13)$ Å, $\beta =91.460^\circ(8)$ and $V =2314.0(3)$ Å³. The analysis through SEM confirmed the single crystal elemental ratios $\text{Sb}_2\text{O}_3/\text{Sr}(\text{OH})_2 \cdot 8\text{H}_2\text{O}/\text{KF}= 2.2:1:0.2$. A cubic structures for Sr doped antimony oxide compound $\text{Sr}(\text{Sr}_{0.5}\text{Sb}_{0.5})\text{O}_{3-y}$ was also reported [32]. The ceramic method was used for the synthesis (ceramic method involve mixing of powder chemical precursor with water and then pre firing in order to hard the mixture) of $\text{Sr}(\text{Sr}_{0.5}\text{Sb}_{0.5})\text{O}_{3-y}$. The mixture of high purity Sb_2O_3 and SrCO_3 was

fired at 900°C for 24 h after grinding. After firing powder was again ground, pelletized and sintered at 1200°C for 48 h, the solid-state reaction expressed as,



2.4 Transition metals doped antimony oxide

2.4.1 Sc doped antimony oxide: Sc doped Antimony oxide, the ScSbO compound was reported to obtain by solid state reaction between Sc(NO₃) and the Sb₂O₃. At 1st metallic scandium was dissolved into the nitric acid in order to obtain the scandium nitrates upon evaporation to dryness. The scandium nitrate and antimony oxide were than crushed, mixed and compacted in an equimolar ratio followed by heating slowly upto 500°C in order to get oxidized product. After the oxidization that mixture was cooled ground and compacted again and heated in an oxidizing atmosphere for 8h at 750-850°C than for next 20h at 1000°C. The final product was single phase ScSbO rutile type crystal structure with Sb ion is +5 oxidation state characterized by PXRD. The PXRD analysis also revealed that the reaction between ScO and SbO started at 950°C and completed at 1050°C XRD analysis confirm the crystal structure [33].

2.4.2 Ti doped antimony oxide: Synthetic inorganic ion exchange material got remarkable significance due to high stability and strong resistance toward high level of radiation [34]. Oxides and hydroxide of zirconium [35-36] antimony [37-39], titanium [40] and manganese [41] [42] were studied for ion exchange materials. M.abe and Ito were the first who studied antimonate of Sn and after synthesizing Sn antimonate they discover its ion exchange capability [43]. Ti doped antimony oxides are important as an ion exchange materials. M.abe synthesized Ti antimonate for this purpose from 4M (aq) SbCl₅ and 120 cm₃ of 4M (aq) TiCl₄ were mixed at 60°C followed by an immediate addition of 5dm³ DI water. And then with 960mL demineralized water at same temperature. The white precipitates obtained, were allowed to stand overnight in mother solution at 60°C, then filtered and washed with demineralized water through centrifuge @ 10,000 rpm until the pH of solution become higher than 1.5. The product was dried at 60°C for 4d then grounded and sieved through mesh size 100-200. Re washing was performed with demineralized water remove any adherent particle then precipitate were treated with 1M HNO₃ to remove chloride ion then again washed with demineralized water and finally dried at room

temperature. Thermal analysis and XRD were done and result was $a = 4.66 \text{ \AA}$ $c = 2.97 \text{ \AA}$. Another group of scientists also has reported the Ion exchange properties of titanium antimonates they have synthesized it by prehydrolysing SbCl_5 in water and then mixing it with TiCl_4 . Different ratio of antimony and titanium salts were used to prepare 5 mixtures. The XRD analysis indicated poor rutile type crystal structure ($a=4.593 \text{ \AA}$, $c=2.959 \text{ \AA}$ space group P42/mnm) [44].

Antimonates show unusual properties when compared with phosphate, molybdate, arsenate and tungstate. They also act as an inorganic ion exchange material and large number of scientists worked on inorganic ion exchangers [45]. M. Qureshi and V. Kumar did experiment to study ion exchange capacity of titanium antimonates. For this purpose they synthesized titanium antimonate by mixing 0.1 M TiCl_3 and 0.1 M SbCl_5 solutions in the volume ratio 1:1. Then liquid NH_3 was added dropwise with constant stirring till the required pH was attained. White ppt obtained after 24 h stirring at room temperature. After washing by decantation and filtration, drying was done at 40°C . This dried material cracks into small particles when sat in water. Addition of 2M HNO_3 converted this material into hydrogen form which was washed with demineralized water and dried at 40°C . After drying, sieving operation was done with 100-200 mesh size. After sieving material was ready for column operation to study its ion exchange properties [46]. Antimonates of titanium synthesized by this method capture many hydrogen ions in its structure during nitric acid treatment which were responsible for its ion exchange ability.

TiO_2 exists naturally in three crystalline phases, rutile, anatase and brookite. Out of these rutile type phase is thermodynamically stable one, possess smaller band gap energy than its other polymorphs. Anatase and brookite are metastable [47]. Rutile is a mineral composed primarily of titanium dioxide TiO_2 [48].

XRD analysis indicated the following result for rutile type crystal structure with lattice parameters; $a=0.4594\text{nm}$ $c=0.29589\text{nm}$, cell volume = 0.0624 nm^3

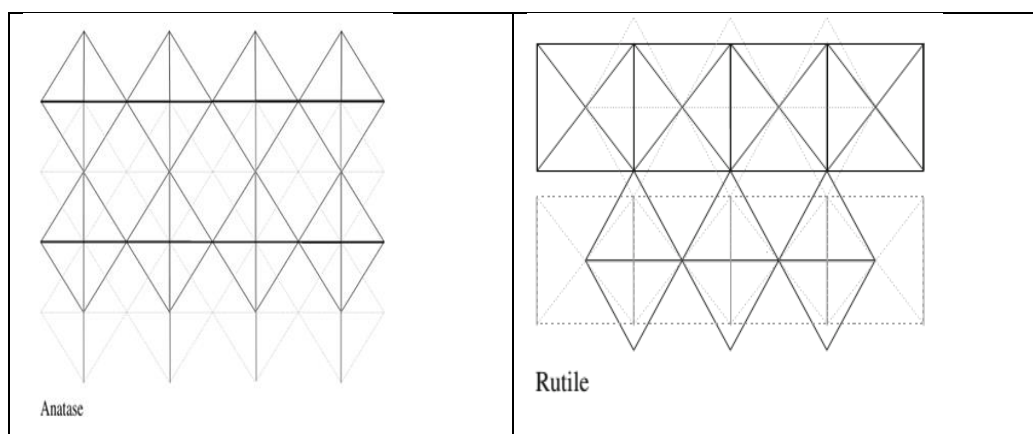


Figure:2.2: represent Anatase and rutile phase of titanium oxide.

F.J berry et al, worked on shear planes formation when a crystalline materials was doped into another crystalline material. They reported shear planes and twin boundaries formation when SbCl_5 was doped with rutile type of TiO_2 . For this purpose antimony oxide doped with titanium was synthesized by calcination method. Mixture of SbCl_5 and TiCl_4 solution was stabilized by addition of ammonia and HCl for pH maintenance. Then mixture was filtered, precipitated and washed. After washing material was calcined in air at 1000°C for 1 day. Characterization was performed after calcination by XRD, which indicated the lattice parameters; $a = b = 4.598(3)\text{\AA}$, $c = 2.968(3)\text{\AA}$ [49].

2.4.3 Vanadium doping in antimony oxide

Frank et al, in 1983 synthesized antimony oxide doped with vanadium by reacting the respective oxides [50] Composition and structural properties of V-Sb oxide synthesized by three different routes were studied by Taufiq et al, following XRD, FTIR and BET analysis. VSbO is used as a catalyst for ammoxidation of propane to acrylonitrile it converts propane into propene [51-52]. For a long time propene is used as a starting material for acrylonitrile synthesis, but now a days an attempt was made to prepare acrylonitrile from propane. For this purpose VSbO was used as a catalyst which play its good part for synthesis of acrylonitrile. Three methods of VSbO synthesis were followed.

- (i) Deposition on Antimonic Acid (DAA) Method.
- (ii) Sol-Gel (GS) Method.

(iii) Solid State Reaction (SS) Method [53].

(i). **Deposition on antimonite acid:** H_2O_2 solution was prepared by mixing 30% of H_2O_2 in water and this aqueous mixture was placed in ice bath then SbCl_5 was added into it. This mixture was aged for 6 hour in ice bath. Light yellow ppt of antimonite acid were produced. After filtration ppt were washed with distilled water and drying operation were carried out at 120°C overnight. V_2O_5 solution was prepared in water with oxalic acid addition and 3 hour boiling to maintain V in +4 oxidation state. Antimonite acid was added into V_2O_5 solution. The solution was refluxed for 3 hours with continuous stirring. After evaporation of water obtained solid was grinded and dried at 120°C for 1 night. Sb/V ratio was =3 and mixture was calcined at 700°C For 3 h.

(ii). **Sol gel method:** Aqueous solution of 30% H_2O_2 was added slowly into another solution of V_2O_5 in 300ml water placed in ice bath. Solution was continuously stirred for 2 hour on ice bath. After 2h solution was heated upto 100°C with stirring and refluxing. Then Sb_2O_3 was added into that solution until solution become viscous and desired ratio of Sb/V was obtained. Solution turns into dark green then again this solution was stirred and refluxed for 3h. After this operation water was evaporated by hot plate and product was dried at 120°C for 1 night. Sb/V ratio was=2. Then mixture was calcined for 3h at 600°C .

(iii) **Solid State Reaction (SS) Method:** V_2O_5 and Sb_2O_3 separately grinded and after grinding mixed together. Time was required to obtain the homogeneity of mixture. After mixing the mixture was calcined at 500°C for 3 hours. Sb/V ratio was =1. Commercial Li ion batteries used carbon as anode material. Morales et al did extensive research to introduce a substitute of carbon anode in lithium ion batteries. Antimony based intermetallic compound capture the attention of researchers to used these compound as an anodic material. Electrochemical properties of nanometric vanadium antimonite was studied for battery anode. Synthesis involved fine grinding of V_2O_5 and Sb_2O_3 in 1:20 ratio. The mixture was ball milled in air using stainless steel vials (250 ml) and ball size 20mm for 70h at 200 rpm. Characterization was carried out by XRD, TEM and Mossbauer spectroscopy (MS) [54].

Sundana in 1984 studied the redox properties of compound having binary oxide system V_2O_5 - Sb_2O_3 . Solid state reaction at high temperature was carried out to synthesize VSbO. Equal weight of powdered V_2O_5 and Sb_2O_3 were mixed and introduced into a quartz tube in open air and temperature was gradually raise to 900°C . Then the product was water quenched to room

temperature which was black flowing crystalline powder. Characterization with XRD revealed the tetragonal unit cell with $a = 4.60 \text{ \AA}$, $c = 3.02 \text{ \AA}$ lattice parameters. ESR study indicated V^{+4} oxidation state act as impurity in VSbO structure [55].

Doping of different metals in antimony oxide has profound effect on its structural chemistry and properties. This change in properties of $\beta\text{-Sb}_2\text{O}_4$ when small quantity of dopant metal was added studied by Raymond and his colleagues. Synthesis involve coprecipitation method or sintering method. In 1st method Sb_2O_5 sol was prepared from Sb_2O_3 or Sb_2O_4 . NH_4VO_3 was dissolved in water then Sb sol was coprecipitated with ammonium vandate then evaporation and denitrification was done. 2ND method of synthesis of vanadium doped antimony oxide involve grinding of both oxide then firing at temperature 800°C . Characterization through XRD, SEM and neutron diffraction was carried out. Vanadium antimonate possess a rutile type structure with space group $P4_2/mnm$ and lattice paramerters; $a=4.6321(2)\text{ \AA}$ $c= 3.0355(2)\text{ \AA}$ $V= 65.12(1)\text{ \AA}_3$. [56].

Ballarini et al, studied the catalytic activity of VSbO prepared from two different methods for ammoxidation of alkane to acrylonitrile. Two methods of VSbO synthesis were mechanochemical method which involve ball milling and coprecipitation method. Catalyst obtained by the both methods were characterized by XRD, BET, FTIR and TGA. Result indicated that co precipitation method yield highly active catalyst for ammoxidation of propane. In coprecipitation method $\text{VO}(\text{acac})_2$ and SbCl_5 (V/Sb ratio=1) was dissolved in absolute alcohol. The pH 7 was maintained by adding buffer solution the precipitate was separated from the supernatant by centrifugation, and then filtration was carried out. Precipitates obtained were dried at 140°C for 1 night and finally calcined by gradually increasing the temperature from 300°C , 450°C , 550°C and was 700°C . Mechanochemical method involve mixing of V_2O_5 and Sb_2O_3 in anticipated proportion ($V/\text{Sb} = 1$ at. ratio). Then mixture was placed into vessel in which stainless steel sphere were present the ratio of stainless steel sphere and metal oxide sphere was =20/1. Milling was done to sample for 70 hour and finally this sample was calcined at 700°C . Characterization was done by XRD, BET and FTIR techniques. Catalytic test for propane ammoxidation was also carried out. Catalyst prepared by mechanochemical method has small crystallite size and large morphological defect and in this type of synthesis compound show rutile type structure. Sample prepared by coprecipitation method do not show high catalytic activity toward ammoxidation of propane [57].

The effect of preparation method of VSbO catalyst on ammoxidation of propane has been revealed by Gabrielli et al. The VSbO has been synthesized by four different methods and their catalytic behavior has been studied. During catalytic reaction V was reduced from its +5 to +4 oxidation state and the compound formed was V_2O_4 . Antimony in its +5 oxidation state on surface of vanadium antimonate was highly active to catalyse the ammoxidation of propane to acrylonitrile. V reoxidize the Sb and play effective role in catalytic ammoxidation. Method of synthesis involve solid state reaction, sol gel method and redox reaction in solution method.

i. Solid state reaction: This method involves mechanical mixing and grinding of V_2O_5 and Sb_2O_3 samples. Mixing involved the maintenance of Sb:V as 1:3. After mixing calcination was done with mixture at 400°C for 6 h then at 600°C for 3h. In order to enhance the possibility of happening of solid state reaction between two oxide the mixture during calcination was recurrently taken out from oven and ground and mixed. After this step small portion of calcined sample was re calcined at 750°C or 850°C for 3 h.

ii. Redox reaction in solution: Slurry method for the preparation of VSbO was already reported in patents [58-59]. VSbO preparation involves refluxing of NH_4VO_3 solution with Sb_2O_3 for 8h then solvent evaporation was done in a rotavapour following drying at 100°C for 1 night. Solid after drying undergone heat treatment at 350°C for 4 hour then 500°C for 6 hour in the presence of air or vacuum at pressure 10^{-3} torr. When heat treatment was completed the sample was ground and mixed then calcined at 600°C for 2 h then 850°C for 2 h.

ii. Sol gel: Sol gel method used for VSbO synthesis was similar to those reported in patents. [60-61]. 30% aqueous H_2O_2 solution was added into V_2O_5 solution. Mono peroxovanadium ion will form in the reaction vessel. Continuous stirring was done for 2 h which resulted formation of a sol. When stirring was continued for 16 hours the sol was converted into gel. Then Sb_2O_3 was added into the gel in such a quantity to attains desired ratio of Sb/V. Little quantity of water was also added in order to reduce the viscosity of mixture then solution was refluxed with stirring for 3 h. After water evaporated through heating on hot plate, drying was done at 110°C for 1 night. After drying the solid was crushed and calcined.

iv. Coprecipitation: $SbCl_5$ was added into 10% H_2O_2 solution at 0°C. After filtration the solid was dried at 110°C. V_2O_5 solution was prepared by reducing V^{+5} into V^{+4} by addition of oxalic

acid at 100°C. Then antimony oxide was added into it final ratio of Sb/V was 1-3. Slurry was refluxed and stirred for 3h. Then evaporation remove the water and resulted solid was dried at 110°C. After drying calcination was done.

2.4.4 Doping of Cr in Sb₃O: The ion exchange properties of antimonates with different metals as an ion exchange material has been studied by J. Mathew et al, For this purpose chromium antimonate was synthesized. Synthesis of chromium antimonate involved precipitation method using CrCl₃ and H₂K₂O₇Sb₂ precursors. Antimonic acid was prepared by potassium pyroantimonate solution [62].

2.4.5 Doping of Mn in antimony oxide: Subramanian et al synthesized Mn₂Sb₂O₇ compound by using MnCO₃ and Sb₂O₃ as a starting material. Both chemicals were thoroughly milled in the presence of CCl₄ which was added to enhance contact points during grinding in 1:1 ratio. After grinding mixture was dried to evaporate the CCl₄ then pelletized. The pellet was fired in air on Pt foil at 1100°C for 72h.. The first compound that was formed MnSb₂O₃ at 950°C and the reaction was completed after 72h heating. Samples were weighed during firing operation in order to check the occurrence of chemical reaction by losing of elements during evaporation. Characterization involve XRD analysis which indicated trigonal structure in space group= p3₁21 with lattice parameters; a=7.191(1) c=17.398(1)Å for the Mn₂Sb₂O₇ compound [63-64]. In this paper the crystal structure of the compound reported was distorted pyrochlore

Table 2.1: Product of solid state reaction of Mn₂CO₃ with Sb₂O₃ at different temperature.

| Temperature (°C) | Reaction time (hr) | Reaction products |
|------------------|--------------------|--|
| 600 | 24 | Mn ₂ O ₃ + γ-Sb ₂ O ₄ |
| 900 | 24 | Mn ₂ O ₃ + γ-MnSb ₂ O ₆ |
| 950 | 24 | Mn ₂ O ₃ +Mn ₂ Sb ₂ O ₇ +γ-MnSb ₂ O ₆ |
| 950 | 96 | Mn ₂ Sb ₂ O ₇ +γ-MnSb ₂ O ₆ + unidentified phase |
| 1100 | 72 | Mn ₂ Sb ₂ O ₇ |
| 1200 | 24 | Mn ₂ Sb ₂ O ₇ |
| 1250 | 24 | Mn ₂ Sb ₂ O ₇ + unidentified phase |

A new crystal structure of MnSb₂O₆ has been reported by Vincent et al with hexagonal symmetry. According to previously reported work the crystal structure of manganese doped

antimony oxide was orthorhombic, distorted pyrochlore and tetragonal etc. [63]. Synthesis involved heating of Mn_2O_3 and Sb_2O_3 mixture in different steps for 24h in ratio 2:5 and 5:2.

Then in next step sample was heated slowly 700-1200°C. Specimen obtained after heating at 1000°C, and 1200°C were analysed by XRD, SEM and thermogravimetry, lattice parameters, $a = 8.8056(1)$, $c=4.7232(1)\text{\AA}$ for hexagonal symmetry. Single crystal was also prepared by mixing and grinding Mn_2O_3 and Sb_2O_3 in ratio 2:5 and the obtained mixture weight was almost 5g. Then mixture was pelletized under the pressure of 5 ton at room temperature in 5mm diameter pellet. The pellet was heated on platinum foil for 24h at different temperatures. Temperature ranges from 700, 800, 900 and 1000°C. There were no intermediate grinding after 24 h annealing sample was quenched to room temperature. The single crystals obtained were needle shaped showing a little hexagonal section [65].

Subramanean et al, synthesized $\text{Mn}_2\text{Sb}_2\text{O}_7$ by following solid state reaction and determined the crystal structure by employing the MnCO_3 and Sb_2O_3 and CdO presursors. After fine grinding heating was done in platinum crucible for 6h at 600- 900°C. At 600°C MnCO_3 was decomposed and at 900°C Sb_2O_3 was oxidized to Sb_2O_5 . Samples were again ground then sealed to platinum tubes and heated at 1100°C for 20h. XRD, Mossbauer spectroscopy and chemical analysis characterize the product. XRD indicated that $\text{Mn}_2\text{Sb}_2\text{O}_7$ has rhombohedrally distorted pyrochlore structure. Electrical study revealed that compound as an insulator [63].

2.4.6 Doping of Fe in antimony oxide: Synthesis of FeSbO_4 was carried out by adding the aqueous solution of $\text{Fe}(\text{NO}_3)_3$ into Sb sol. Then this mixture was heated and stirred to drying and firing for 3 h at 425°C. XRD and NDA indicated the presence of two phases in the reaction product; the FeSbO_4 and Sb_2O_4 . FeSbO_4 found to be in space group= P_{42_1}/mnm , $a=4.6365(6)$ $b=4.6365(6)$ $c=3.0742(6)\text{\AA}$, $V=66.09 \text{\AA}^3$ [66]. Synthesis of iron antimonite involved heating of Sb_2O_3 and $\alpha\text{-Fe}_2\text{O}_3$ at 925°C in air. XRD and Mossbauer spectroscopy revealed magnetic ordering at temperature ranges from 42.5 to 45 K [67].

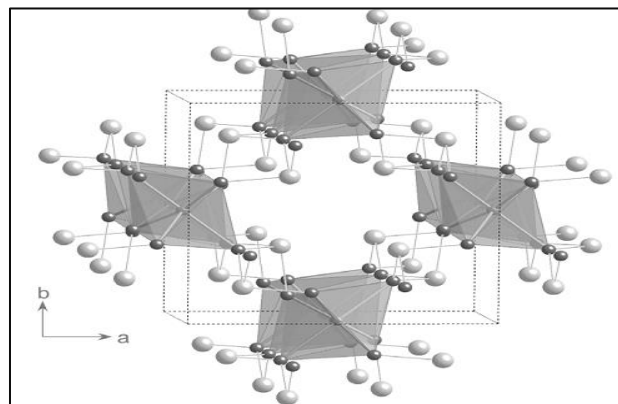


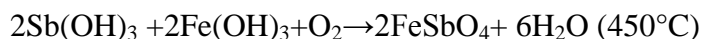
Figure 2.3: Structure of $FeSb_2O_4$ shaded octahedral are Fe^{+2} ion located within O ion are (black sphere) and Sb (white) .

Now a days inorganic Ion exchange material get special attention due to their unique properties like thermal stability and selectivity etc. Iron(iii) antimonates was also studied. In order to ensure exchanging property, Rawat et al, worked on iron antimonates. For this purpose they synthesize $FeSbO$ by using salts of $Fe(NO_3)_3$ and $SbCl_5$. While the Antimony pentachloride was diluted with 4M HCl. Solutions of 0.1 M iron antimonate and antimony pentachloride were mixed and pH was adjusted by adding NH_3 solution dropwise the the Fe/Sb ratio 2:1 was maintained. The solution was aged for 24 h then the product was filtered, washed with demineralized water at pH=6 and dried at $100^\circ C$. After drying the ppts were immersed in water when ppt make contact with water they were broken down. The sample was dried at $40^\circ C$ the ppt were converted to H^+ form. By changing pH value different sample has been synthesized and their ion exchange property have been measured. Ion exchange ability of compound synthesized at lower pH was higher than those samples which were synthesize at higher pH [68].

The $FeSbO_4$ nanoparticles have been synthesized by following sonochemical method [Paratnu]. The 0.2 M solutions of $Fe(NO_3)_3$ nonahydrate and Sb_2O_3 were prepared in slightly acidic solution. After mixing both the solutions the mixture was sonicated for 30 min with gradual addition of dropwise NH_3 until pH = 9-10 and precipitation was completed. Sonication was continued for 0.5h then cooled to room temperature. Brown ppt were obtained after cooling. Solution was centrifuged and ppt obtained after filtration were washed with distilled water and acetone for many times. Precipitates after washing were dried in air, ground and calcined at

300/450°C for 6h in air. XRD analysis indicated rutile type of phase for FeSbO₄ nanoparticle whereas XPS analysis indicated proper valence of Sb⁺⁵ and Fe⁺³ in nanoparticles [69]. Satyendra et al, did researches on LPG gas sensing material using FeSbO₄ the Synthesis involved sol gel and spin coating method. 0.1M solution of FeCl₃ and SbCl₃ were prepared in alcohol by continuous stirring of 6h at 50°C. Both gel after 6h stirring were mixed properly into each other and the solution after mixing was refluxed at 50°C for 6h in rotary vacuum evaporator. Then precipitation of iron and antimony hydroxide take place after drop wise addition of NH₄OH with continuous stirring. Precipitates after filtration annealed at 450°C. Resultant compound was FeSbO₄. Chemical reactions taking place are following

Ethanol solution of (FeCl₃+SbCl₃) → ppt.of Fe and Sb hydroxides(NH₄OH dropwise)



XRD suggested much smaller particle size of FeSbO₄. Single phase of FeSbO₄ obtained at 450°C annealing due to high diffusion rate of chemicals. The material has tetragonal crystal structure and lattice parameter were a=b=4.5820 and c=3.0854Å (P 42/mnm space group) [70].

The FeSbO₄ nanorods were synthesized by solid state reaction method followed by the ball milling. Dry milling was done with measured quantity of Sb₂O₅ and β-FeCOOH at 300r/min for 6h in PTEF vial. After milling the mixture was heated from 700- 900°C for 6h in air at the rate of 10°C/min. Structure characterization was done by PXRD and elemental analysis with SEM. P42/mnm space group was reported and crystals were of rutile type tetragonal with lattice parameters; a=0.4629 and c = 0.3072nm. Electrochemical properties were measured further its reaction with Li was studied which indicated that it can be used as cathodic material for primary rechargeable Li ion battery. Further investigation in this regard are required [71].

The catalytic behavior of iron antimony oxide for ammoxidation of propene has been reported. Synthesis involved slurry impregnation method, at 333K Fe(NO₃)₃ 9H₂O was heated in a beaker on hot plate/magnetic stirrer in this way solution of iron nitrate was formed from its own water of crystallisation. Sb₂O₃ was added into iron nitrate solution brown fumes were formed and temperature was raised to 350K. Aqueous NH₃ was added into the solution to adjust the pH= 3. After filtration the brown ppt were obtained which were dried at 400K for 16h. Then calcination was done in air at 1173K for 7h which increases the rate of diffusion of ions. Sb:Fe ratio was 2:1

which can be adjusted by adjusting the amount of starting chemical precursors. Characterization was performed by XRD, BET and TEM techniques. XRD indicated high temperature calcination yield ordered structure of the product [72].

2.4.7 Co doped antimony oxide: Cobalt doped antimony oxide nanoparticle has the potential to act as a chemical sensor and a photocatalyst for environmental pollution. Synthesis of CoSb_3O_6 follow hydrothermal process, 0.1 M solutions of CoCl_2 and SbCl_3 solution were added into 100mL double distilled water whose pH = 10.5 was adjusted by addition of NH_4OH . This reaction mixture was transferred to Teflon autoclave and placed in oven at 150°C for 16h. Brown ppt of CoSb_2O_6 were obtained after washing with acetone. The ppt were dried at room temperature and were grinded into fine powder than heated at 400°C in oven. Heating induced uniform nanosize crystal of CoSb_2O_6 . The photo catalytic activity was measured by using acridine solution [73].

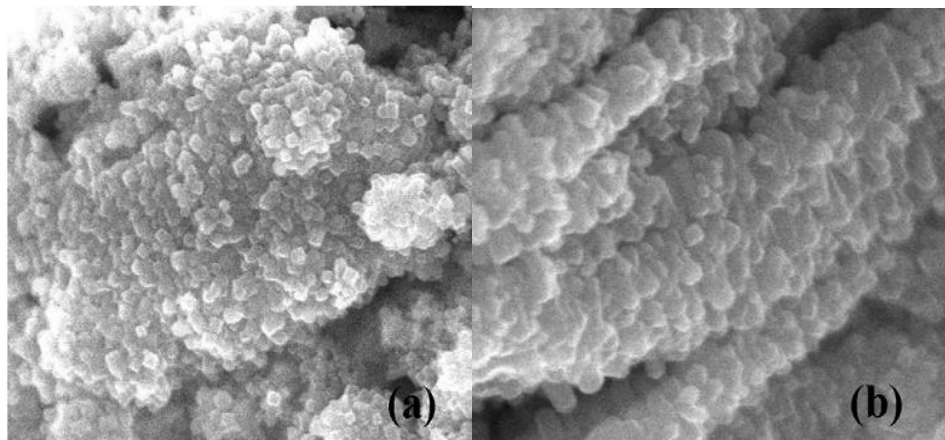


Figure 2.4: CoSb_2O_6 SEM image [73]

The hydrothermal synthesis of CoSbO nanoparticles has been reported by Peter Norby et al., which involved in situ and ex situ experimentation. *In situ* experiment sapphire capillary tubes were used which is Al_2O_3 anisotropic, monoaxial, crystalline, substance, hardest and durable material, possess excellent thermal stability upto 1600°C . Chemical precursors were $\text{Co}(\text{CH}_3\text{COO})_2 \cdot 4\text{H}_2\text{O}$, SbCl_3 , NaOH and HCl . Solution of SbCl_3 was added into 4M HCl then aqueous solution of $\text{Co}(\text{CH}_3\text{COO})_2 \cdot 2\text{H}_2\text{O}$ was added into it. The pH of mixture was maintained by adding NaOH which also changed the solution from red to blue. A little amount of this solution was injected into sapphire tube at pressure of 256 bar. Then heating was done by

applying jet of hot air and desired temperature was attained within 20 s. *Ex situ* experimentation involved mixing 10ml of 1.33M SbCl_3 solution in 4M HCl and 0.66M $\text{Co}(\text{CH}_3\text{COO})_2 \cdot 2\text{H}_2\text{O}$ aqueous solution with magnetic stirring. Afterwards 16mL of 8M NaOH solution was added in order to maintain the pH. An autoclave was filled with the 70 ml of reaction mixture and placed into oven for 53h at 220°C. The powder was obtained from filtered, washed and dried reaction mixture which was characterized by PXRD and SEM analysis. An electrochemical analysis was also performed to check the conductivity of CoSbO [74]. The synthesis of mesoporous CoSb_2O_6 . H.bonilla et al studied gas sensing ability of nano CoSb_2O_6 for this study they prepare its nanoparticles by colloidal method by using $\text{Co}(\text{NO}_3)_3$, SbCl_3 , n-dodecylamine ($\text{C}_{12}\text{H}_{27}\text{N}$) and $\text{C}_2\text{H}_5\text{OH}$. Synthesis involve dissolution of SbCl_3 and dodecylamine in alcohol and $\text{Co}(\text{NO}_3)_2$ also dissolve separately in alcohol with dodecylamine. Cobalt solution was red in colour and SbCl_3 solution was colorless. Cobalt solution was continuously stirred for 1h than SbCl_3 solution was added into it red colour of cobalt solution turn blue after SbCl_3 solution addition due to formation of blue ppt and pH of this suspension was 2 this suspension was stirred for 24h at room temperature. Then using microwave oven the solvent was evaporated by microwave radiation (160 W). The temperature of suspension was kept at 50 °C in microwave oven. For maintenance of temperature inside the microwave the microwave radiation was applied 10 time for 20s. After this operation the sample became viscous and was dried at 200 °C in air for 5h then further calcination was carried out from 300 °C to 700 °C for 5h. The temperature of furnace was raised @ of 100 °C/h. XRD analysis indicated that several phases are present in the sample [75].

2.4.8 Doping of Ni in antimony oxide: Synthesis of mixed metals oxide, their properties and applications were studied by Osama et al. The materials synthesized were Ca_2CuO_3 , $\text{Ca}_3\text{Co}_2\text{O}_6$, and NiSb_2O_6 involving solid state calcination method. In which NiCO_3 and Sb_2O_3 powders were mixed and calcined in stoichiometric amounts at 900°C for 2h after grinding. These oxide showed good heat resistance and corrosion resistance properties [76].

The effect of temperature changes on NiSb_2O_4 structure prepared by sol gel method was investigated by Sandrella et al. The compound, NiSb_2O_4 was prepared by using 1M NiCl_2 , 2M SbCl_3 and 8M NaOH solutions. In NaOH solution, NiCl_2 and SbCl_3 solution were added slowly with constant stirring. Afterwards the precipitates formed were filtered and washed many times with dist. water. Chemical reaction took place during synthesis followed the given equation,



Then product obtained was calcined at different temperatures, i.e, 500 ,900 and 1100°C. Characterization was carried out by DTA and XRD. Sample calcined at 1100°C showed intense peak of NiSb₂O₄ and small peak of NiO and Sb₂O₃ by XRD, whereas sample calcined at 900°C showed single phase of NiSb₂O₄ while the sample calcined at 500°C shows peaks of two different compounds (NiO,Sb₂O₃) [77].

Ion exchange ability of Ni and Co antimonates were studied by Qureshi et al, in 1978. They synthesized nickel antimonate by sol gel method, by addition of 0.05M H₂Sb₂O₇ into 0.05M Ni(NO₃)₂ and by maintaining the pH = 11. The ratio of Ni/Sb was 1 : 2. Then gel was refluxed in the mother liquor for 10h. After 10 h refluxing, the mixture was filtered, ppt were washed with dist. water and dried at 100°C [78].

Ni antimonate synthesis and catalytic activity for ammoxidation of propane was reported by T.J. Cassidy. Synthesis involved dissolution of NiCl₄ and SbCl₅ in aq. solution of HCl. Then this green solution was added dropwise into buffer solution of NH₄CH₃COO, which was stirred thoroughly (pH = 7). Precipitates were washed with dist. water three times and centrifuged after very time of washing. Drying at 120 °C for 1 night then temperature was raised to 300 °C for 2h, then finally to 700 °C for 16h. [79].

2.4.9 Doping of Cu in antimony oxide: Copper compounds(Cu₅SbO₆ or Cu₄SbO₄) having honey comb lattices show fantastic magnetic properties at low temperature. E.Climent et al, studied five compounds of copper for their magnetic properties in this paper. These compounds have delafossite crystal structure (delafossite is copper iron oxide mineral with formula CuFeO₂. Gabriel delafosse gave the name to this material in 1873 and Friedel first time discovered this material CuFeO₂. After this, many compounds having delafossite structure have been discovered including CuInO₂, CuScO₂, CuYO₂ etc. In delafossite structure, every Cu atom is linearly coordinated with two oxygen atom and form O-Cu-O dumbbells parallel to c-axis having rhombohedral unit cell) [80].

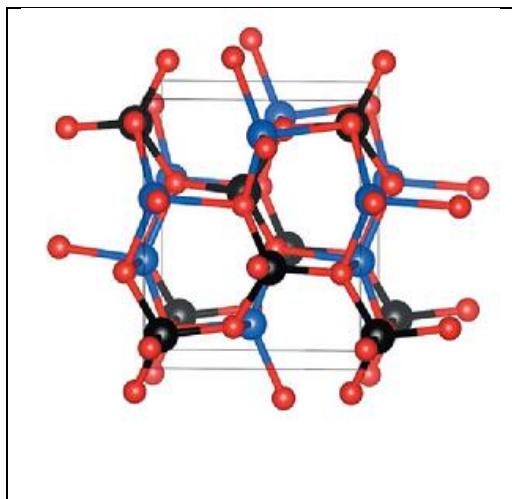


Figure 2.5: Delafossite structure [80]

John teller distortion in Cu^+ d9 system also result formation of Cu^{+2} - Cu^{+2} dimer which give copper containing compounds magnetic property. These dimerization leads to triangular lattice rather than rectangular. Powder Cu_5SbO_6 were prepared by following solid state reaction method from mixture of CuO and Sb_2O_3 in ratio of 5:1 and heated in air at 950°C @ 100°C per hour for 16 h. Then reheated at 1000°C for 24h in air. PXRD analysis indicated the monoclinic structure with $a=8.93$, $b=5.60$, $c =11.85$ Å, and $\beta = 103.6^\circ$. A magnetic property of Cu_5SbO_6 was also measured by VSM (vibrating sample magnetometry), which indicates magnetic behavior of Cu_5SbO_6 [81].

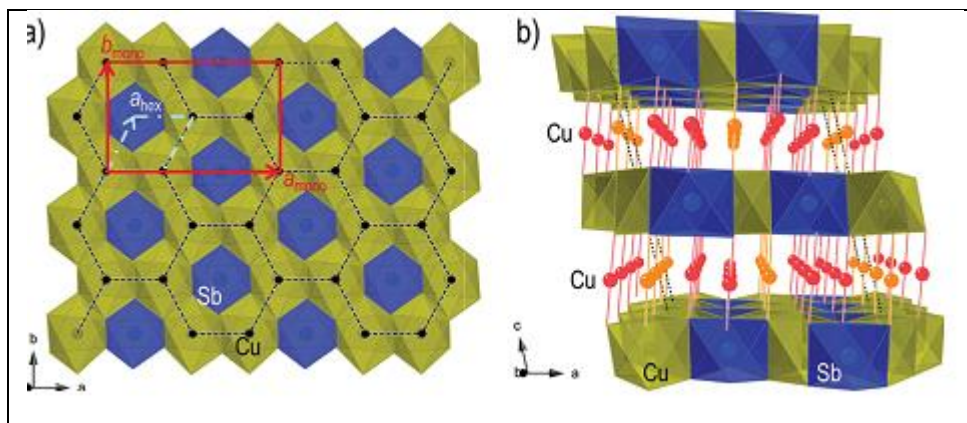
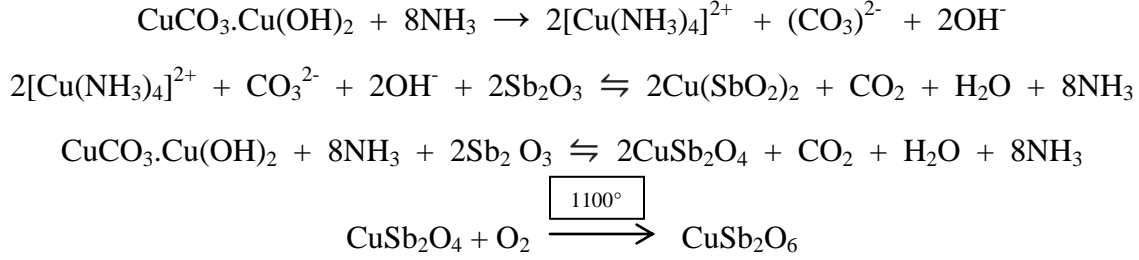


Figure 2.6: Delafossite honeycomb crystal structure of Cu_5SbO_6 . (a). View perpendicular to the honeycomb layer with the Cu^{2+} honeycomb arrangement emphasized (black dashed lines and dots). Sb(V)O_6 octahedral are shown in blue (dark) while Cu(II)O_6 octahedral are shown in yellow (light). A schematic illustration of the relationship of the unit cell axes between the hexagonal (light-gray dashed-dot arrows) and monoclinic (red solid arrows) cells is also included. (b) View parallel to the honeycomb layers. The two types of $\text{O}-\text{Cu(I)}-\text{O}$ sticks that separate the planes are [81].

Walter synthesized copper antimonite by following facile synthesis route and studied its application as a future candidate oxidant for using in delaying of time for mining detonation. The copper antimonite was prepared by refluxing method in three necked flask attached with condenser. In 28g NH_3 solution, 10g of $\text{CuCO}_3 \cdot \text{Cu(OH)}_2$ and 282 gram distilled water were added (mixture was magnetically stirred at 500 rpm). Then 26g Sb_2O_3 was added into the stirred suspension and mixture was heated in an oil bath to reflux. Temperature was settled at 60-70°C. Stirrer speed was increased upto 700 rpm to ensure homogeneity of suspension. Cooling water was passed through condenser in order to prevent NH_3 escaping. Refluxing was done for 6h. The NH_3 was allowed to evaporate by stopping the cooling water. Suspension was filtered, ppt obtained were washed and calcined at 1000°C for 2h. Chemical reactions took place during the process is given below,



CuSb₂O₆ powder sample was characterized by SEM, PXRD, UV-Visible Spectroscopy and TGA analysis [82-83].

Koltsova et al, studied the phase relation of Cu-Sb-O system at 700°C to 1000°C. They concluded that Sb₂O₄ in CuSbO exist in two polymorphic form Sb₂O₄ and β-Sb₂O₄ at 800°C. Synthesis of CuSbO involved mixing of CuO and Sb₂O₃ in ethanol. Then mixture was heated in a crucible at 700 °C, 800 °C and 950 °C for 30h in air with intermediate regrindings. Products obtained after heating were cooled to room temperature, different samples were prepared at different heating duration and temperature followed by quenching.

Table 2.2: Sb₂O₃ and CuO phase relation at different temperature.

| Synthesis temperature, °C | Phase composition |
|---------------------------|--|
| 700 | CuO + CuSb ₂ O _{6-δ} + α-Sb ₂ O ₄ |
| 800 | CuO + CuSb ₂ O _{6-δ} |
| 800 | CuSb ₂ O _{6-δ} |
| 800 | CuSb ₂ O _{6-δ} + α-Sb ₂ O ₄ + β-Sb ₂ O ₄ |
| 1000 | CuO + Cu ₅ SbO ₆ |
| 950 | CuO + Cu ₅ SbO ₆ |
| 950 | Cu ₅ SbO ₆ |
| 950 | CuSb ₂ O _{6-δ} + Cu ₅ SbO ₆ |
| 1000 | CuSb ₂ O _{6-δ} + Cu ₅ SbO ₆ |
| 950 | CuSb ₂ O _{6-δ} |
| 950 | α-Sb ₂ O ₄ , β-Sb ₂ O ₄ |

Then analysis indicated orthorhombic cell with $a = 4.6047$, $b = 4.6603$, and $c = 9.2531 \text{ \AA}$ [84].

2.4.10 Doping of Zn into antimony oxide: A.singh et al, prepared ZnSb_2O_6 by single step hydrothermal method of synthesis. Ilmenite (NaSbO_3) was added into the teflon lined autoclave divalent metal chloride solution of ZnCl_2 and CdCl_2 were also added into the autoclave along with an appropriate amount of water. Then heating was done in oven at $150\text{-}240^\circ\text{C}$ for different durations. Product obtained by heating at 210°C for 3 d was CdSb_2O_6 while heating at 240°C for 4 d the product obtained was ZnSb_2O_6 . After heating solution was filtered and ppt. obtained were washed and dried. Characterization was performed by SEM, XRD UV-Visible analysis revealed the trirutile structure of ZnSb_2O_6 with space group ($P42mnm$) and lattice parameters were $a = 4.6827(8)$ and $c = 9.277(1)$ Å. Optical and photocatalytic activity was also measured for ZnSb_2O_6 [85].

The generation of carrier in the structure of ZnSbO has been studied by Naoto et al., which is semiconducting nature and it is n type carrier. Its conductivity depends on method of synthesis. Sol gel method of ZnSbO preparation show different conductivity as compared to that of prepared by solid state method. In this paper ZnSbO a synthesis has been reported which involves Sb_2O_3 powder addition to dist. water and H_2O . This sol was heated to $363\text{-}373$ K for 2h during this process Sb_2O_3 gets converted into Sb_2O_5 . With continuous stirring of Sb_2O_5 sol at 368K $3\text{ZnCO}_3.4\text{Zn(OH)}_2$ was slowly added. The ZnSb_2O_5 was produced as a product of this reaction while the main product was Zn and Sb rich. Zn_2SbO_6 , obtained after filtration and drying at $373\text{-}573\text{K}$. Obtained powder was sintered in air at three different temperatures and time durations ; at 893K for 12h, 1173K for 6h and 393K for 24h. In order to control the crystallinity and electrical properties, different sample of ZnSbO prepared in different conditions. Characterization was done by SEM and XRD analysis which indicated trirutile phase of ZnSb_2O_6 with the existence of rutile chains. Due to these chains the mobility of electron carrier was considered to be high [86].

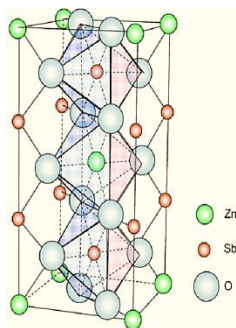


Figure 2.7. Crystal structure of ZnSb₂O₆. Edge-shared octahedrons represent the rutile chain [86]

2.5 Lubricating oils

Lubrication is a technique used to reduce the wear of surfaces in close contact and move relative to one another by introducing a substance called lubricant between them. Vast varieties of lubricating oils are introduced at commercial level in vehicles and machines. Such lubricants enhance the life of engines and machineries by reducing the friction between the rubbing parts. Engine lubricating oils are widely used for transportation and machinery lubrication [137]. In order to get good quality of lubricants scientist are trying to introduce new chemicals as additives in lubricating oil. Lubricating oils properties are greatly influenced by addition of certain additives, in terms of flash point, viscosity, surface tension, wear, oxidation and specific gravity etc.

2.5.1 Addition of chemicals in lubricating oil

Large number of researches are conducted to improve the performance of lubricating oil by introducing new additives into it. Following survey concentrates the past work done by scientist to enhance the efficiency of lubricating oil.

2.5.2 ZDDP

Allyson et al in 2000 determined the function and mechanism of action of ZDDP (Zinc dialkyl dithiophosphate) as an additive and determined its effect on properties of lubricating oil. ZDDP retards oxidation of lubricating oil during service because when engine is working it produces heat and due to heating lubricating oil start oxidation and there is production of free radicals (the peroxy radicals). ZDDP react with these radicals and retard their propagation and it acted as radical scavengers and stopped production of free radicals. ZDDP also acted as an antiwear chemical by forming thick layer on rubbing parts [138]. Following the ZDDP additive scientist used metals other than zinc and form metal DDP including Mo, Ca, Cd and Pb. Anti-oxidant and

anti-wear properties of these MDDP were studied and found inferior than ZDDP [139]. Other antiwear additives metal free dithiophosphate [140], aminothiophosphate, *O,O*-dialkylphosphorodithioic disulfides $[(RO)_2P(S)S-SP(S)(RO)_2]$ as potential replacements for ZDDP [141], metal organophosphates including those of Ca, Zn and Al [142], tricresyl phosphate (TCP), dialkylphosphonates [143], Dithiocarbamates of several different metals and metalloids including Zn [141], molybdenum, Cu [144], Ce, Pb, Sb [145] and Bi, Mo dialkyldithiocarbamates (MoDTC) [146] were also introduced in lubricating oil and their effect were studied, all acted as good antiwear additives.

2.5.3 CuO, TiO₂ and nano diamond as an additives

Y.Y.Wu et al introduced nano CuO, TiO₂ and nano diamond into lubricating oil as an additives and studied the effect on properties of lubricating oil. In order to protect oxidation of nanoparticles of following materials were soaked in glycol and in the presence of glycol were added into lubricating oil. Friction analyser and Viscometers revealed the good friction reduction and antiwear properties of these materials. Nano diamond had very little effect but CuO has tremendously reduced the wear and friction by forming a layer on worn surfaces which decreased the shearing stress and improved tribological properties. Viscosity of oil was greatly enhanced by TiO₂ and CuO nanoparticles at high temperature which led to proper lubrication [147].

2.5.4 CuO additive

Ehsan ollah et al in 2013 studied the effect of CuO nanoparticles addition on lubricating oil properties. They measured the quality parameters of lube oil with CuO including; viscosity, flash point, antiwear ability and pour point etc. in comparison to virgin oil. Results indicated the improvement in performance of lube oil. Viscosity and flash point increased and pour point of the lubricating oil decreased which produces good effect during service [148].

2.6. Properties of antimonates

Lithium antimonates has ionic conductivity used in batteries and other electronic devices as an electrodes material. Antimonates of Na show flame retardant ability [92], antimonates of Ca are used in glass industry for creation of opacity [99], and also it possess photocatalytic activity [100]. Antimonate of Sr have double perovskite like structure used in fuel cell, solar cell [32], and as a semiconducting material [94]. Antimonates of Fe serve as LPG sensing material [70]. Ti antimonates show ion exchange property [97], V antimonates show magnetic susceptibility [50],

electrical property [54], and catalytic property for ammoxidation of propane. Cr antimonates also show ion exchange property [62]. Manganese antimonates show magnetic property [149]. FeSbO used as a catalyst [72], as an ion exchange material and possess various analytical applications [68], including electrochemical property [71]. Ni antimonates show ion exchange ability [78] and heat resistant pigment in paints [101]. Co antimonates have magnetic property along with the electrochemical ability these compound will used in batteries [74]. Co antimonites are the candidate oxidants in the time delays for mining detonators [96] also show electrical properties [94]. Co antimonate show electrochemical ability [74], as a chemical sensor and photocatalyst for environment pollutants [98] also show magnetic properties [83]. Zn antimonates show photocatalytic property [85], it also shows optical and electrical properties [86]. And other metals antimonates also have unique and worthwhile properties which serve as a milestone for the researchers to do extensive research on synthesis of antimony oxide doped with different metals.

2.7. Properties of lubricating oil

When certain additives are added into lubricating oils they directly influence the properties of lubricating oil. Density, viscosity, flash point, wear resistance, oxidation and corrosion resistance of lubricating oil increases by addition of additives. Such oils considered good for service inside the engine possess high values of following quality parameters.

2.8 Properties of doped antimonates

2.8.1 Optical properties

U.V visible spectroscopic analysis for Sr antimonates was carried out and spectrum shows that compound has no absorption from 400-800nm .and absorption edges appear near 375 nm. Which indicates that strontium antimonates is an insulator with optical band gap of 3.3 eV [31].

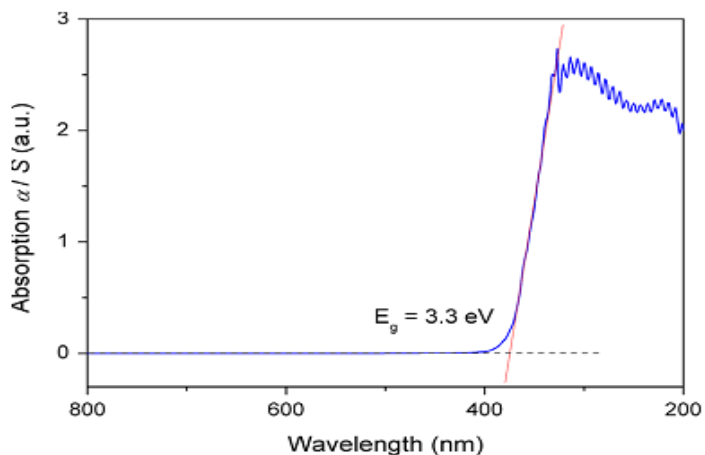


Figure 2.8 Optical absorption spectrum converted from optical diffuse reflectance spectrum for polycrystalline sample of strontium antimonates [31].

$Ba_2Sb_2O_3$ also possess indirect band gap semiconductor properties Its optical diffuse reflectance spectrum were measured and result deduced from the spectra indicated in figure that $Ba_2Sb_7O_{13}(OH)$ belongs to a semiconductor with optical band gap of 2.7eV [150].

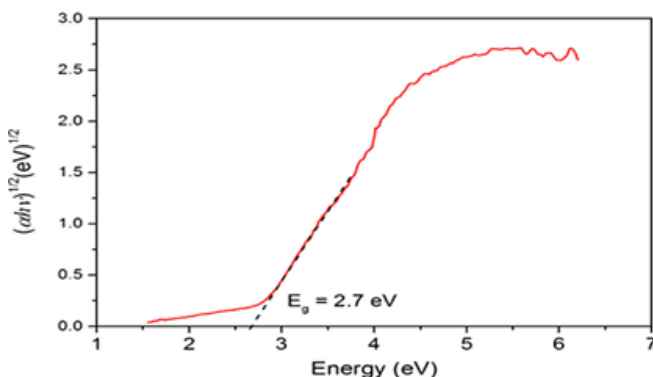


Figure 2.9. Optical band gap estimated from the plots of $(\alpha h\nu)^{1/2}$ versus energy $(h\nu)$ for polycrystalline sample of $Ba_2Sb_7O_{13}(OH)$.

Semiconductor-based photocatalytic oxidation has been established to be one of the most auspicious technologies for the environment remediation and has been employed in the treatment of all kinds of organic contaminants [151-153]. The require photocatalyst should be of high photocatalytic activity if it can be use for environmental remediation. Therefore incredible researches are done for the development of new photocatalysts [154]. $CaSb_2O_5$ and $CaSb_2O_5(OH)_2$ show photocatalytic property This property was measured by degradation of

methyl orange and gaseous benzene [102]. Photocatalytic experiment was carried out in a quartz tube having 17cm length and 4.6cm inner dia under UV light irradiation. Four UV lamps with $\lambda=254$ nm was used as illumination source. The photocatalyst was added in an amount of 80 mg into 80 mL methyl orange solution and stirred for 2h before irradiation to assure that adsorption desorption equilibrium was reached. At given irradiation time interval 4mL of suspension was collected, centrifuged and filtered to separate the photocatalyst particle. Degraded solution of methyl orange were analysed by U.V vis spectrophotometer. Changes in concentration of methyl orange were monitored by maximal absorption in U.V vis spectra at 464 nm. Result after irradiation indicated that methyl orange was degraded completely by irradiating $\text{CaSb}_2\text{O}_5(\text{OH})_2$ for 60 min. While $\text{Ca}_2\text{Sb}_2\text{O}_7$ show little photocatalytic activity comparable to $\text{CaSb}_2\text{O}_5(\text{OH})_2$, in the same time for illumination the methyle orange degradation only 70%. Both photocatalyst show high stability towards UV radiation. Following figure indicated the irradiation.

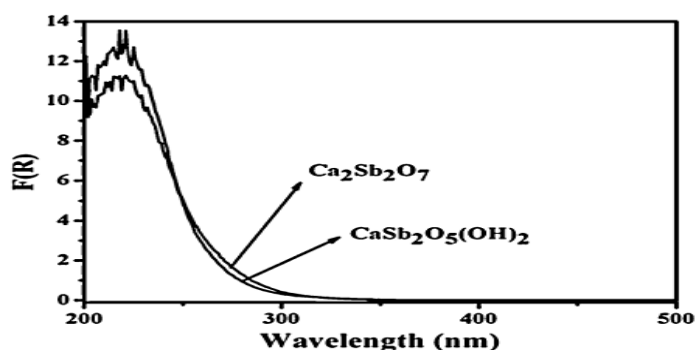


Figure 2.10: UV-visible degradation spectra of $\text{CaSb}_2\text{O}_5(\text{OH})_2$ prepared at pH=1 and cubic CaSb_2O_5

ZnSb_2O_6 also show photocatalytic activity which can be measured by degradation of RhB and Methyl orange dyes. dyes aqueous solution is required and for irradiation purpose 4 UV lamps of tungsten with 254nm wavelnegth were used. Photocatalytic reaction was carried out in a quartz tube having 4.6cm inner diameter and 17cm length. In 150 mL RhB solution 150 mL ZnSb_2O_6 was added and continuously stirred for 1 night. Then suspension was irradiated with different time intervals. 4 mL of suspension was taken and centrifuged then filtered to collect photocatalyst particles. Degraded solutins of RhB and Methyle orange were analysed by UV-vis spectrophotometer. Absorption peak of RhB at 554 nm was observed. ZnSb_2O_6 photocataalytic

activity was measured by degradation value of RhB and MO dyes under UV light irradiation. Sequential changes in RhB concentration monitored by the maximal absorption in UV-vis spectra at 554 nm over ZnSb_2O_6 are given below.

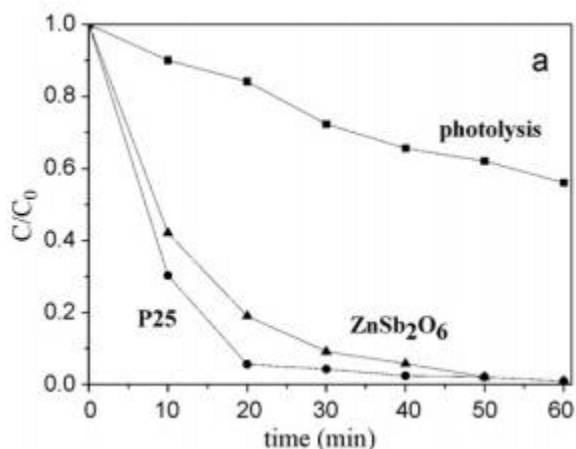


Figure 2.11: Temporal changes of RhB concentration as monitored by the UV-vis absorption spectra at 554nm over illuminated ZnSb_2O_6 , illuminated P25 and UV irradiations only

When UV light fall on RhB solution in the presence of ZnSb_2O_6 for 40 min 95% of RhB was degraded and when 60 min irradiation was done complete degradation of RhB was carried out. In the absence of ZnSb_2O_6 only 40% RhB was degraded by uv radiation. photocatalytic activity of nano ZnSb_2O_6 was compared with commercial Degussa P25 in above figure. C represent absorption of RhB at different time interval of irradiation. C° is the absorption of starting concentration. Similarly degradation of methyl orange was measured in the presence of ZnSb_2O_6 its initial concentration was 20 ppm and absorption peak at 464nm was monitored [155]. antimonates of cobalt also show photocatalytic ptoperties [98].

2.8.2. Photoluminescence Properties.

ZnSb_2O_6 show photoluminescence ability which is measured at room temperature. He-Cd laser is used as an excitation source at 325nm range indicated by figure below,

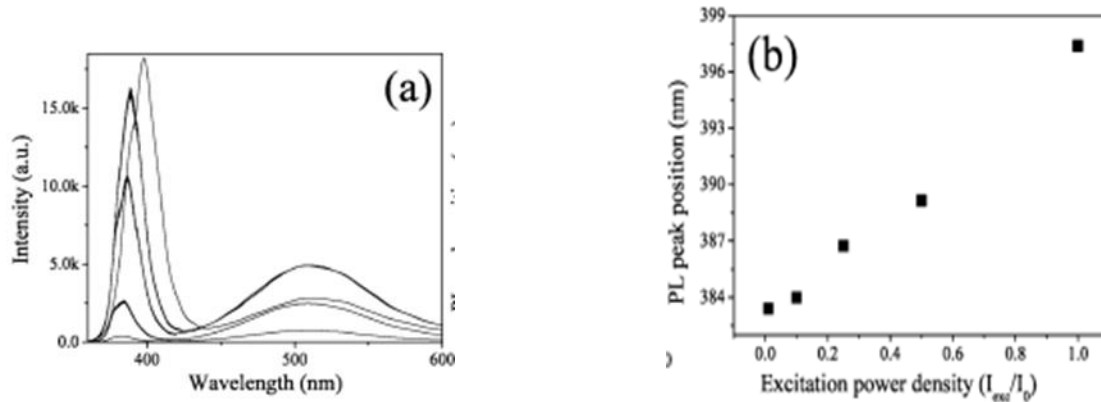


Figure 2.12:Excitation power intensity-dependent PL of the nanostructures measured at room temperature, where I_0 is about 20 kW/cm^2 . Position (b) and integrated intensity

It is excitation power dependent photoluminescence. Intensity of excitation light ranges about 0.2 and 20 kW/cm^2 . Sample possess narrow UV emission which is associated to near band emission and a broad green emission band which is related to deep level defects [a]. Substantial red shift from 383-398nm is shown with increasing intensity of excitation power from 0.2-20 KW/cm^2 by near band edge emission[b]. Near band edge excitation is dominant by bound exciton transition at room temperature when excitation power intensity is low. When intensity is high for excitation photogenerated electrons discharge phonons by Auger recombination and relaxation happen from conduction band to trap states. It result saturation of Near band edge emission and cause redshift by increasing intensity of excitation [156].

2.8.3. Surface photovoltage property

Surface photovoltage spectroscopy is very versatile and powerful characterization technique it is applied to study different semiconductor bulk material and various nanostructures studies.it gives information about electronic structure and optical behavior of a material at room temperature. Sps is performed by using kelvin probe and material is illuminated by a light source [157]. Surface photovoltage property of a material can be calculated by surface photo voltage spectrum. This property provides information about electrons and holes when light fall on the surface of material [158]. ZnSb_3O_6 show surface photovoltage property.and it is measured by taking the spectra of ZnSb_2O_5 .2 sample of ZnSb_2O_6 were studied by sps analysis. Pure ZnSb_2O_6 and doped ZnSb_2O_6 .The pure ZnSb_2O_6 show absorption band from 320 to 380 nm.and doped ZnSb_2O_6 do not show absorption peak. Difference between doped and un doped material is due to

modification of doped material with dopant. Maximum signal was at 320nm which shows transition from 2p orbital of oxygen to 4d orbital of Sb [159]. Intensity of spectra gives the information about photocatalytic activity [160]. Photocatalytic activity will be higher if surface photovoltage signals are weak [161].

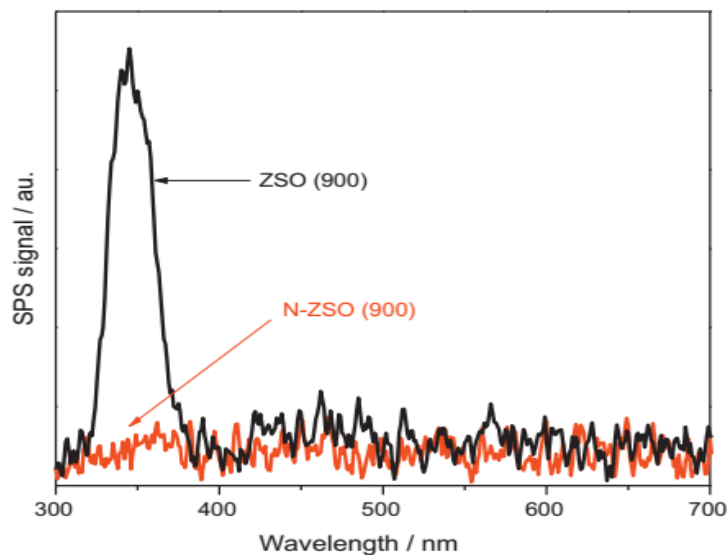


Figure 2.13: SPS spectra of ZSO(900) undoped and N-ZSO(900)doped $ZnSb_2O_6$ without external bias.

2.8.4. Electrical properties

2.8.4.1. Conductivity. Antimonates of Ti show electrical conductivity with temperature. The electrical conductivity was measured as a function of frequency range in the temperature ranging from 76-350K. Graphical representation of the relationship between temperature and conductivity is shown in figure 2.14. .

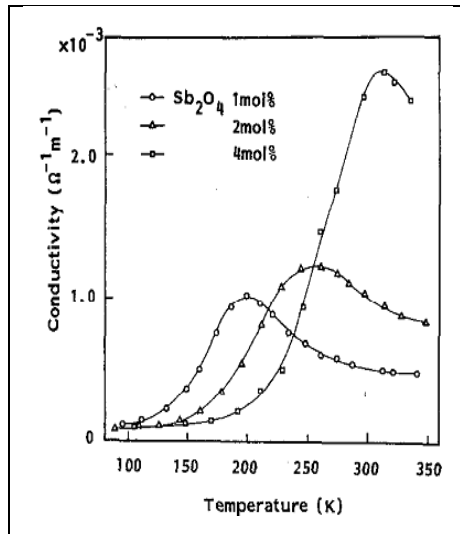


Figure 2.14: conductivity vs temperature

Three samples of different antimony oxide concentration were studied graph indicated convex curves when antimony oxide concentration increased the maximum shift of line move toward higher temperature and higher conductivity side. Similarly when frequency increased the maximum shift move toward higher temperature [162]. The V antimonates also show electrical properties [163].

NaSbO₃

Ilmenite phase of NaSbO₃ show little ionic conductivity figure below indicated the typical ac impedance spectrum of ilmenite type NaSbO₃ at 182°C.

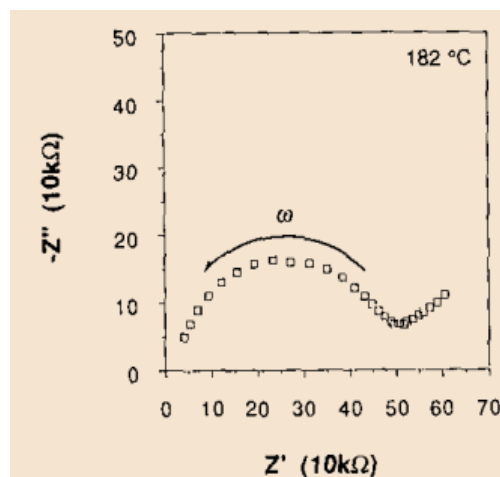


Figure 2.15: The ac complex impedance spectrum of ilmenite NaSbO₃.

Semicircle is present at higher frequency and an inclined straight line is present at lower frequency. Ionic conductivity of ilmenite phase also be measured by Arrhenius plot figure below indicated the plot.

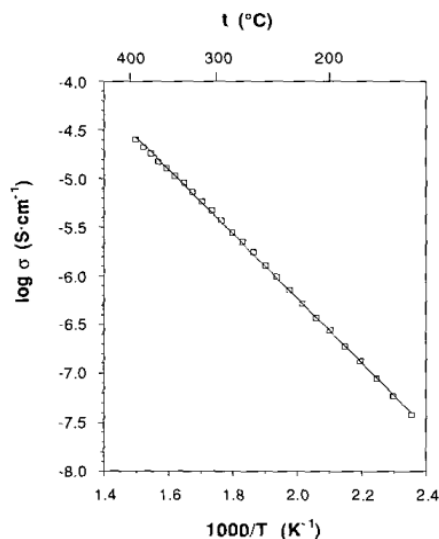


Figure 2.16; Arrhenius plot for NaSbO_3 ionic conductivity for ilmenite phase.

Arrhenius plot indicated Linear behavior in the temperature range of 150-400°C for ionic conductivity. Highest conductivity is shown at 400°C by ac impedance is $3.0 \times 10^{-5} \text{ S.cm}^{-1}$ and having activation energy $E_a=0.66 \text{ eV}$.

In ilmenite NaSbO_3 the Na^+ ions are orderly arranged between the edge sharing SbO_6 in octahedral sites. movement of Na^+ is 2 dimensional in ilmenite phase instead of three dimensional. Na-O bond is stronger and bond distance is 2.313(5) and 2.535(5)Å Strong bond result reduce ionic conductivity. Na-Na separation is 3.175(2)Å. and activation energy is also higher then other crystalline phase of NaSbO_3 . Lower conductivity is also attributed to higher sodium occupancy factor [164].

2.8.5. Electrochemical properties

Nano CoSb_2O_6 possess electrochemical properties. Future trials are made to use it as ann anode in lithium ion batteries.its potential was measured by half cell of type CR2032. Galvanostatic cycling is mentioned below in the figure for CoSb_2O_6 .

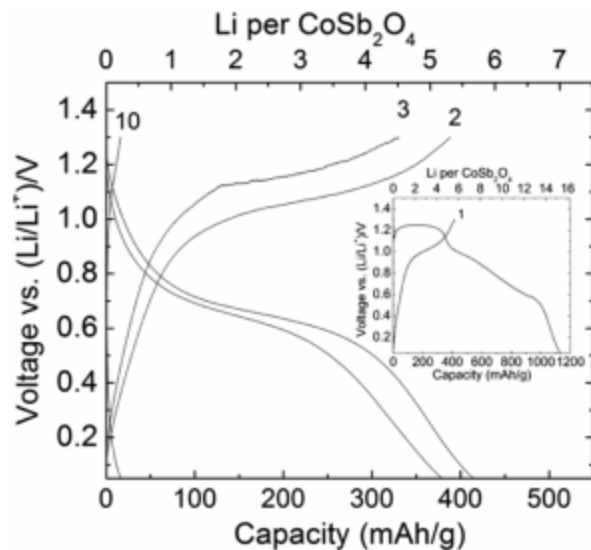


Figure 2.17: Potential (vs Li/Li^+) vs capacity for CoSb_2O_4 under galvanostatic charge/discharge at 30 mA/g between 0.05 and 1.3 V for the second, third, and tenth cycles. The inset shows the initial discharge and charge curves.

15 Li atoms reacted with CoSb_2O_6 when initial discharge reached at 1131 mAh/g. It is analogous to the 1127 mAh/g already reported. Initial charge capacity was 417 mAh/g which is parallel to dealloying below Li_3Sb two formula units. It is renowned that in half cell unreacted cobalt is inactive electrochemically. On successive cycling capacity was faded up quickly. After 10th cycle only 20 mAh/g reversible capacity was remaining. CoSb_2O_6 potential for using it as an anode material in Li battery is not suitable. Because material possess large irreversible capacity in 1st cycle and this capacity fades up in 10th cycle. Further research is required to use CoSb_2O_6 as an anode material for batteries [74]

2.8.6 Ion exchange property. Antimonates of Ti show ion exchange ability [44], chromium [62], FeSbO_3 also possess ion exchange capacity [68].

2.8.7. Magnetic properties.

Magnetic studies of FeSbO_4 indicated the magnetic nature of iron antimony oxide at room temperature. A vibrating sample magnetometer was used for magnetization studies. Result indicated that magnetization decrease to zero when applied field was removed which resulted superparamagnetic behavior. Superparamagnetism is unique phenomenon possessed by few

nanomaterial which show paramagnetic behavior above a critical size. Figure indicated that FeSbO_4 nanoparticles having average crystallite size 3nm show no magnetization at zero magnetic field strength, which indicated superparamagnetism. The smallest crystallite having 2nm size is single domain particle also exhibit superparamagnetism. This revealed that magnetic domain size of these particles were approximately larger than 2nm. When magnetic particle size was decrease they change from multi domain to single domain [70].

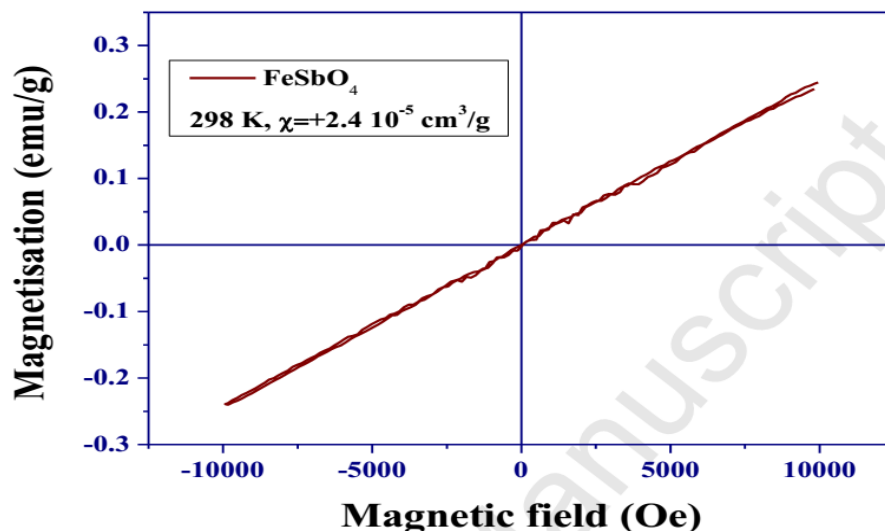


Figure 2.18: Magnetic behavior of FeSbO_4

CoSb_2O_6 and CuSb_2O_6

Cobalt and copper antimonates also show magnetic susceptibility. Measurement was done by magnetic susceptibility measurement and NMR/NQR techniques. Magnetization (M) and susceptibility (M/H) depends on temperature for CoSb_2O_6 measured at different magnetic field given below in figure:

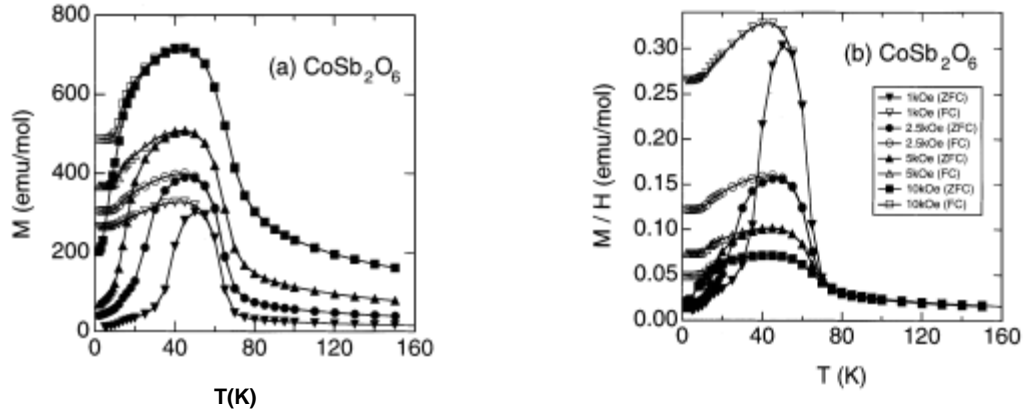


Figure.2.19: Temperature dependence of the magnetization (M) and the susceptibility (M/H) of CoSb_2O_6 compounds measured at various magnetic Fields (H).

Susceptibility (M/H) values do not depend on magnetization H above 70K, and it shows Curie-Weiss behavior. Effective moment (μ_{eff}) estimated value was $4.66\mu_B$ and Weiss temperature expected value was 17.8K [165]. Co^{+2} has a slightly higher value of effective moment due to the presence of d^7 high spin state. Susceptibility values below 70K quickly increase due to the formation of short range ferromagnetic order. After 30K, at low temperature susceptibility values are going to decrease for zero field cooling, it was constant below 30K for field cooling measurement. Spin freezing behavior is observed 1st time in CoSb_2O_6 structure which was caused by spin frustration due to low dimensional magnetic structure. Further researches are in progress to find the electronic and magnetic state of cobalt.

CuSb_2O_6

Magnetic susceptibility of CuSb_2O_6 depends on temperature. Figure below indicated this dependence when a field of 2.5kOe is applied.

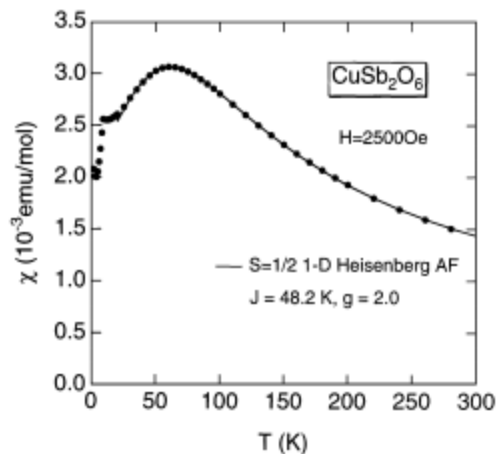


Figure 2.20: Temperature dependence of the magnetic susceptibility of the CuSb_2O_6 sample. The solid line represents a result of the curve fitting $S=1/2$ 1-D antiferromagnetic Heisenberg model.

Cu^{+2} sublattice is 2-D square but its magnetic susceptibility matches well with numerical calculation of 1-D antiferromagnetic Heisenberg model. This 1-D behavior indicated that superexchange pathways are not similar for $[1\ 1\ 0]$ and $[1\ \bar{1}\ 0]$ directions [166]. In 1st case Cu-O-O-Cu coupling takes place and bond angle is 180° . In 2nd case Cu-O-Cu coupling is present with bond angle 160° . In figure magnetic susceptibility decreases quickly at 8.5 K, which signifies that magnetic transition is undergoing inside the system. This indicates that magnetic moment of Cu^{+2} is less than $1.0\mu_B$ if 3-D antiferromagnetic long range order is present. Magnetic transition at 8.5 K is not due to antiferromagnetic long range order. It is an open question for researchers. NMR and NQR measurements indicated that it is due to spin-pierls transition. Further researches are required to prove this data [167].

Antimonates of vanadium [50], manganese [168], and FeSb_2O_4 show magnetic property [67].

2.8.8 Catalyst

Vanadium antimonates are used as effective catalysts for ammoxidation of alkanes. FeSbO is also used as a substitute catalyst for alkane ammoxidation [72].

Vanadium antimonate acts as a catalyst for conversion of hydrogen sulfide to sulfur. Petroleum refinery gases and natural gases use VSbO for removal of H_2S pollutant and converted into

elemental sulfur it serve as an excellent source for H₂S removal. Various catalyst were used for this purpose which poses their own hazards but vsbo proof itself to be a good substitute for previous one. Catalytic activity of vsbo for conversion of H₂S into sulfur was studied by using a flow reactor with temperature 180-280°C. VSBO catalyst was prepared in five different ratios of V/Sb 1/0, 5/1, 1/1, 1/5.0/1 In a tubular reactor catalytic reaction with hydrogen sulfide was studied. Reactor consist of a pyrex tube with diameter 0.007m. Before measuring the catalytic reaction reactor was heated with a tube furnace.presulfurization of catalyst was carried out in an environment of 15 vol %H₂S, 25 vol%O₂ and 60 vol%N₂ for 8h at 250°C. Reactor temperature was decreased from 250°C to 180°C after presulfurization. Then gaseous feed was introduced at the top of the reactor which carry 1vol% H₂S , 94vol % N₂ and 5 vol%H₂. Gaseous feed was flowing into the reactor at 200 mL/min and catalyst contact with gas feed for 0.03s. Gas product analysis was carried out.

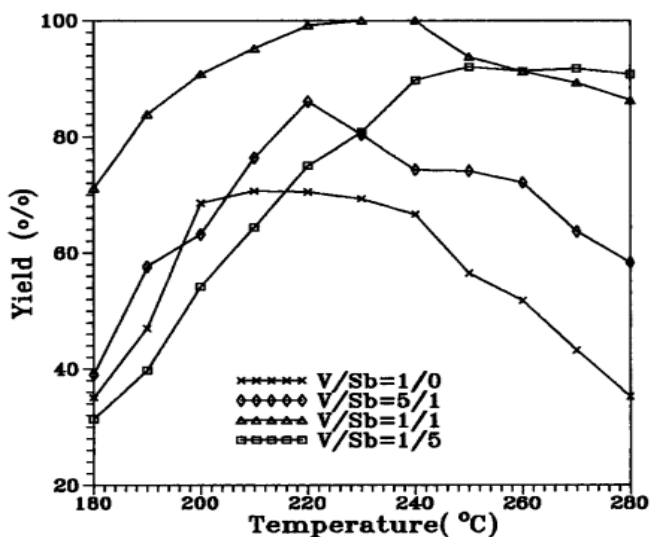


Figure 2.21: Sulfur yield as a function of reaction temperature

Yield of sulfur as a function of temperature shown above for vsbo catalyst having four different concentration pure antimony oxide is excluded due to its low activity. Different concentration of catalyst having different yield.5/1, 1/1, 1/5 concentrations having maximum yield of 86.1%, 100% and 92%. Yield was maximum for 1/1 ratio of V/Sb .VSbO₄ which contain Sb+5 in oxidized state and vanadium in reduced state [169].

2.8.9 Acid base property

iron antimonates show acidic and basic nature due to presence of iron and antimony. Iron antimonates strongly acidic sites possessing Fe^{+3} cations are obstructed by weakly acidic Sb^{+3} cation. strength and nature of acidic and basic sites and relative concentration of these sites can be determined by IR spectroscopy of adsorbed molecules. pretreatment of prepared sample of iron antimonates was done in a vacuum of 10^{-4} to 10^{-5} torr at 273 K then in the presence of oxygen at 400 -600 torr. Cooling was done in the presence of oxygen to room temperature. And evacuation to 10^{-3} torr. spectra was recorded at room temperature by using UR-20 spectrometer. recorded spectra was decomposed into individual component on SC-2 curve synthesizer. iron antimonate surface has two type of basic centres and responsible for bands at 2242 cm^{-1} and 2259 cm^{-1} in CdCl_3 spectra. This relates to pka of basic centres +2 and -3 [170].

2.8.10 Sorption behavior

Titanium antimonates show sorption behavior their ability was tested in nuclear power plant. it removes radiocobalt in the presence of complexing agent [171].

2.8.11 Opacifying agent

Large number of opacifier are used in early history Calcium antimonates got special attention due to its very long time use in early antiquity for opacification of glass [98]. Antimonates of sodium is used in glass industry as a fining agent or degasser, especially in colour television bulbs and optical glass, as an oxidizing agent at high temperature, enamel opacifier, glass fining agent, as a decolourizer in glass tube and fiber glass [165].

2.8.12 Flame retardant

When Na antimonate is used with halogen especially with chlorine it shows fire retardant property with low tinting characteristic. As such it is used in plastics, paints, fibre glass, resins and various textile goods The colloidal antimony pentoxide produced from Sodium antimonates hexa hydrate is used as flame retardant. Extremely high purity antimony metal and high purity antimony oxide is also produced by antimonates of sodium.

2.8.13 Gas sensing ability

FeSbO₄ powder show gas sensing property. Fabricated film has improved gas sensing ability with high sensitivity and fast response. Sensing ability was checked by using different concentration of H₂ gas. From 1000ppm to a higher concentration of 8% H₂ gas. In figure 2.23 different concentration of H₂ gas (1000ppm, 1,2,4 and 8%) are plotted as a function of temperature. Operating temperature was 350°C. At 300°C sensor displayed a response of 65% toward 1% H₂ and 80% toward 2% H₂ gas. When sensor exposed to 4% H₂ for 20s resistance of sensor decreased which result in high sensitivity of 83.5% toward 8% H₂ gas. The sensitivity increased linearly with gas concentration at all temperatures. At 350°C the sensitivity was maximum and then decreased. At 250°C and 300°C operating temperature the same sensor response was 70% and 76% toward 4% H₂ gas [69].

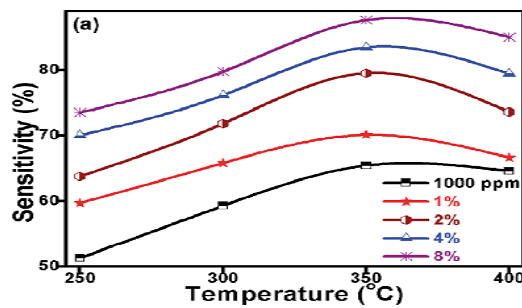


Figure 2.22. Percentage response characteristics as a function of temperature toward different concentrations of H₂ gas exhibited by the sensors fabricated using 300 °C calcined FeSbO₄ powder[69]

NiSb₂O₆ also possess gas sensing property. Thin film of NiSb₂O₆ was prepared on alumina substrate. This thin film was placed in a chamber having inlet and outlet knob for gases. Film has silver contacts. On both sides of film ohmic contacts are made with the help of silver paste to make it a sensing film. Ability of gas sensing was measured for this film by introducing this film into chamber where LPG and CO₂ gases were used as a target material. The measured volume of gases are introduced into the gas chamber which was filled with air. Electrical resistance of the thin film was measured before and after exposing it to the target gases [172]. Using Keithley electrometer. After 1000s recovery the chamber was opened to the atmosphere and sensing plate was studied. Figures given below indicated the morphology of thin film fabricated on alumina

before and after the exposure to gases. SEM analysis of the film before gases exposure indicate the diameter of nanoparticle that was 50-70nm. After exposing this thin film to gases SEM analysis was also done which indicated the diameter of nanoparticle to be 50-400nm range.

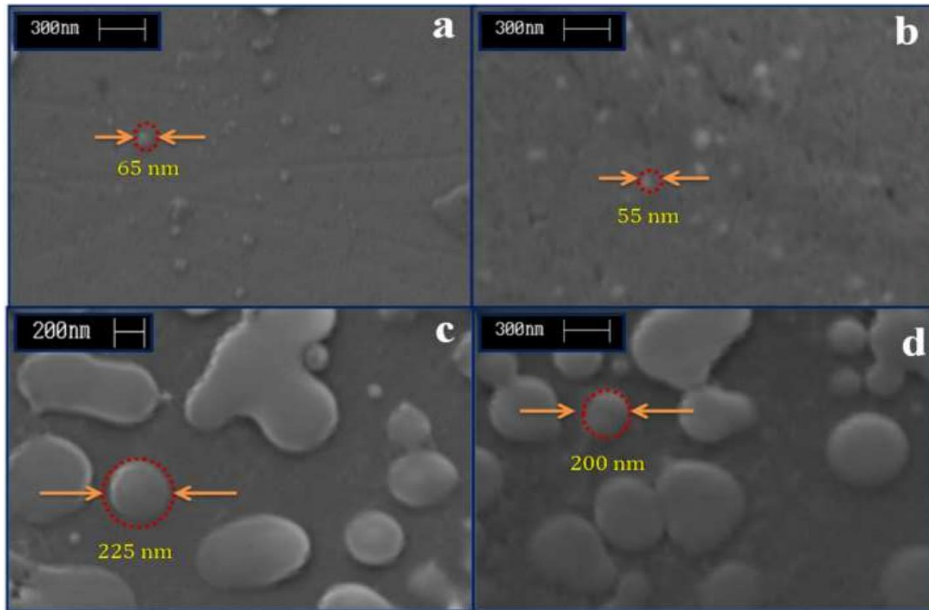


Figure 2.23: SEM analysis of thin film

Enhanced diameter revealed that LPG was in contacted with sensing film surface. On the surfaces there are dangling bonds which cause the high chemical reactivity of the surface. Due to this reactivity surface of the thin film easily absorb LPG when it comes in contact with it [173].

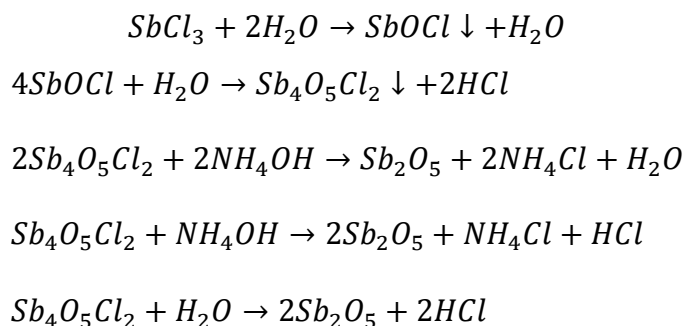
Chapter 3

Materials and Methods

3.1 Synthesis of precursors

Indirect synthesis method has been followed; in the first step, high purity NaCl and antimony oxide was synthesized from $SbCl_3$ via wet chemical methods [174]. Antimony trichloride ($SbCl_3$) from BDH chemicals Ltd Poole England with purity 99.9%, liquid Ammonia (NH_3) from BDH chemicals Ltd Poole England with purity 70%, hydrochloric acid (HCl) from Sigma Aldrich with 70% were used without further purification.

Synthesis of Sb_2O_5 was carried out by precipitation method from 0.8 M $SbCl_3$ maintained at pH 11 by addition of NH_3 solution. After 40 min stirring, the suspension was filtered and washed with ethanol (thrice) and then it was subjected to drying at $100^\circ C$ for 5h, resulting material was then characterized.



3.2 Synthesis of $NaSbO_3$

Purified NaCl and Sb_2O_5 were mixed and ground in 1:3 ratio and pelletized. Pellets were first annealed at $650^\circ C$ for 4d afterwards reground, pelletized and annealed at $700^\circ C$ for next 21h. The resulting material was characterized to ensure the complete removal of chlorine from the

samples. Synthesized material was then annealed at four different temperatures; 700, 800, 900 and 1000°C for 1d.

3.3 Characterization

X-Ray powder diffraction (XRPD): X-ray powder diffraction data was collected for each sample in as cast and annealed state employing a Model STOE Germany operating at 40kV and 40mA, using monochromatic $CuK_{\alpha 1}$ radiation in range of $10^{\circ} \leq 2\theta \leq 80^{\circ}$. For qualitative analysis POWDER CELL program has been used [175] while quantitative Rietveld refinements were performed with the FULLPROF program to calculate crystal structure [176-177].

Scanning electron microscopy (SEM): The as cast and annealed samples were coated with gold employing standard procedures. Micro-Analyses was performed (EPMA) on a MIRA3 TESCAN equipped with an EDX system operated at 40kV.

Ultra Violet Diffused reflectance Spectroscopy (UV DRS): Optical properties were measured by PerkinElmer UV/VIS/NIR spectrometer Lambda 950 having the spectral range of $190-3300\text{cm}^{-1}$. Small amount of pellet is introduced into sample holder for reflectance scan.

Electrical properties LCR (Inductance Capacitance and Resistance) meter: The pellets of 12mm diameter were fixed one by one between the electrodes using Wayne Kerr model-6500B LCR meter having frequency range of 100Hz - 5MHz for dielectric properties measurements at room temperature.

Micro Vickers hardness test: Pellets of sodium antimonate prepared at different annealing temperatures, i.e. 700, 800, 900 and 1000°C were tested one by one for Vickers hardness. Single pellet was placed on sample holder and load of 1kg was applied by pressing the diamond indenter into the material surface for 10 second.

Flash point: The effect of Sodium antimonate addition on the flash point of lubricating oils obtained from four different locally available companies, including; Havoline, Castrol Active, Shell and Zic were studied. Fine crushed 0.3g of NaSbO_3 annealed at different temperatures have been mixed with above mentioned oils, in total 16 samples were prepared for flash point testing. Flash point of virgin oils was also measured for comparison. Close cup flash point tester (SETA series 3) maximum temperature range 300°C. Time taken for analysis was 2 min for 4mL volume.

Density: Densities of virgin lubricating oils and with NaSbO_3 powder were measured by using pycnometer having volume 25mL at room temperature i.e, 30°C . Specific gravity was also measured for 16 samples prepared by addition of little amount of NaSbO_3 powder. Density of water was measured first and then it is compared to the density of each oil sample and the obtain ratio of both densities gave us specific gravity of each sample.

Viscosity: Kinematic and dynamic viscosities of above prepared samples were measured by using Ostwald viscometer. Before starting the experiments, the viscometer was calibrated by measuring the kinematic and dynamic viscosity of water. Later, viscosities of virgin oils and with NaSbO_3 were measured at 30°C .

Chapter 4

Results and discussion

4.1 Structural and morphological analysis

X-Ray diffraction study of synthesized samples was carried out. Phase analysis, crystal structure and crystallite size was measured. X-Ray study was carried out to analyse the phase and crystal data of the synthesized material. XRPD of NaSbO_3 annealed at different temperatures revealed that material is similar unless annealing temperature was raised and intensity of peaks increases by increasing the annealing temperature which indicated the growth of grains to certain axis. At higher annealing temperature material become multiphase.

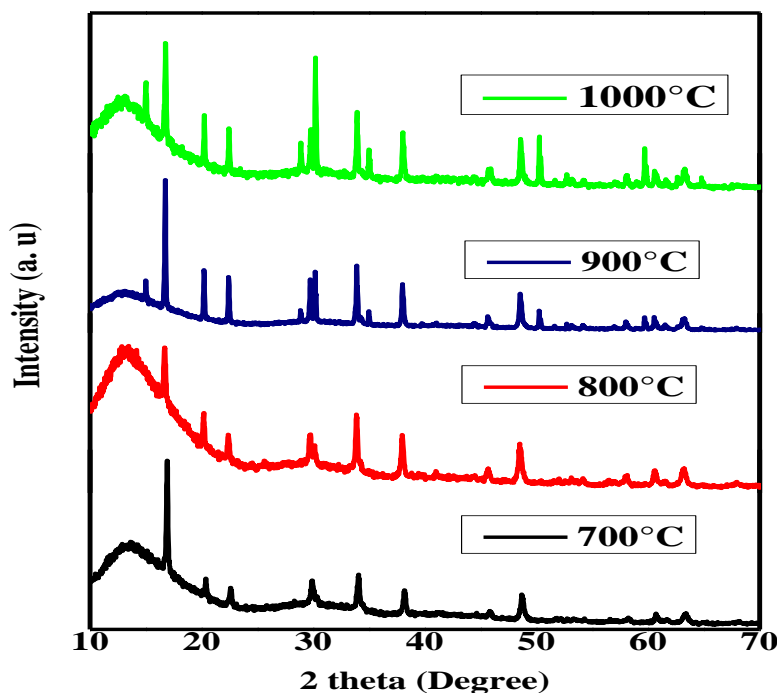


Figure 4.1; X-Ray Powder diffraction pattern of NaSbO_3 annealed at different temperatures

Rietveld Refinement

The Rietveld method refines user-selected parameters to minimize the difference between an experimental pattern (observed data) and a model based on the hypothesized crystal structure and instrumental parameters (calculated pattern) and This method is used to characterize the crystalline material. Data obtained after Rietveld refinement shows the minimum difference between the calculated values and experimentally determined values figure below

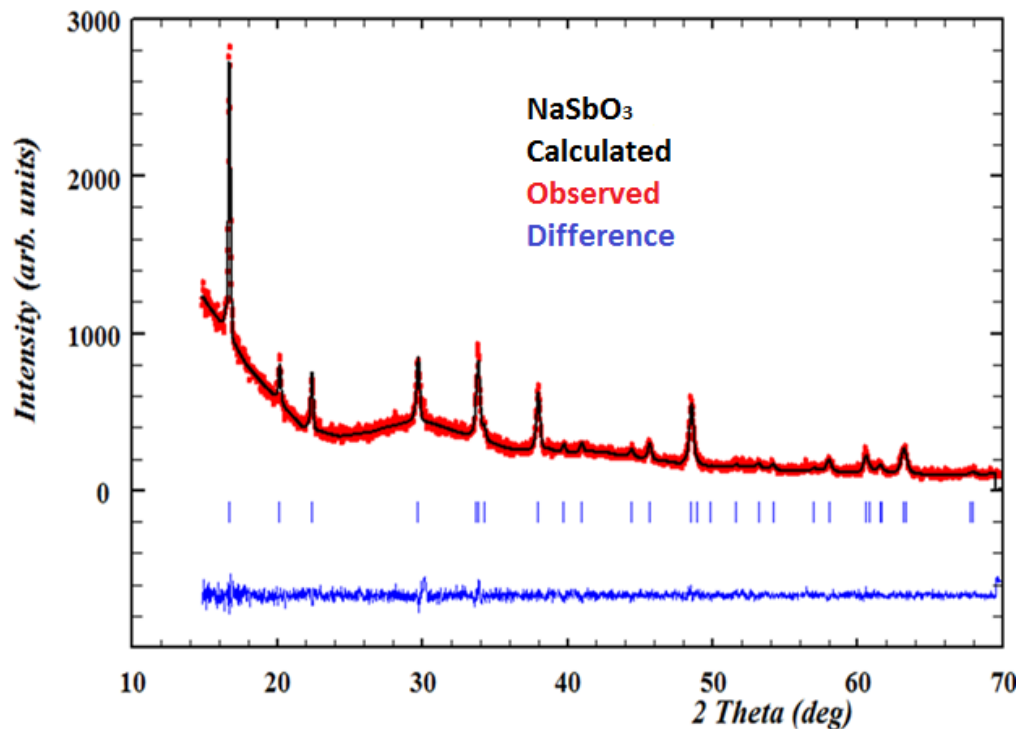


Figure 4.2; Rietveld refinement result of NaSbO₃

Calculated Crystal structure of the NaSbO₃ indicated the pyrochlore type in which sodium atoms are present between the layers of Sb and O. oxide of rare earth and transition metals usually exist in this type of crystal structure.



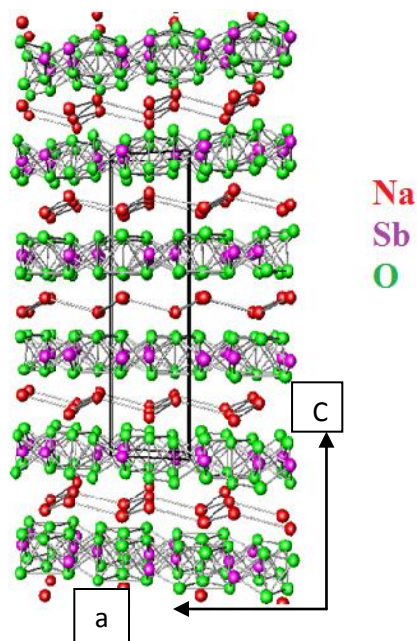


Figure 4.3; Crystal structure of NaSbO₃

Crystal structure data obtained after unit cell study indicated the lattice parameter and density given below in table 4.1

Table 4.1. unit cell data of NaSbO₃

| Annealing temperature | 700°C | 800°C | 900°C | 1000°C |
|------------------------|------------|-----------|------------|-----------|
| a (Å) | 5.29039(6) | 5.2920(1) | 5.2882(8) | 5.3025(2) |
| c (Å) | 15.937(3) | 15.947(4) | 15.9390(4) | 15.959(5) |
| D (g/cm ³) | 5.15 | 5.129 | 5.420 | 4.942 |

4.2. Scanning electron microscopy (SEM)

Scanning electron microscopy was performed for different samples annealed at 700, 800, 900 and 1000°C. Figure below clearly indicates the morphology of samples annealed at different temperatures. Material annealed at 1000°C showed good results, as it become homogenous at higher temperature and particle size indicated that the material is in bulk range.

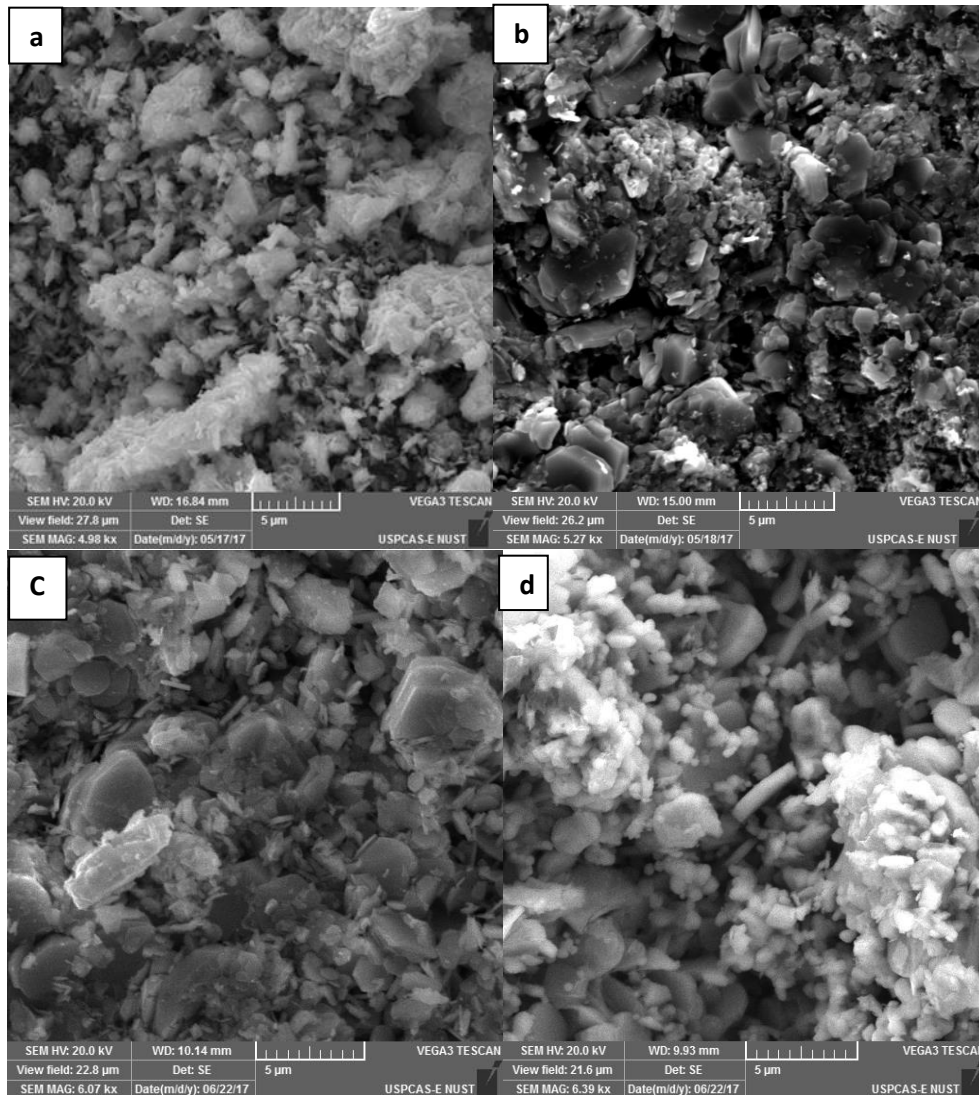


Figure 4.4: SEM images of samples annealed at (a) 700°C (b) 800°C (c) 900°C (d) 1000°C.

Figure 4.5 reveals the EDS spectra of samples prepared at various temperatures. EDS spectra of all four samples show the chemical composition of prepared sample in a ratio of 1:1:3 (NaSbO₃). Extra peaks appeared due to gold coating on material.

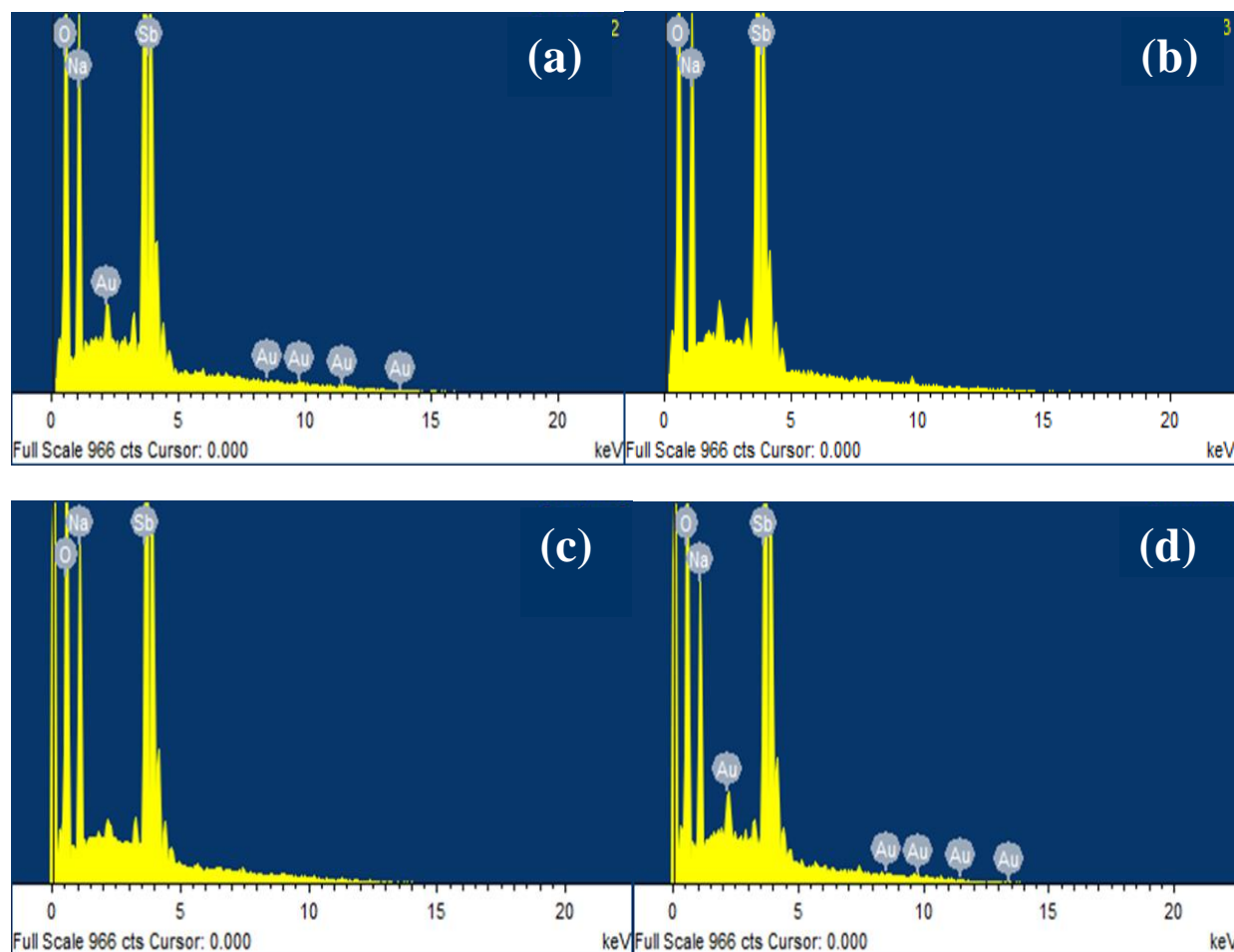


Figure 4.5: EDS spectra of samples prepared at different temperatures; (a) 700°C, (b) 800°C, (c) 900°C, (d) 1000°C.

4.3 Optical properties

4.3.1 Diffuse Reflectance Spectroscopy

UV-Vis spectroscopy was not a fruitful method because sodium antimonite was neither soluble in common available solvents nor produced ideal suspension even after 6h sonication. Diffuse reflectance spectroscopy technique was employed for calculation of optical properties and band gap. Band gap of samples annealed at different temperatures was measured through DRS and then obtained values were compared.

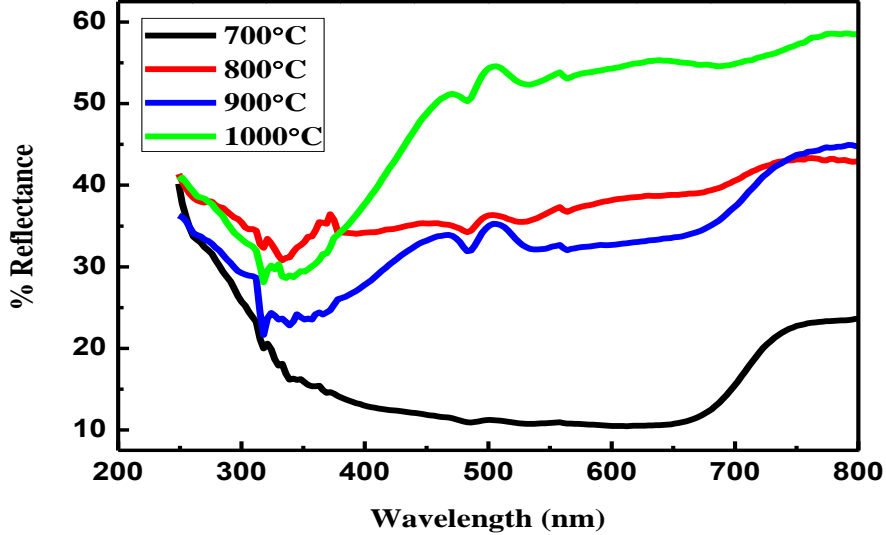


Figure 4.6: UV-DRS spectra of NaSbO₃ samples %Reflectance vs ln F.

The reflectance spectra provided in figure 3 indicates an increase in reflectance with increasing wavelength. Better reflectance ability is observed in sample annealed at 1000°C as compared to other samples annealed at different temperatures. Tauc plot (a plot of energy (eV) Vs $(h\nu\alpha)^n$ [178] for calculation of band gap is also plotted using Kubelka-Munk expression. Absorption factor in DRS-UV is replaced by reflectance factor $F(R)$ given below [179]:

$$F(R) = \frac{(1 - R)^2}{2R} = \frac{K}{S}$$

where:

R-Absolute reflectance

K-Molar absorption coefficient

S-Scattering coefficient

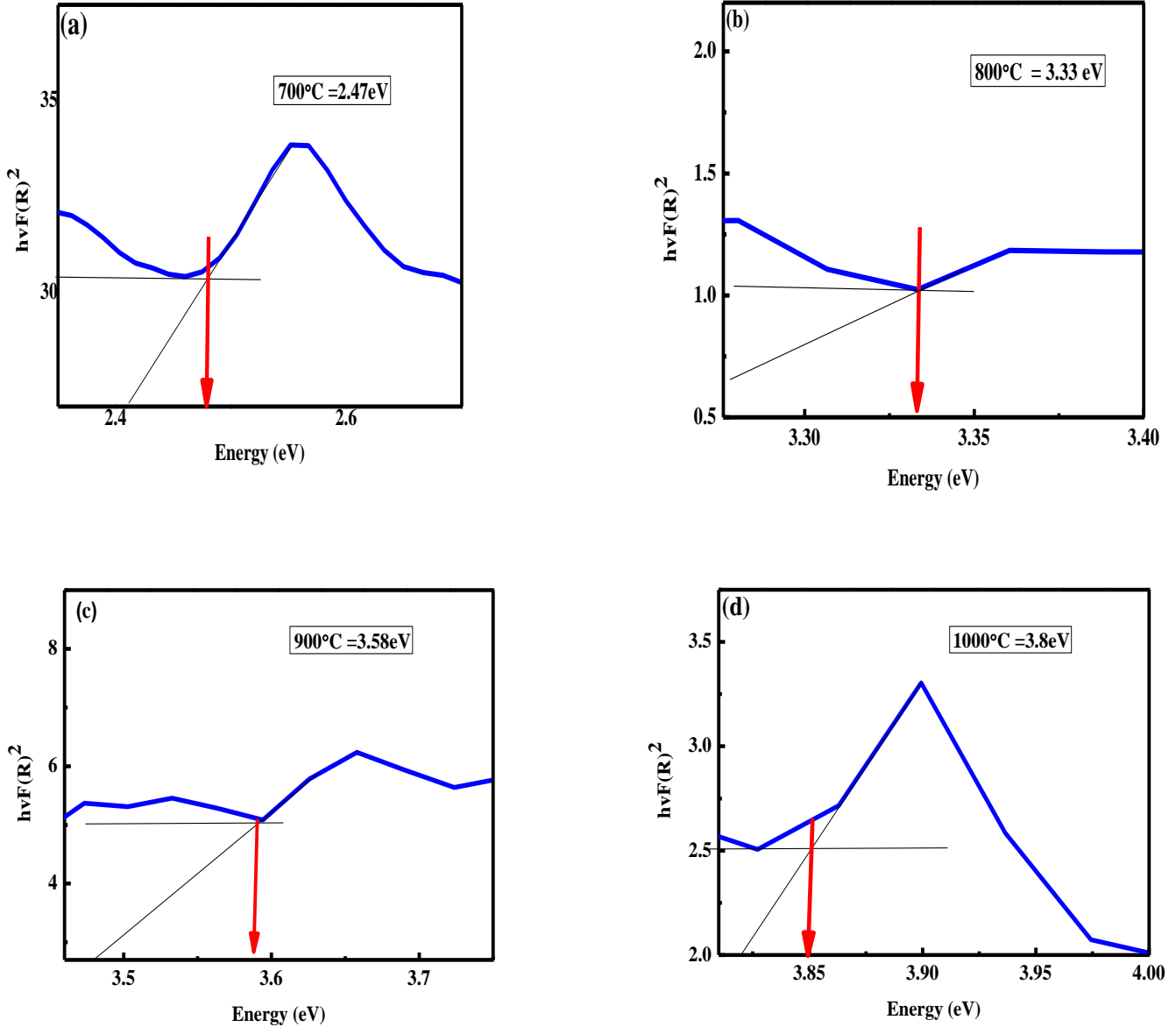


Figure 4.7: Tauc plot, of $[hv \times F(R)]^2$ vs energy for sample annealed at:(a) 700°C, (b) 800°C, (c) 900°C (d) 1000°C

The average band gap was estimated from the intercept of linear portion of the $hvF(R)^2$ vs energy plots shown in Figure 4.7 For calculation of approximate value of E_g a plot of energy (eV) Vs

$h\nu \times F(R)^2$ has been plotted. Figure 4.7 shows estimated values of band gaps for samples annealed at 4 different temperatures including 700, 800, 900 and 1000°C. Results obtained from these graph showed that band gap increases by increasing the annealing temperature. Band gap of samples annealed at different temperatures are 2.47, 3.33, 3.59 and 3.8. Sample annealed at 700°C is semiconducting in nature and sample annealed at 1000°C is going toward insulating behavior. Results obtained by measuring the band gap of material are in close connection with results obtained by measuring the dielectric behaviour of the material.

Table 4.2: Optical band gaps of samples at different temperatures.

| Samples at different temperatures | Band gap (eV) |
|--|----------------------|
| 700°C | 2.47 |
| 800°C | 3.33 |
| 900°C | 3.59 |
| 1000°C | 3.80 |

4.4 Dielectric Properties

Dielectric properties are usually measured for those compounds which are insulator or semiconductor in nature because dielectric has no influence on direct electric current and they get influenced by electric field. Dielectric properties are categorized into four important parameters; dielectric constant, dielectric loss, tangent loss and AC conductivity. When semiconducting material is subjected to electric field four types of polarization can be developed, i.e. ionic, electronic, space charge and orientation which give rise to dielectric constant. These dielectric properties of materials are important to know the charge transport phenomena and the lattice dynamics in the crystals.

4.4.1 Dielectric constant (ϵ)

It is also called relative permittivity which reveals that how easily a material is polarized in the applied field. The dielectric constant can be calculated by the following formula,

$$\varepsilon = \frac{C \times d}{\varepsilon_0 \times A}$$

Where C represents capacitance, d is the sample thickness, ε_0 is permittivity of free space having value $8.85 \times 10^{-12} \text{ Fm}^{-1}$ and A is the surface area of the sample [180]. High value of dielectric constant at low frequency indicates lower electrostatic binding strength which is due to polarization of charge near the grain boundaries. Both dielectric constant ε' (real part) and dielectric loss ε'' (imaginary part) provide information about charge storing capacity and energy dissipation [181-182].

4.4.2 Dielectric loss factor (ε'')

When alternating current is applied to the material the amount of energy loss to align the charges of such material along the direction of applied electric field is called dielectric loss. It is an imaginary part of dielectric loss and calculated by using the formula [183],

$$\varepsilon'' = \varepsilon \times D. factor$$

The dielectric loss factor relates to the inability of molecules in the insulating material to reorient with an alternating electric field. This ability is dependent on the temperature of the sample, the size of the molecules involved, and their polarity. It is also dependent on the frequency of the alternating field. Low value of dielectric loss factor at high frequency suggests that material has fewer defects.

4.4.3 Dissipation factor ($\tan\delta$)

Dissipation factor is direct measure of dielectric loss. Real part for energy loss calculation is called tangent loss. It is measured by using the following formula [184],

$$\tan\delta = \frac{\varepsilon''}{\varepsilon}$$

4.4.4 AC conductivity

It is measure of materials ability to conduct an alternating current (σ_{ac}) which can be calculated σ_{ac} by the given formula,

$$\sigma_{ac} = 2\pi f \epsilon_0 \epsilon' \tan \delta$$

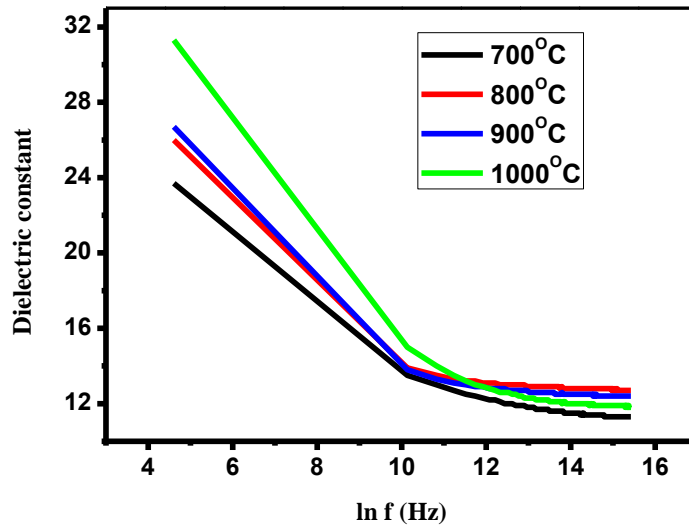


Figure 4.8: Variation of dielectric constant with frequency.

Behaviour of dielectric constant with respect to frequency is explained by knowing the polarization types. The dielectric constant is directly related to the electronic, atomic and orientational polarization of the material. Atomic and electronic polarization is persuaded by the applied field and it is caused by electronic displacement within the atoms. Orientational polarization exists only in polar compounds which possess permanent dipole moments. The first two polarizations do not vary with temperature but orientational polarization depends on temperature. All these polarization take place to a limited range of frequency after that range of frequency they start disappearance [185-186]. The plot of $\ln(F)$ and ϵ (figure 4.8) shows a higher value of ϵ for material annealed at 1000°C as compared to material annealed at other temperature. High value of dielectric constant (31) for sample annealed at 1000°C indicated that this material can be easily polarized by application of external electric field later its value decrease. The value of dielectric constant decreases with increasing frequency is due to decrease in polarization of space charge because dipole do not orient themselves fast when alternating electric field is applied with increasing frequency [187]. Sample annealed at 700°C shows minimum value of dielectric constant as compared to other samples which is even lower at high frequency. This sample has large number of dislocations which do not allow the charges to

orient. Upon annealing of same material at 800°C number of dislocations decreases and material allow orientation of charges in applied alternating current. By increasing the annealing temperature further in sample at 1000°C material response toward applied electric field changes. Semiconducting properties are greatly influenced by annealing because annealing increase the degree of ordering and affect physical properties of material. By increasing frequency Dielectric constant ϵ decreases. At higher temperature and lower frequency this decrease is very sharp. Because at low frequency all type of polarizability contributes including ionic, electronic, orientational and interfacial polarizability. The material acts as multicomponent of polarizability [188].

When frequency increases the rotation of dipoles is no longer to continue rapidly and dielectric constant going to decrease and reaches to a constant value at higher frequency. This constant value is due to interfacial type of polarization and is common for nonpolar material. Above figure 4.8 indicates that dielectric constant increases with increasing annealing temperature of material for all frequency ranges. This increased value of dielectric constant is very clear at low frequency and it is due to the reason that dipoles in polar material cannot be oriented at lower temperature and this orientation of dipole take place when we raise the temperature of synthesized material and value of dielectric constant increases as we increase the annealing temperature.

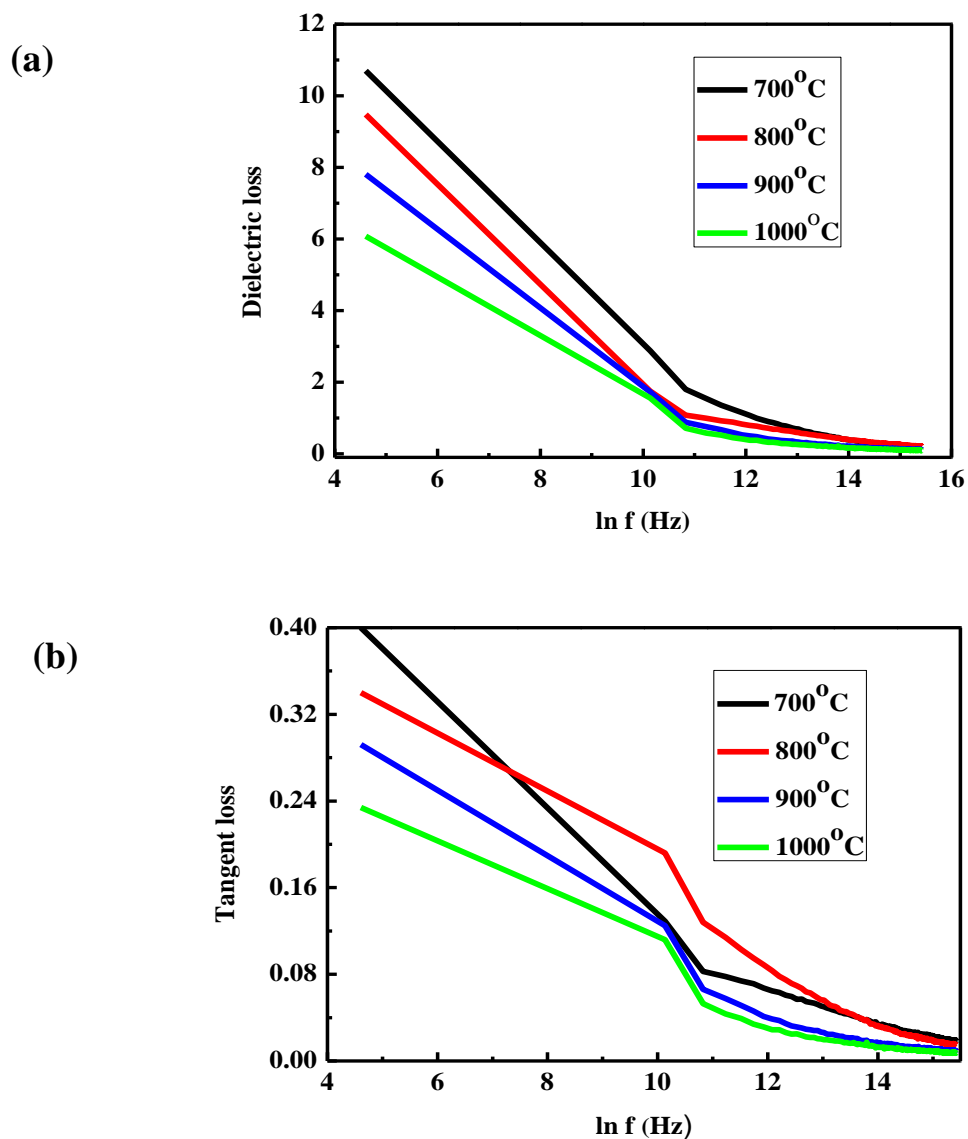


Figure 4.9: (a) plot of dielectric loss vs $\ln F$ (b) plot of tangent theta loss vs $\ln f$.

Dielectric loss and tangent loss show similar trend with frequency change (figure 4.9a and 4.9b). Values measured for dielectric loss for samples annealed at different temperatures (700, 800, 900 and 1000°C) are 10.7, 9.4, 7.8 and 6 respectively. The tangent loss or dissipation factor values for samples are 0.4, 0.3, 0.29 and 0.23. The value of tangent loss decreases with increasing annealing temperature because there is augmentation in the degree of crystallinity in a material by increasing temperature. Material annealed at 700°C has highest value of dielectric loss and

tangent loss and when same value is taken for material annealed at 1000°C these values are lower with respect to other three samples annealed at different temperatures. Conduction losses, dipolar losses and vibrational losses take place inside the material by application of alternating current which is responsible for dielectric loss factor and tangent loss [189].

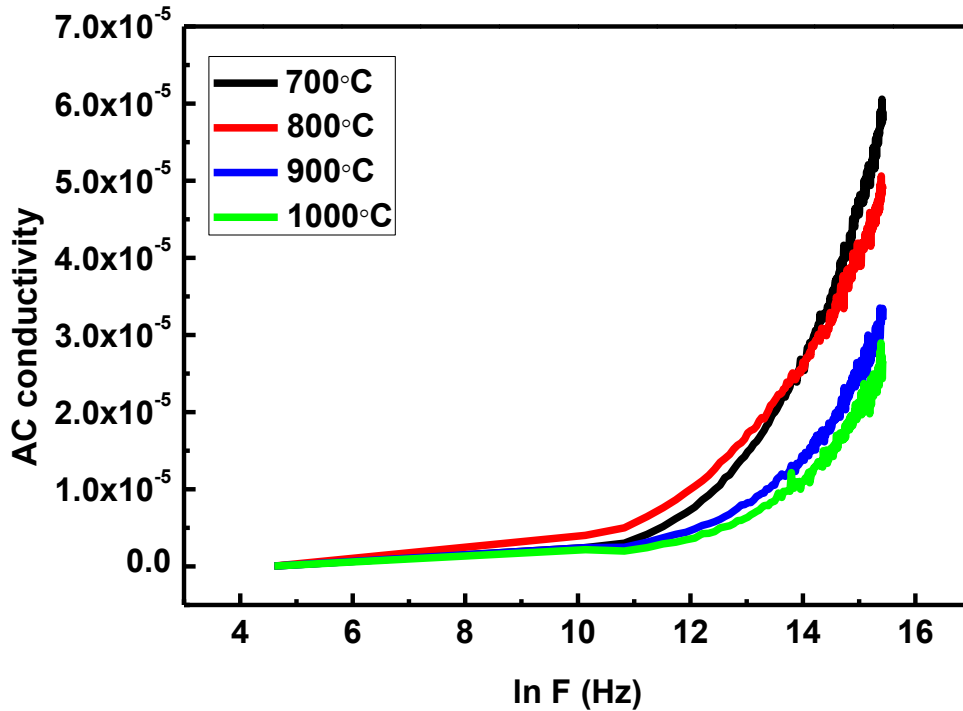


Figure 4.10: Variation of AC conductivity with frequency.

4th parameter is AC conductivity to designate the dielectric behavior of material. Figure 4.10 indicates the trend of AC conductivity in materials annealed at different temperatures. All materials show similar trend of AC conductivity at the starting point then at certain frequency changes are observed. Material annealed at 700°C show increase in AC conductivity at higher frequency due to alignment of particles. At high frequency there is phenomenon of electrons hopping which cause accretion in AC conductivity with frequency. Same trend is happened in material synthesized at 800°C. Figure 4.10 shows different behavior observed in materials annealed at 900°C and 1000°C [190],[178-179].

4.5 Mechanical Properties

Physical properties that a material exhibits by the application of force are called mechanical properties, for example tensile strength, elongation, hardness and modulus of elasticity etc. Indentation method is preferred over all other methods for measurement of mechanical properties because there is no specific requirement for a material i.e. any shape and size can be used for indentation method and it is a non-destructive method utilizing little amount of sample [191-195]

4.5.1 Hardness

Hardness is the ability of a material to resist the external mechanical action [196] and permanent deformation by indentation. It is a complex property which depends on loading forces, indentation size, grain size, defects and crystallographic orientations[119]. Rockwell, Brinell and Vickers methods are used for hardness measurements out of which Vickers hardness is the standard one for hard surfaces. Four samples of NaSbO_3 annealed at different temperatures (700°C , 800°C , 900°C , and 1000°C) were tested by Vickers hardness tester. The hardness of materials in terms of Vickers number (HV) is calculated by the following formula

$$\text{HV} = 1.854(\text{F}/\text{D}^2)$$

Where

F= applied load in Kgf

D= area of diagonal in mm

Table 4.3: Vickers hardness of samples.

| S/no | Sample | Hardness in (Hv) |
|------|----------------------------------|------------------|
| 1 | Annealed at 700°C | 792.3 |
| 2 | Annealed at 800°C | 457.3 |
| 3 | Annealed at 900°C | 301.4 |
| 4 | Annealed at 1000°C | 276.7 |

Material annealed at 700°C shows maximum hardness value as compared to other sample annealed at 800, 900 and 1000°C having hardness in Vickers number 457, 301 and 276Hv. Sample at 700°C annealed show hardness of 792.3Hv because this material has defects and dislocations as we are going to increase the annealing temperature the defect inside the material is reduced and particles inside become more organized making the material brittle due to development of perfect crystal planes. Increasing the annealing temperature results in increasing

the grain size of the material and there is inverse relation between grain size and hardness. Hardness decreases with increase in grain size [197-199], [148]. There is reduction in the grain boundary energy which causes reduction in grain boundary total area. During growth of grains, some grains are grown at the expense of already present grain in the material. Few grains ingest fine grained region and combine with large grain. Higher annealing temperatures are driving force for growth of grains and grain agglomeration [200-203].

1. Applications

Antimony in its pentavalent form retard the flammability when combined with halogens and form halogenated antimony compound which omits oxygen from the flame front [204-206]. Due to flame retardant property of sodium antimonate, it is tested as an additive for engine lubricating oil and it has tremendous effect on lubricating oil behavior by raising the flash point. This is great success of this work. For improvement of chemical and physical properties of lubricating oil, large number of chemicals were added into base oil these chemicals are called additives [207]. Additives provide desirable results in cheaper and economical way. Oil additives are usually added to prevent undesirable changes taking place during service in lubricating oils [208-209]. The purpose of the present research is to add sodium antimonate into engine oil and evaluate the produced changes in some of its properties [148].

4.6 Flash Point Elevation

It is the minimum temperature of petroleum products or other combustible fluids at which vapours are produced and form combustible mixture and it is the lowest temperature at which vapours and air mixture in the presence of small flame, flash. Flash point indicates the presence of volatile and combustible chemicals in a material. Measurement of flash point is necessary for lubricating oil used in transportation and storage requirement. High flash point is prime requirement for lubricating oils used in different engines of transports. Very heavy flash point is required for lubricating oils used in ships engine and heavy machinery vehicles. Because low flash point lubricating oils easily capture fire during service inside the engine [209]. Formerly, the flash point was developed for the purpose of determining the fire hazard of oils and fuels being used for storage and transportation. Sodium antimonates, when introduced in little amount in lubricating oil, enhance the flash point. In the present research work, the effect of NaSbO_3

addition as an additive is studied in 4 different engine lubricating oil. For this purpose 4 lubricating oils including Havoline, Castrol Active, Shell and Zic are taken for testing.

Table 4.4: Effect of NaSbO₃ on flash point of lubricating oil.

| Oil samples | Flash point °C | | | |
|-------------|----------------|-------|----------------|-----|
| | Havoline | Shell | Castrol Active | Zic |
| Virgin oil | 240 | 240 | 225 | 256 |
| 700°C | 250 | 245 | 235 | 262 |
| 800°C | 252 | 250 | 238 | 263 |
| 900°C | 253 | 254 | 244 | 264 |
| 1000°C | 255 | 260 | 248 | 265 |

It is clear from all data obtained from the experiment that NaSbO₃ addition in lubricating oil raises the flash point of lubricating oil and this trend is observed in different companies lubricating oils. This is great results of synthesized compound. Powder NaSbO₃ lower the surface area of the oil and its vapour pressure is reduced when vapour pressure of oil reduced it take higher temperature to produce vapours and flash point of oil was raised. Oils having high flash point are considered good for service inside the engine.

4.7 Effect on density of lubricating oil

Densities are affected by mass and volume. Lubricating oils densities are measured at 30°C for all samples prepared in 4 different oils. Mass of empty bottle was 16g and volume of bottle was 25ml.

$$\text{Density} = \text{mass} / \text{volume} = 18 \text{ [120]}$$

m_1 = mass of empty bottle

m_2 = mass of oil filled bottle

$$m = m_2 - m_1$$

Table 4.5: Effect of NaSbO₃ addition on densities of lubricating oil.

| Samples | Density (g/cm ³) | | | |
|---------------------------------|------------------------------|-------|----------------|-------|
| | Havoline | Shell | Castrol Active | Zic |
| Standard oil | 0.892 | 0.908 | 0.908 | 0.896 |
| Oil + NaSbO ₃ 700°C | 0.896 | 0.912 | 0.920 | 0.900 |
| Oil + NaSbO ₃ 800°C | 0.900 | 0.916 | 0.924 | 0.904 |
| Oil + NaSbO ₃ 900°C | 0.904 | 0.960 | 0.928 | 0.908 |
| Oil + NaSbO ₃ 1000°C | 0.908 | 0.964 | 0.932 | 0.912 |

Above table indicates that density of lubricating oil increases by increasing the annealing temperature of the added material in all types of lubricating oil mentioned above.

4.8 Specific gravity

It is the ratio of liquid density with water density at particular temperature 30°C density of water is noted in the same way as given above. The density of water calculated by following above method is 1 g/cm³.

Specific gravity = Density of sample / Density of water [122]

Table 4.6: Effect of NaSbO₃ addition on specific gravities of lubricating oils.

| Samples | Specific Gravity | | | |
|---------------------------------|------------------|-------|----------------|-------|
| | Havoline | Shell | Castrol Active | Zic |
| Standard oil | 0.892 | 0.908 | 0.908 | 0.896 |
| Oil + NaSbO ₃ 700°C | 0.896 | 0.912 | 0.920 | 0.900 |
| Oil + NaSbO ₃ 800°C | 0.900 | 0.916 | 0.924 | 0.904 |
| Oil + NaSbO ₃ 900°C | 0.904 | 0.960 | 0.928 | 0.908 |
| Oil + NaSbO ₃ 1000°C | 0.908 | 0.964 | 0.932 | 0.912 |

After adding little amount of powdered NaSbO₃ into lubricating oil, the specific gravity of oil sample was measured. The value of specific gravity of lubricating oil was increases by adding NaSbO₃ and it was further increases by adding the material annealed at higher temperature.

4.9 Viscosity

Resistance offered to the flow of liquid is called viscosity. Two types of viscosity of lubricating oils are measured after addition of little amount of NaSbO₃ powder kinematic viscosity and dynamic viscosity or absolute viscosity

4.9.1 Kinematic viscosity

It was measured by using IP method number 71/78 (ASTM D445-87). Viscometer was used after thorough cleaning and time for liquid flow was calculated between two marks on the bulb of viscometer. Following formula is used for measuring kinematic viscosity of oils after NaSbO₃ addition [123].

$$\mu = C.t$$

Where

μ = kinematic viscosity

C = calibration constant of viscometer

t = time of flow between two marks

Table 4.7: Effect of NaSbO₃ addition on kinematic viscosity of lubricating oils.

| Samples | Kinematic Viscosity (cSt) | | | |
|---------------------------------|---------------------------|-------|----------------|-------|
| | Havoline | Shell | Castrol Active | Zic |
| Standard oil | 229.1 | 238.1 | 237.7 | 232.1 |
| Oil + NaSbO ₃ 700°C | 208.1 | 215.2 | 214.2 | 212.1 |
| Oil + NaSbO ₃ 800°C | 216.4 | 218.3 | 217.3 | 216.2 |
| Oil + NaSbO ₃ 900°C | 223.2 | 221.5 | 220.4 | 220.3 |
| Oil + NaSbO ₃ 1000°C | 224.1 | 223.3 | 223.2 | 222.1 |

The addition of NaSbO₃ powder annealed at 700°C decreased the kinematic viscosity and at higher annealing temperatures it increases. Powder NaSbO₃ trapped within the layer of oils and affect its viscosity and material annealed at higher temperature raised the viscosity of lubricating oil.

4.9.2 Dynamic Viscosity

Dynamic viscosities of all samples were calculated from kinematic viscosity, μ and density (ρ) by means of following equation

$$V = d\mu$$

Where

V = dynamic viscosity

d = density of sample

μ = kinematic viscosity

Table 4.8: Effect of NaSbO₃ addition on Dynamic viscosity of lubricating oils.

| Samples | Dynamic Viscosity (cP) | | | |
|---------------------------------|------------------------|-------|----------------|-------|
| | Havoline | Shell | Castrol Active | Zic |
| Standard oil | 204.3 | 216.1 | 215.8 | 207.9 |
| Oil + NaSbO ₃ 700°C | 186.4 | 196.2 | 197.0 | 190.8 |
| Oil + NaSbO ₃ 800°C | 194.7 | 199.9 | 200.7 | 195.4 |
| Oil + NaSbO ₃ 900°C | 201.7 | 212.6 | 204.5 | 200.0 |
| Oil + NaSbO ₃ 1000°C | 203.4 | 215.2 | 208.0 | 202.5 |

Value of dynamic viscosity decreases by adding NaSbO₃ powder annealed at 700°C and then gradually increases by raising the annealing temperature. Viscosities of all types of lubricating oil increased by increasing the annealing temperature of the added material.

Summary and future prospect

Sodium antimonite is successfully synthesized by solid state method using cheap precursor NaCl and synthesized compound is further annealed at four different temperatures i.e. 700, 800, 900, and 1000°C. All previous method of NaSbO₃ synthesis reported in literature used salts excluding NaCl and different synthesis routes have been followed. XRPD analysis was carried out to confirm the phases, crystallite size purity and crystal structure of synthesized compound. Crystal structure was rhombohedral and material was polycrystalline at higher temperature. SEM analysis reveals the elemental composition which was 1:1:3 NaSbO₃ and material annealed at higher temperature show uniform geometry. Optical band gap was calculated by using DRS technique and its value is increased at higher temperature because material become insulator at higher annealing temperature. Material annealed at 700°C has 2.eV band gap and material at 1000°C has 3.80eV band gap energy. Dielectric behavior of the material is measured by LCR meter and material annealed at higher temperature show maximum value of dielectric constant with frequency. tangent loss and dielectric loss values are inversely proportional to dielectric constant these values are maximum for material annealed at lower temperature because material at low annealing temperature is not organized and its particle dissipate maximum energy to orient according to applied electric field. AC conductivity is higher for material annealed at lower temperature than other annealed at higher temperatures. By increasing the frequency electron overhopping phenomenon is more prominent which result high value of AC conductivity. Mechanical properties of the material is measured and material annealed at lower temperature show maximum value of hardness (792Hv) and by raising the annealing temperature material become brittle and its hardness is reduced. Due to stable and flame retarding ability of NaSbO₃ it is introduced as an additive into lubricating oil in little quantity and after addition quality parameters of lubricating oils were measured and compared with virgin oil. flash point of lubricating oils was increased to 10 degree by NaSbO₃ addition. Viscosity including kinematic and dynamic also lower by NaSbO₃ addition. Specific gravity and density of lubricating oils with NaSbO₃ also increased. Improvement in quality parameters results better lubricating oil quality.

NaSbO₃ is used as a semiconducting material due to having optical band gap 2.4 and having dielectric behavior it is used in electronics and capacitors. having good impact on properties of lubricating oil it can be used as an additive in future to improve the quality of lubricating oil.

References

- [1] D. R. Lide, "Magnetic susceptibility of the elements and inorganic compounds", CRC Handbook of Chemistry and Physics, 86th ed. 474, 2005.
- [2] K. H. Alber, "Types of Alloys,". Battery Technology Handbook. CRC Press. 60–61, 2003.
- [3] J. Carlin, F. James, "Mineral Commodity Summaries: Antimony," *United States Geological Survey*. Retrieved 23 January 2012.
- [4] W. C. Butterman, J. F. Carlin, "Mineral Commodity Profiles: Antimony," *United States Geological Survey*, 2003.
- [5] Willardson, R. K. Beer, C. Albert, "Infrared detectors," 15, 1970.
- [6] W. Omara, R. B. Herring, L.P. Hunt, "Handbook of semiconductor silicon technology," 2007.
- [7] A. Harder, "Chemotherapeutic approaches to schistosomes: Current knowledge and outlook,". *Parasitology Research*, **88**, 395–7, 2002.
- [8] A. Kassirsky, N. N. Plotnikov, "Diseases of Warm Lands," A Clinical Manual, 262–265.1 august 2003.
- [9] D. L. Reger, R.S. Goode, D. W. Ball, "Chemistry: Principles and Practice," 3rd ed. Cengage Learning. 883, 2009.
- [10] M. Dratovsky and J. Karlicek, "Lithium and sodium antimonate," *J. Chem. Zvesti*, 35 (5), 629—640, 1981.
- [11] P. Benjamin, D. Laune, D. Ryan, Bayliss and C. Greaves, "LiSbO₂ Synthesis, Structure, Stability, and Lithium-Ion Conductivity," *J. Inorg. Chem*, 50, 7880–7885, 2011.
- [12] E. R. Meneses, "Synthesis and characterization of NaSbO₃," *J. Superficies y Vacío*, 20, 14-18, 2007.
- [13] L. Y. long, L. Z. Hua, "Investigation on Technology of Sodium Antimonate Synthesis from Antimony Concentrate by Chloridizing Leaching Process," *J. CNKI*, 2007.
- [14] D. P. Chen, W. Bowers and S. E. Skrabalak, "Aerosol-Assisted Combustion Synthesis of Single-Crystalline NaSbO₃ Nanoplates A Topotactic Template for Ilmenite AgSbO₃," *J. Chem. Mater*, **27**, 174 –180, 2015.
- [15] D. J. Stewart and O. Knop, Pyrochlores. VI. "Preparative chemistry of sodium and silver antimonates and related compounds," *Canadian journal of chemistry*, **48**, 1970.
- [16] B. A. Wechsler and C. T. Prewitt, "Crystal structure of ilmenite (FeTiO₃) at high temperature and at high pressure," *J. American Mineralogist*, **69**, 176-185, 1964.
- [17] R. A. P. Rabiero, S.R. de Lazaro, "Structural, electronic and elastic properties of FeBO₃ (B = Ti, Sn, Si, Zr) ilmenite: a density functional theory study," *RSC Adv.*, **4**, 59839-59846, 2014.
- [18] J. L. Waring, R. S. Roth, H. S. Parker, and W. S. Brower, "Phase Equilibria and Crystal Growth in the Alkali Antimonate Systems Sb₂O₄-NaSbO₃, Sb₂O₄-KSbO₃, and Sb₂O₄-NaSbO₃-NaF," *Journal of research of the National Bureau of Standards-A. Physics and Chemistry*, **80**, 5-6, 1976.
- [19] V. B. Nalbandyan, M. Avdeev, A. A. Pospelov, "Ion exchange reactions of NaSbO₃ and morphotropic series MSbO₃, *Solid State Sciences*," **8**, 1430–1437, 2006.
- [20] W.S. Brower, D. B. minor, "flux synthesis of cubic potassium antimonates," *J. pergamon press inc*, **9**, 1974.
- [21] S. B. Kasenova, S. A. Khaidargalieva, B. K. Kasenov, "Heat capacity and thermodynamical functions of RbSbO₃ within range 289.15-673K," **6**(1), 34-36; 1999.

- [22] G. kalpana and M.T. weller, $\text{Rb}_2\text{Sb}_4\text{O}_{11}$, *J. Acta Cryst*, **65**, 41, 2009.
- [23] B. Mason and Charles, "Bystromite, Magnesium antimonate, A new mineral," *J. Vitaliano*, Indiana University, Bloomington, Indiana 1951.
- [24] B. G. Deboer, R.A young and A. sakthivel, "X-Ray Rietveld structure refinement of Ca, Sr and barium meta antimonates," *J. Acta, Cryst C50*, 476-482, 1994.
- [25] V. V. Zyryanov, V. G. Ponomareva and G. V. Lavrova, "Preparation, Structure, and Electrical Conductivity of Calcium-Antimonate-Based Materials," *J. inorganic material*, **42**, 2006.
- [26] R. Huang, X. Xu, J. Zhu, W. Liu, R. Yuan, X. Fu, Y. Zhang, Z. Li, "Nanocrystalline $\text{CaSb}_2\text{O}_5(\text{OH})_2$ and $\text{Ca}_2\text{Sb}_2\text{O}_7$: Controlled syntheses, electronic structures and photocatalytic activity," *J. Applied Catalysis B: Environmental*, **127**, 205–211, 2012.
- [27] L. Chelazzi, T. B. Ballaran, F. Nestola, L. Bindi, P. Bonazzi, "High-pressure behavior of the synthetic $\text{Ca}_2\text{Sb}_2\text{O}_7$ weberite-type compound," *J. solid state sciences* **13**, 1092-1095, 2011.
- [28] G. Cornelis, T. V. Gerven, R. Snellings, B. Verbinnen, J. Elsen, Carlo Vandecasteele, "Stability of pyrochlores in alkaline matrices: Solubility of calcium antimonate," *J. Applied Geochemistry*, **26**, 809–817, 2011.
- [29] L. Geng, C. Y. Meng, M. M. Wang, K. Dai, C. Shingli, W. D. Cheng, "Synthesis and crystal structure of a novel layered Barium Antimonate $\text{Ba}_2\text{Sb}_7\text{O}_{13}(\text{OH})$ with mixed valence antimony," *J. solid state sciences*, **44**, 27–31, 2015.
- [30] H. Xue, Yanying Chen, Nan Ding, Qinghua Chen, Yongjin Luo, Xiping Liu, Liren Xiao, Qingrong Qian, "Hydrothermal synthesis of $\text{Sr}_{1.36}\text{Sb}_2\text{O}_6$ nano-octahedrons with photocatalytic activity for overall splitting of water," *J. Catalysis Communications*, **74**, 5–9, 2016.
- [31] L. Geng, C. Y. Meng, C. S. Lin, W. D. Cheng, "A new strontium Antimonite III $\text{Sr}_5\text{Sb}_{22}\text{O}_{38}$: Synthesis, Crystal structure and characterizations," *Journal of Solid State Chemistry*, **203**, 74–78, 2013.
- [32] E. Chinarro, G. C. Mather, A. Caballero, M. Saidi, E. Moran, "Synthesis, characterizati and ionic conductivity of $\text{Sr}_{1.5}\text{Sb}_{0.5}\text{O}_{3-y}$ ($y = 0.25$)," *J. Solid State Sciences*, **10**, 645-6 (2008).
- [33] B. Gerhard, "Process for preparing indium and scandium antimonates," US 3449064 A Jun 10, 1969.
- [34] C. B. Amphlett, L. A. McDonald and M. J. Redman, "Synthetic inorganic ion-exchange materials-I zirconium phosphate," *J. Inorg. Nucl. Chem*, **6**, 236, 1958.
- [35] G. H. Nancollas and R. Paterson, "Thermodynamics of ion exchange on hydrous Zirconia," *J. Inorg. Nucl. Chern*, **29**, 565, 1967.
- [36] L. Kullberg, "A review of "Inorganic Ion Exchange Materials,"". Edited by A. Clearfield (Texas ASM University). CRC Press, Inc, Boca Raton, Fl. 304, 1982.
- [37] M. Abe and T. Ito, Bull, "Synthetic Inorganic Ion-exchange Materials. X. Preparation and Properties of So-called Antimonic(V) Acid," *Soc. Jpn., i!* 333, 1968.
- [38] L. H; Baetsle, D. Huy and Guerry, "Structure and ion exchange characteristic of polyantimonic acid," *J. Inorg. Nucl. Chem.*, **30**, 639, 1968.
- [39] F. Girardi, R. Pietra and E. Sabbioni, "Radiochemical separation by retention on ionic precipitate .adsorption test on ionic materials," *J. Radioanal. Chem.*, **5**, 141, 1970.
- [40] Y. Inoue and M. Tsuji, "Hydrous Titanium Oxide Ion Exchanger," *j.nuclear science and technology*, **13**, 51, 1976.

- [41] M. Tsuji and M. Abe, "synthetic inorganic ion-exchange materials xxxvi. synthesis of cryptomelane-type hydrous manganese dioxide as an ion-exchange material and their ion-exchange selectivities towards alkali and alkaline earth metal ions Solv. Extr. and Ion Exchange," **2**, 253-274, 2007.
- [42] M. tsuji and M. abe, "Separation of trace amounts of Ca²⁺ and Sr²⁺ from K⁺ and Rb⁺ with a hydrous manganese dioxide ion exchanger.radioisotopes," **21**, 218, 1984.
- [43] M. Abe, R. Chitrakar, M. Tsuji and K. Fukumoto, "Synthesis of titanium(IV) antimonates and their ion exchange properties for alkali and alkaline earth metal ion," **11**, 693-712, 1993.
- [44] T. Moller, R. Harjula, P. Kelokaski, K. Vaaramaa, P. Karhu and J. Lehto, "Titanium antimonates in various Ti : Sb ratios: ion exchange properties for radionuclide ions," *J. Mater. Chem* , **13**, 535–541, 2003.
- [45] V. Vesely and V. Pekarek, "Synthetic inorganic ion exchangers—II: Salts of heteropolyacids, insoluble ferrocyanides, synthetic aluminosilicates and miscellaneous exchangers," *J. Inorg. Nuclear Chem*, **84**, 697,1963.
- [46] M. Qureshi and V. Kuma, "Synthesis and Ion-exchange Characteristics of Titanium Antimonate," *J. Chem. SOC.(A)* 1970.
- [47] Dorian, A. H. Hanaor, C. Charles, Sorrell, "Review of the anatase to rutile phase transformation," *J Mater Sci.*, **46**, 855–874, 2011.
- [48] J. F. Banfield, D. R. Veble, D. Smith, "The identification of naturally occurring TiO₂ (B) by structure determination using high resolution electron microscopy, image simulation, and distance-least-squares refinement," *J., Am. Mineral*, **76**, 343, 1991.
- [49] F.J. Berry and P. M. Gogarty, "Twin boundaries in antimony(v)-doped rutile titanium(iv) oxide, *J. Solid State Communications*," **64**, pp. 273-275, 1987.
- [50] F. J. Berry and M. Brett, "Reactions Between the Oxides of Antimony and Vanadium," *J. Inorganica Chimica Acta*, **81** 133-135, 1984.
- [51] Centi, G., S. Perathoner and F. Trifiro. (1997). V-Sb-oxide catalysts for the ammoxidation of propane. *Appl. Catal. A: General*. **157**: 143-172.
- [52] Grasselli, R.K. (1999). Advances and Future Trends in Selective Oxidation and Ammoxidation Catalysis. *Catal. Today*. **49**: 141-153(1999)
- [53] Y. H. Taufiq-Yap¹, Ita Yee-Ping Jong¹, Mohd. Zobir Hussein¹, Zulkarnain Zainal¹, Irmawati Ramli¹ and Rusnah Samsuddin, Physico-Chemical Characterisation of V-Sb-Oxide Catalysts Prepared by Three Different Methods, *Malaysian Journal of Analytical Sciences*, Vol. 7, No. 2, 423-430(2001)
- [54] J. N. Moralesa, L. S. Ncheza, M.N. Francisco, F. Berry, "Electrochemical reaction of lithium with nanosized vanadium antimonate," *Journal of Solid State Chemistry* **179**, 2554 – 2561, 2006.
- [55] C. S. Sunandana, "ESR evidence for the existence of rutile-type, non stoichiometric vanadium antimonate," *Mat. Res. Bull.*, **19**, 325-329, 1984.
- [56] R. G. Teller, M.R. antonio, J. F. brazdil, and R. K Grasselli, "New Materials Synthesis: Characterization of Some Metal-Doped Antimony Oxides," *journal of solid state chemistry* **64**, 249-260, 1986.
- [57] N. Ballarini, F.J. Berry, F. Cavani, M. Cimini , X. Ren, D. Tamoni, F. Trifiro, "The synthesis of rutile-type V/Sb mixed oxides, catalysts for the ammoxidation of propane to acrylonitrile A comparison of high-energy milling and co-precipitation methods," *Catalysis Today* **128**, 161–167, 2007.
- [58] A.T. Gutmann, R.K. Grasselli, J.F. Brazdil, U.S. Patent 4,746,641 and 4,788,317(1988).
- [59] L.C. Glaeser, J.F. Brazdil, D.D. Suresh, D.A. Omdoff, R.K. Grasselli U.S. Patent
- [60] M.A. Tort, J.F. Brazdil, L.C. Glaeser, U.S. Patent 4,784,979 (1988).

- [61] C.S. Lynch, L.C. Glaeser, J.F. Br, M.A. Tort, U.S. Patent 5,094,989 (1992).
- [62] J. Mathew, S. N. Tandon, "Chromium Antimonate as an Ion-Exchanger," *Chromatographia*, Vol. **9**, No. 5, May 1976
- [63] M. A. Subramanian and a.clearfield, synthesis and solid state studies on $Mn_2Sb_2O_7$ and $(Mn_{1-x}Cd_x)_2Sb_2O_7$ pyrochlores," *journal of solid state chemistry*, **52**, 124-129, 1984.
- [64] H. G. Scott, "Synthesis and Crystal Structures of the Manganous Antimonates $Mn_2Sb_2O_7$ and $MnSb_2O_5$," *journal of solid state chemistry* **66**, 171-180, 1987.
- [65] X. Turrillas, H. Vincent, "Manganese antimony oxide, i. rasines. manganese antimony oxide," *rev. chirn le minrale*, **22**, 625, 1985
- [66] R. g. teller, mark r. antonio, james f. brazdil, and robert k. grasselli, New Materials Synthesis: Characterization of Some Metal-Doped Antimony Oxides, *journal of solid state chemistry* **64**, 249-260 (1986)
- [67] R. D. Bayliss, F. J. Berry, B. P. de Laune, C. Greaves, O. Helgason, J. F. Marco, M F Thomas, L Vergara and M. J. Whitake, "Magnetic interaction in ferrous antimonite, $FeSb_2O_4$, and some derivatives," *J. Phys.: Condens. Matter*, **24**, 7, 2012.
- [68] J. P. Rawat and D. K. Singh, "synthesis, ion-exchange properties and analytical applications of iron(iii) antimonate," *Analytica Chimica Acta*. **87**, 157-162, 1976.
- [69] P. Nag, S. Banerjee, Y. Lee, A. Bumajdad, Y. Lee and P. Sujatha Devi, "Sonochemical Synthesis and Properties of Nanoparticles of $FeSbO_4$," *Inorg. Chem*, **51**, 844 –850, 2012.
- [70] S. Singh, V. Gupta, B.C. Yadav, P. Tandon, A. K. Singh, "Structural analysis of nanostructured iron antimonate by experimental and quantum chemical simulation and its LPG sensing, sensor and actuator," **195**, 373-381, 2014.
- [71] Z. Qinggang, H. U. Xiaohong, Z. Dan, Z. Guozhu, P. Tianyou, "Synthesis and Electrochemical Properties of $FeSbO_4$ Nanorods," *Wuhan University Journal of Natural Sciences*, **18** No.3, 2013.
- [72] M. D. Allen, S. Poulston, E. G. Bithell, M. J. Goringe and Mike Bowke, "An XPS, TEM, and TPD Study of the Oxidation and Amoxidation of Propene Using Mixed Fe–Sb Oxide Catalysts," *journal of catalysis* **163**, 204–214 (1996).
- [73] Aslam, M. M. Rahman, Sher Bahadar Khan, Mohd. Faisal , Kalsoom Akhtar, Malik Abdul Rub, Abdullah M. Asiri , Abdulrahman O. Al-Youbi, Cobalt doped antimony oxide nano-particles based chemical sensor and photo-catalyst for environmental pollutants, *Applied Surface Science* **261**, 52–58(2012)
- [74] P. Norby, M. Roelsgaard, M. Søndergaard and B. B. Iversen, "Hydrothermal Synthesis of $CoSb_2O_4$: In Situ Powder X-ray Diffraction, Crystal Structure, and Electrochemical Properties," *Cryst. Growth Des.* **16**, 834 –841, (2016).
- [75] C. R. Michael, H. G. Bonilla, A. H. M. Preciado, J. P. M. Lazaro, "Synthesis and gas sensing properties of nanostructured $CoSb_2O_6$ microsphere," *sensors and actuators*, **143**, 278-285, 2009.
- [76] O. A. Fouad , A. M. Hassan, H. AbdElWahab, A. MohyEldin, AbdelRahman, M. Naser, Osama, A.G. Wahba, "Synthesis, characterization and application of some nanosized mixed metal oxides as high heat resistant pigments: Ca_2CuO_3 , $Ca_3Co_2O_6$, and $NiSb_2O_6$," *Journal of Alloys and Compounds* **537**, 165–170(2012).
- [77] S. Z. Alabdeen1 Ibrahim Ismail2, Studying the Structural Changes of $NiSb_2O_4$ by Temperature Using Sol-Gel Method, *Chemistry and Materials Research*, **8**, 2224-3224, 2016.
- [78] M. Qureshi, K. G. Varshney and N. Fatima, "synthesis and ion-exchange behaviour of nickel and cobalt antimonates," *Journal of Chronofography*, **169**, 365-372(1979).
- [79] T. J. Cassidy, M. Pollastri and F. Trifiro, "Amoxidation of Propane on Nickel

- Antimonates The Role of Vanadium as Promoter,” *Journal of catalysis*, **172**, 55–63, 1997.
- [80] D. O. Scanlona and A. Walsh, “Polymorph engineering of Cu M O₂ (M = Al, Ga, Sc, Y) semiconductors for solar energy applications: from delafossite to wurtzite,” *J. Acta Cryst.*, **71**, 702–706, 2015.
- [81] E. C. Pascual, P. Norby, N. H. Andersen, P. W. Stephens, H.W. Zandbergen, J. Larsen and R. J. Cava, “Spin 1/2 Delafossite Honeycomb Compound Cu₅SbO₆,” *J. American chemical society Inorg. Chem.* **51**, 557–565, 2012.
- [82] W.W. Focke, S. F. Mkhize, R. Storey, O. D. Fabbro and Elmar Muller, “facile synthesis of copper antimonite,” *Taylor & francis group, chem. eng. comm.*, **201**, 153–159, 2014.
- [83] M. T. Atanasova, A. M. Strydom, C. J. H. Schutte, L. C. Prinsloo, W. W. Focke, “Crystal structure and magnetic properties of CuSb₂O₄,” *J Mater Sci* , **49**, 3497–3510, 2014.
- [84] T. N. Koltsova and A. E. Chastukhin, “Phase Relations in the Cu–Sb–O System,” *Inorganic Materials*, **38**, No. 12, 1228–1234, 2002.
- [85] J. Singh, N. Bhardwaj and S. Uma, “Single step hydrothermal based synthesis of M(ii)Sb₂O₆ (m = cd and zn) type antimonates and their photocatalytic properties,” *Bull. Mater. Sci.*, **36**, No. 2, 287–291, 2013.
- [86] N. Kikuchi, W. Z. H. Hosono and H. Kawazoe, “Carrier Generation in Wide-Gap Conductor, Zinc Antimonate,” *J. Am. Ceram. Soc.*, **88**, 2793–2797, (2005).
- [87] G. Z. Zang, J. F. Wang, H. C. Chen, W. B. Su, C.M. Wang, P. Qi, B.Q. Ming, J. Du, L.M. Zheng, “Perovskite (Na_{0.5}K_{0.5})_{1-x}(LiSb)_xNb_{1-x}O₃(Na_{0.5}K_{0.5})_{1-x}(LiSb)_xNb_{1-x}O₃ lead-free piezoceramics,” *Appl. Physics. Lett.* **88**, 212908 (2006).
- [88] S. C. Grund, H. Kunibert, H. J. Breunig, H. U. Wolf , "Antimony and Antimony Compounds," *Ullmann's Encyclopedia of Industrial Chemistry*, Wiley-VCH, Weinheim, 2000.
- [89] Norman, C. Nicholas, “Chemistry of arsenic, antimony, and bismuth,” 45, 1998.
- [90] N. J. Wilson, D. Craw, K. Hunter, "Antimony distribution and environmental mobility at an historic antimony smelter site, New Zealand,” *Environmental Pollution* **129**, 257–266, 2004.
- [91] E. D. Weil, S. V. Levchik, “Flame retardants for plastics and textiles: Practical applications,” **4**, 2009.
- [92] X. Lin, F. Huang, W. Wang, Y. Wang, Y. Xia, J. Shi, Photocatalytic activities of M₂Sb₂O₇ (M = Ca, Sr) for degrading methyl orange, *Appl. Catal. A: Gen*, Vol 313, 218-223(2006)
- [93] J. N. Moralesa, L. S. ncheza, F. Martin, F. Berry, “Electrochemical reaction of lithium with nanosized vanadium antimonate,” *Journal of Solid State Chemistry* **179**, 2554 – 2561, (2006).
- [94] Donaldson, J. D. Kjekshus, Nicholson, D.G, “ Properties of Sb-Compounds with Rutile-like Structures,” *Acta Chem. Scand., Ser.*, **29**, 803–809, 1975.
- [95] S. Bang, S. Lee, T. Park, Y. Ko, S. Shin, S.Y. Yim, H. Seo, H. Jeon, “Dual optical functionality of local surface plasmon resonance for RuO₂ nanoparticle–ZnO nanorod hybrids grown by atomic layer deposition,” *J. Mater.chem.*, **22**, 14141-14148, (2012).
- [96] Ricco, I. M. M., Conradie, C., and Focke, W. W. (2004). Alternative oxidants for silicon fuel in time-delay compositions, *Combust. Sci. Technol.* , 176, 1565–1575(2004)
- [97] M. Abe and T. Ito, Bull, “Synthetic Inorganic Ion-exchange Materials. X. Preparation and Properties of So-called Antimonic(V) Acid,” *Chem Soc. Jpn.*,

- 333 (1968).
- [98] A. Jamal, M. M. Rahman, S. B. Khan, M. Faisal, K. Akhtar, M. A. Rub, A. M. Asiri, A. O. Al-Youbi, "Cobalt doped antimony oxide nano-particles based chemical sensor and photo-catalyst for environmental pollutants," *J. Applied Surface Science*, 261, 52–58, 2012.
- [99] S. Lahlil, I. Biron, M. Cotte, J. Susini, "New insight on the in situ crystallization of calcium antimonate opacified glass during the Roman period," *J. Appl Phys A* **100**, 683–692, (2010).
- [100] W. E. S. Turner, H. P. Rooksby, Sonderband:, "A Study of the Opal-ising Agents in Ancient Opal Glasses throughout Three Thousand Four Hundred Years," Sonderband: V. Int. Glaskongreb, 28, (1959).
- [101] O. A. Fouad , A. M. Hassan, H. AbdElWahab, A. MohyEldin, AbdelRahman, M. Naser, Osama, A.G. Wahba, "Synthesis, characterization and application of some nanosized mixed metal oxides as high heat resistant pigments: Ca₂CuO₃, Ca₃Co₂O₆, and NiSb₂O₆," *Journal of Alloys and Compounds* **537**, 165–170(2012).
- [102] R. Huang, X. Xu, J. Zhu, W. Liu, R. Yuan, X. Fu, Y. Zhang, Z. Li, "Nanocrystalline CaSb₂O₅(OH)₂ and Ca₂Sb₂O₇: Controlled syntheses, electronic structures and photocatalytic activity," *J. Applied Catalysis B: Environmental*, **127**, 205–211, 2012
- [103] Y.Cho, C. Lee, Y. Hwang, M. Park, J. Lee , C. Choi, M. Jung, "Tribological behavior of copper nanoparticles as additives in oil," *Curr Appl Phys* **9**:124–127, (2009).
- [104] C.G. Lee, Y. J. Hwang, Y. M. Cho, J. K. Lee, C. Choi, J. M. Oh, "A study on the tribological characteristics of graphite nano lubricants," *Int J Precis Eng Manuf* **10**:85–90, (2009).
- [105] Purdue University, West Lafayette, IN 47907, (765) 494-4600, 2014
- [106] C. Zeiss, "Applications of Scanning Electron Microscopes in Forensic Investigations," *AZO Materials*, nov 16, 2010.
- [107] J.Goldstein, "Scanning electron microscopy and x-ray microanalysis". Kluwer Academic / Plenum Publishers, 689, 2003.
- [108] ASTM D 150, Standard Test Methods for A-C Loss Characteristics and Permittivity (Dielectric Constant) of Solid Electrical Insulating Materials
- [109] ASTM D 1531, Standard Methods for Relative Permittivity (Dielectric Constant) and Dissipation Factor by Fluid Displacement Procedures
- [110] H. G. Scott, "Synthesis and Crystal Structures of the Manganous Antimonates Mn₂Sb₂O₇ and MnSb₂O₅," *journal of solid state chemistry* **66**, 171-180, 1987.
- [111] P. Hanrahan and W.Krueger,"Reflection from layered surfaces due to subsurface scattering," *SIGGRAPH* , **27**, 165–174, 1993
- [112] F. Kawano, T. Ohguri, T. Ichikawa, I. Mizuno, Hasegawa "A. Shock absorbability and hardness of commercially available denture teeth" *Int J Prosthodont*, **15**, 243–247, 2002.
- [113] Y. Ab, Y. Sat, Y. Akagawa, S. Ohkawa, "An in vitro study of high-strength resin posterior denture tooth wear," *Int J Prosthodont*, **10**, 28–34, 1997.
- [114] Y. Abe, Y. Sato , T.Taji , Y. Akagawa, P. Lambrechts , G. Vanherle, "An in vitro wear study of posterior denture tooth materials on human enamel," *J Oral Rehabil* **28**, 407–412 , 2001.
- [115] A.Yap, K. Wee, S. Teoh, "Effects of cyclic temperature changes on hardness of composite restoratives," *Oper Dent*, **27**, 25-29, 2002.
- [116] J.S Tse, "Intrinsic hardness of crystalline solids," *J. Superhard Mater*, **32**, 177-191, 2012.
- [117] R. Kaner, J. Gilman, S. Tolbert, "Designing superhard materials," *Science*, **308**, 1268, 2005.

- [118] A.Szymanski, J. Szymanski, "Hardness estimation of minerals rocks and ceramic materials," Amsterdam: *Elsevier*, 1989.
- [119] J. Gilman, "Hardness e a strength microprobe," The science of hardness testing and its research applications, *American Society of Metals*, Metal Park ohio, 1973
- [120] Test method for density and specific gravity of plastic by displacement. ASTM standard D 792 Vol 81.01 American society for testing and material.
- [121] ASBC method of analysis Extract in wort and beer, American society of brewing chemists, St paul, 2009
- [122] F.P. Incorporea , P. D. Dewit, "Fundamentals of heat and mass transfer", Wiley, 2007.
- [123] M. Gerstein and W.B. Stine, "Anomalies in flash points of liquid mixtures," *Ind Eng Chem Prod Res Dev*, **12**, 253–255, 1973.
- [124] J. L. Scheffey and D.C. Tabar, "Hazard rating system for flammable and combustible liquids," *Process Safety Prog*, **15**, 230–236, 1996.
- [125] B.C. Sharma and O. P. Gandhi, "Performance evaluation and analysis of lubricating oil using parameter profile approach," *Industrial Lubrication and Tribology*, **60**, 131 – 137, 2008
- [126] ASTM D 445-04, Standard test method for kinematic viscosity of transparent and opaque liquids (and the calculation of dynamic viscosity), Annual Book of Standards, American Society for Testing and Materials, West Conshohocken, PA,35, 2004
- [127] R. R. Mohammed, I. A.R. Ibrahim, A. H. Taha, G. McKay, " Waste lubricating oil treatment by extraction and adsorption," *Chemical Engineering Journal.*, 220 343–35, 2013.
- [128] (ASTM) Test method for flash point by the equilibrium method with a closed cup apparatus
- [129] H. Emmerson, "The advantage of used oil re-refining," Technical Report, Bartlesville Energy Technology Center, Bartlesville, USA, 1980.
- [130] (ASTM D2896-98) standard test method for base number of petroleum products by potentiometric titration
- [131] J. H. Gilks, "Antioxidants for petroleum products," *J Inst Petrol*, 50(491), 309.1964
- [132] L. R. Mahoney, "Antioxidants." *Angew Chem Int Ed* 8(8), 547–55, 1969.
- [133] S. Schuber and N. Husing, "Solid state chemistry synthesis of inorganic material" *John willey and sons*, 414, 2002.
- [134] T. Adschiri, T. Hakuta, Y. Arai, K, "Hydrothermal synthesis of metal oxide fine particles at supercritical conditions," *Ind. Eng. Chem. Res*, **39**, 4901–4907, 2000.
- [135] M.O. Donoghue, "A guide to man made gemstones.great Britain;" Van Nostrand Reinhold company, 40-44, 1983.
- [136] A. R. west, "Solid state chemistry and its application," *Wiley and sons*, 2005.
- [137] Thorsten, "lubricants and lubrication,"Ullman encyclopedia of industrial chemistry, Weinhem. 423, 2005.
- [138] A.M. Barnes, K. D. Bartle, V. R. A. Thibon, "A review of zinc dialkyldithiophosphates (ZDDPS):characterisation and role in the lubricating oil," *Elsevier Tribology International*, 34, 389–395, 2001
- [139] W. A. Givens, W. H. Buck, A. S. Jackson, A. Kaldor, A. Hertzberg, W. Moehrmann , S. Mueller-Lunz , N. Petz, G. Wenninger, "Lube formulation effects on transfer of elements to exhaust after-treatment system components," SAE -01-3109, 2003.
- [140] R. Schumacher, H. Zinke, "Tribofragmentation and antiwear behaviour of isogeometric phosphorus compounds,". *Tribology International*, **30**:199–208, 1997.
- [141] R. Sarin, D. K. Tuli, M. M. Rai, A. K. Mehta, A. K. Bhatnagar, "Titanium dithiophosphates: a new class of multifunctional lubricant

- additives,” *Lubrication Engineering*, **51**:313–320. 1995.
- [142] B. B. Farrington, J. O. Clayton, “Compounded mineral oil,” US Patent 2228658, 1941
- [143] E. S. Forbes, J. Battersby, “The effect of chemical structure on the load-carrying and adsorption properties of dialkyl phosphites,” *ASLE Transactions*, **17**:263–270. 1947.
- [144] G. Chen, L. Chen, J. Dong, “Preparation and tribological behaviour of oil-soluble cerium dioctyl dithiocarbamate,” *Lubrication Engineering*, **53**:24–29. 1997.
- [145] J. M. Palacios, “Thickness and chemical composition of films formed by antimony dithiocarbamate and zinc dithiophosphate,” *Tribology International*, **19**:35–39. 1986.
- [146] T. Sakurai, K. Sato, “Chemical reactivity and load carrying capacity of lubricating oils containing organic phosphorus compounds,” *ASLE Transactions*, **13**:252–261. 1970
- [147] Y.Y. Wu, W.C. Tsui, T.C. Liu, “Experimental analysis of tribological properties of lubricating oils with nanoparticle additives,” *Wear* **262**, 819–825. 2007.
- [148] E. Etefaghi, H. Ahmadi, A. M. Rashidi, S. S. Mohtasebi and M. Alaei, Etefaghi, “Experimental evaluation of engine oil properties containing copper oxide nanoparticles as a nanoadditive,” *International Journal of Industrial Chemistry*, **44**, 2013.
- [149] A. M. Abakumov, M. G. Rozova, and Evgeny V. Antipov Joke Hadermann and Gustaaf Van Tendeloo Maxim V. Lobanov and Martha Greenblatt Mark Croft Eugene V. Tsiper “Synthesis, Cation Ordering, and Magnetic Properties of the $(Sb_{1-x}Pb_x)_2(Mn_{1-y}Sb_y)O_4$ Solid Solutions with the Sb_2MnO_4 -Type Structure,” *Chem. Mater.* **17**, 1123-1134(2005)
- M.A. Butler, Photoelectrolysis and physical properties of the semiconducting electrode WO_2 *J. Appl. Phys.* **48**, 1914-1920(1977)
- [150] M.R. Hoffmann, S.T. Martin, W. Choi, D.W. Bahnemann, Environmental Applications of Semiconductor Photocatalysis *Chemical Reviews* **95**,69-96(1995)
- [151] A. Fujishima, T.N. Rao, D.A. Tryk, Titanium dioxide photocatalysis *Journal of Photochemistry and Photobiology C1*, 1–21 (2000).
- [152] C.C. Chen, W.H. Ma, J.C. Zhao, Semiconductor-mediated photodegradation of pollutants under visible-light irradiation, *Chemical Society Reviews* **39**, 4206–4219 (2010)
- [153] L. Zhang, W.Z. Wang, L. Zhou, M. Shang, S. Sun, Fe_3O_4 coupled BiOCl: A highly efficient magnetic photocatalyst *Applied Catalysis B: Environmental* **90**, 458–462. (2009)
- [154] W. Liu, Pingyong Lin, Hua Jin, Hun Xue, Yongfan Zhang, Zhaohui Li, Nanocrystalline $ZnSb_2O_6$: Hydrothermal synthesis, electronic structure and photocatalytic activity, *Journal of Molecular Catalysis A: Chemical* **349** (2011) 80–85
- [155] B. Cheng, Baixiang Tian, Wei Sun, Yanhe Xiao, Shuijin Lei, and Zhanguo Wang, Ordered Zinc Antimonate Nanoisland Attachment and Morphology Control of ZnO Nanobelts by Sb Doping, *J. Phys. Chem. C* **2009**, *113*, 9638–9643
- [156] V. Donchev, Ts. Ivanov, K. Germanova, and K. Kirilov, Surface photovoltage spectroscopy-an advanced method for characterization of semiconductor nano structures, *Trends in applied spectroscopy vol 8*, 2010
- [157] L. Jing, X. Sun, J. Shang, W. Cai, Z. Xu, Y. Du, H. Fu, *Sol. Energy Mater. Sol. Cells* **79**(2003) 133.
- [158] Z. Wang, W. Cai, X. Hong, X. Zhao, F. Xu, C. Cai, *Appl. Catal. B: Environ.* **57** (2005) 223
- [159]

- [160] W. Wang, G. Li, N. Yang, W. Zhang, *Mater. Chem. Phys.* 123 (2010) 322.
- [161] S. Wu, Guoqiang Li, Yang Zhang, Weifeng Zhang, Surface photoelectric and visible light driven photocatalytic properties of zinc antimonate-based photocatalysts, *Materials Research Bulletin* 48 (2013) 1117–1121
- [162] N. Morita, T. Endo, T. Sato, and M. Shimada, The Oxidation State of Antimony and Electrical Properties in Antimony-Doped Rutile, *Journal of solid state chemistry*, 68, 106-111 (1987)
- [163] Beatriz Irigoyen a, Alfredo Juan b, Susana Larrondo a, Norma Amadeo, The electronic structure of vanadium antimonate A theoretical study, *Catalysis Today* 107–108 , 40–45(2005)
- [164] B. Wang, C. Chen, G. Belt, The crystal structure and ionic conductivity of the ilmenite polymorph of NaSbO₃, *journal of solid state chemistry* , 184-188, 1994
- [165] J.N. Reimers, J.E. Greedan, C.V. Stager, R. Kremer, *J. Solid State Chem.* 83 (1989) 20
- [166] J.C. Bonner, M.E. Fisher, *Phys. Rev.* 135 (1964) A640
- [167] Masaki Kato, Akitsugu Hatazaki, Kazuyoshi Yoshimura, Koji Kosuge, One-dimensional magnetic behavior of CuSb₂O₆, *Physica B* 281&282 (2000) 663-664
- [168] N. Reimers and J. E. Greednam M. A. Subramanian, Crystal Structure and Magnetism in MnSb₂O₆ : Incommensurate Long-Range Order, *journal of solid state chemistry* 79, 263-276 (1989)
- [169] Kuo-Tseng Li* and Ni-Shen Shyu, Catalytic Oxidation of Hydrogen Sulfide to Sulfur on Vanadium Antimonate, *Ind. Eng. Chem. Res.* 1997, 36, 1480-1484
- [170] G. A. Zenkovets, E. A. Paukshtis, D. V. Tarasova, T. A. Nikoro and S. Ya. Khomicheva, Acid base and catalytic properties of iron antimony oxide catalysts, *React. Kinet. Catal. Lett.*, Vol. 16, No. 2-3, 143-146 (1981)
- [171] Leena K. Malinen *, Risto Koivula, Risto Harjula, Sorption of radiocobalt and its EDTA complex on titanium antimonates *Journal of Hazardous Materials* 172 (2009) 875–879,
- [172] A. Singh, S. Singh, B.D. Joshi, A. Shukla, B.C. Yadav, P. Tandon, *Mater. Sci. Semi. Processing* 27 (2014) 934-950.
- [173] archana Singh Ajendra Singh Satyendra Singh Poonam Tandon, Nickel antimony oxide (NiSb₂O₆): A fascinating nanostructured material for gas sensing application, *Chemical Physics Letters* • February 2016
- [174] Y. Hu, H. Zhang, H. Yang, "Direct synthesis of Sb₂O₃ nanoparticles via hydrolysis-precipitation method," *Journal of Alloys and Compounds*, **428**, 327-331, 2007.
- [175] W. Kraus, G. Nolze, "Powder Cell—a program for the representation and manipulation of crystal structures and calculation of the resulting X-ray powder pattern," *Journal of Applied Crystallography*, **29**, 1996.
- [176] T. Roisnel, J. R. Carvajal, "WinPLOTR: A windows tool for powder diffraction analysis." In *Materials Science Forum Proceedings of the European Powder Diffraction Conf. (EPDIC 7)*: Citeseer; 2001.
- [177] L. V. Azaroff and M. J. Buerger, "The Powder Method in X-ray Crystallography," **342**, 1953.
- [178] A. Chandran, N. Francis, T. Jose and K. C. George, "Synthesis Structural Characterization and Optical Band Gap Determination of ZnS Nanoparticles," *Acad Rev*, **17**, 17-21, 2010.
- [179] M. Ganguly, S. K. Rout, H. Y. Park, C. W. Ahn and I. W. Kim, "Structural, Dielectric and Optical Characterization of Cerium Doped Barium Titanate." *Physics Express*, **3**,

- 1-12, 2013.
- [180] Z. Z. Sheng and A. M. Hermann "Superconductivity in the rare-earth-free Ti Ba Cu O system above liquid-Nitrogen temperature," *Nature*, **332**, 55-58 1988.
- [181] J. Chandrasekaran, P. Ilayabarathi, P. Maadeswaran, P. Mohamedkutty, S. Pari, "Synthesis, growth and characterization of a semiorganic nonlinear optical single crystal: L-Valine cadmium bromide," *Optik international journal of light and electron*, **123**, 1407-1409, 2012.
- [182] J. M. Linet, S. Jerome Das, "Optical studies on glycine sodium nitrate: A semiorganic nonlinear optical crystal," *J. Optik*, **123**, 1895-1899, 2012.
- [183] A. M. Hermann and J. V. Yakhmi, "Thallium-Based High-Temperature Superconductors" (New York: Dekker) 1994.
- [184] T. Kayed, "Properties of Boron Doped Ti-Ba-Ca-Cu-O Superconductors," *Materials Research Bulletin*, **38**, 533-538, 2003.
- [185] C. J. F. Botcher, "Dielectrics and Static Fields," **1**, 2nd edn, Elsevier Scientific Publishing Company, 1973.
- [186] C. J. F. Botcher and P. Bordewijk, "Dielectrics in Time Dependent Fields," **2**, 2nd edn, Elsevier Scientific Publishing Company, Amsterdam, 1978.
- [187] S. Ameer, I. H. Gul, N. Mahmood, M. Mujahid, "Semiconductor-to-metallic flipping in a ZnFe₂O₄-graphene based smart nano system: temperature/microwave magneto-dielectric spectroscopy," *J. Mater. Charact.* **99**, 254-265, 2015.
- [188] B. Tareev, "Physics of Dielectric Materials," Mir, Moscow 1975.
- [189] J. M. Stevels, "The electrical properties of glass," *Handbuch der Physik*, Ed. S. Flugge, Vol. xx, Berlin Springer, 350-391, 1957.
- [190] K. Maschke, H. Overhof, P. Thomas, "On the variable range hopping near the fermi energy two dimensional system," *Basic solid state physics*, **62**, 113-122, 1974.
- [191] F. Frohlich, P. Grau and W. Grellman, "Performance and analysis of recording microhardness tests," *physica status solidi*, **42**, 79-82, 1977.
- [192] W. C. Oliver and G. M. Pharr, "An improved technique for determining hardness and elastic modulus using load and displacement sensing indentation experiments," *J. Mater. Res.* **7**, 1564-1583, 1992.
- [193] J. L. Loubet, J. M. Georges, O. Marchesini and G. Meille, "Vickers indentation curves of magnesium oxide (MgO)," *J. Tribology*, **106**, 1984.
- [194] M. Sakai, "Energy principle of the indentation induced inelastic surface deformation and hardness of brittle materials," *J. Acta metall. mater.* **41**, 1751-1758, 1993.
- [195] A. Juhasz, M. Dimitrov, A. Luckas, G. V. Gubicza, P. Tasnadi, P. Luckas and A. Kele, *Fortchrittsberichter der Deutschen Keramischen Gesellschaft* **9**, 1994.
- [196] J. Haines et al, "Synthesis and design of superhard material," *Annu. Rev. Mater. Res.* **31**, 1-23, 2001.
- [119] J. J Gilman, J. H. Westbrook, H. Conrad, "The science of hardness testing and its research applications." Ohio, USA: American Society of Metal, Metal Park; [chapter 4], 1973.
- [197] L. Wang, P. Henrique, L.G. Lopes, J.C. Pereira "Mechanical properties of dental restorative materials: relative contribution of laboratory test," *J. Appl. Oral Sci.* **11**, 2003.
- [198] B. Yang and H. Vehoff, "Grain size effects on the mechanical properties of nanonickel examined by nanoindentation," *J. Mater. Sci. Eng.*, **400-401**, 467-470, 2005.
- [148] E. O. Hall, "The deformation and ageing of mild steel: ii characteristic of luder deformation" *J. Phys. Soc.*, **64**, 747-753, 1951.

- [199] N.J. Petch, "The cleavage strength of polycrystals," *J. of the iron steel inst.* **174**, 25–28, 1973.
- [200] G. M. Pharr, "Measurement of mechanical properties by ultralow load indentation," *Materials Science and Engineering*, **253**, 151–159, 1998.
- [201] V. Weihnacht and W. Bruckner, "Abnormal grain growth in 111 textured Cu thin films," *Thin Solid Films*, **418**, no. 2, 136–144, 2002.
- [202] J. M. Zhang, K.W. Xu, and V. Ji, "Competition between surface and strain energy during grain growth in free-standing and attached Ag and Cu films on Si substrates," *Applied Surface Science*, **187**, 60–67, 2002.
- [203] C. V. Thompson and R. Carel, "Texture development in polycrystalline thin films," *Materials Science and Engineering*, **32**, 211–219, 1995.
- [204] G. A. Gerhartz, Y. S. Yamamoto, F. T. Campbell, R. Pfefferkorn, and J. F. Rounsaville, eds. in Ullman's Encyclopedia of Industrial Chemistry, Vol. A1. Weinheim, Germany: VCH, 124–125, 1985.
- [205] D. R. Lide, Handbook of Chemistry and Physics, 72nd Ed. Boca Raton, FL. CRC Press 1991–1992
- [206] ATSDR (Agency for Toxic Substances and Disease Control). Toxicological Profile for Antimony. Agency for Toxic Substances and Disease Registry, U.S. Department of Health and Human Services, Public Health Service, Atlanta, 1992.
- [207] L. R. Rudnick, "Lubricant Additives, Chemistry and Application," Taylor and Francis, 2003.
- [208] A. U. Obasi, S. G. Udeagbara, O. J. Anusiobi, "Effect of additives on the performance of engine oil," *International Journal of Engineering and Technology Research*, **2**, 1–11, 2014.
- [209] A. Elliot, Evans, "Lubricating and Allied Oils", Chapman and Wall Ltd London, 4th Edition. 1963.

